## ATOMIC STRUCTURE AND NON-ELECTRONIC PROPERTIES OF SEMICONDUCTORS

# Kinetics of the accumulation of radiation defects during the high-dose electron irradiation of $Pb_{1-x}Sn_xSe$ alloys

E. P. Skipetrov, B. B. Kovalev, L. A. Skipetrova, and E. A. Zvereva

*Physics Faculty, M. V. Lomonosov Moscow State University, 119899 Moscow, Russia*
(Submitted April 7, 1998; accepted for publication April 27, 1998)
Fiz. Tekh. Poluprovodn. **32**, 1409–1413 (December 1998)

The kinetics of the variation of the electron concentration in electron-irradiated ($T\approx 300$ K, $E=6$ MeV, $\Phi\leqslant 7.1\times 10^{17}$ cm$^{-2}$) $n$-$Pb_{1-x}Sn_xSe$ ($x=0.2$ and 0.25) alloys in the vicinity of the metal-insulator transition induced by electron irradiation are investigated. The principal parameters of the energy spectrum of the irradiated alloys are determined by comparing the experimental and theoretical dependences of the electron concentration on fluence. It is shown that agreement between the theoretical and experimental data is possible only under the assumption that the defect production rate decreases with increasing fluence, and a model, within which the main defect formation mechanism in the alloys investigated is the formation of complexes of primary radiation defects with structural defects typical of the as-grown crystals, is proposed. © *1998 American Institute of Physics.* [S1063-7826(98)00112-4]

### INTRODUCTION

It has been reported that the electron irradiation of $Pb_{1-x}Sn_xSe$ alloys leads to the appearance of a broad band of acceptorlike radiation defects at $E_t$ in the energy spectrum of these alloys.[1,2] The position $E_t$ of the middle of the radiation-defect band relative to the top of the valence band (the $L_6^-$ term) varies with increasing tin concentration in the alloy according to an essentially linear law: $E_t=L_6^-+(87-250\cdot x)$ meV. Therefore, in alloys with an inverse spectrum ($0.19<x<0.35$) the middle of the band $E_t$ is located in the band gap, and the production of radiation defects during the irradiation of *n*-type alloys causes the overflow of electrons from the conduction band into the radiation-defect band $E_t$ (Fig. 1), a decrease in the free-electron concentration, and a metal-insulator transition under the effects of irradiation.[2,3]

Under these conditions an investigation of the kinetics of the variation of the electron concentration during irradiation in the vicinity of the irradiation-induced metal-insulator transition permits the determination of the radiation-defect production rate and provides information on the parameters of the model of the energy spectrum of irradiated alloys and the microscopic structure of the defects. Therefore, the general goal of the present work was to investigate the influence of electron irradiation on the electron concentration in *n*-type alloys with an inverse spectrum ($x=0.20$ and 0.25) for the purpose of determining the parameters of the defect-formation model and ascertaining the nature of the radiation defects in the alloys investigated.

### 1. MEASUREMENT METHOD AND SAMPLES

Single-crystal samples of $Pb_{1-x}Sn_xSe$, whose parameters are listed in Table I, were irradiated at room temperature in an ÉLU-6 electron accelerator ($E=6$ MeV, $\Phi\leqslant 7.1\times 10^{17}$ cm$^{-2}$). The temperature dependences of the resistivity $\rho$ and the Hall coefficient $R_H$ ($4.2\leqslant T\leqslant 300$ K, $B\leqslant 0.04$ T), as well as the field dependences of the Hall coefficient and the Shubnikov–de Haas effect at $T=4.2$ K ($\mathbf{B}\|\langle 100\rangle$, $B\leqslant 7$ T), were investigated before irradiation and at several fluences for each sample.

The results of the measurements at $T=4.2$ K were used to calculate the free-electron concentration and to construct plots of the dependence of the electron concentration in the irradiated crystals on fluence.

### 2. DEPENDENCE OF THE ELECTRON CONCENTRATION ON FLUENCE

Monotonic increases in the resistivity and the absolute value of the Hall coefficient, which indicate a decrease in the electron concentration in the conduction band of the alloy, were observed for all the $n$-$Pb_{1-x}Sn_xSe$ samples during irradiation (Fig. 2). Distinctive oscillations of the transverse resistivity, which attest to the highly uniform introduction of radiation defects during irradiation, were observed in the samples investigated at all values of the fluence. The electron concentrations calculated from the absolute value of the Hall coefficient and the period of the Shubnikov–de Haas oscillations at $T=4.2$ K coincided to within $\pm 5\%$.

In $n$-$Pb_{1-x}Sn_xSe$ ($x=0.25$), in which the middle of the radiation-defect band $E_t$ is located in the band gap near the top of the valence band $L_6^-$, electron irradiation leads to a decrease in the electron concentration and a metal-insulator transition at a certain fluence $\Phi^*\approx 8\times 10^{17}$ cm$^{-2}$. At the same time, in the alloys with $x=0.2$ the rate of variation of the electron concentration decreases appreciably with increasing fluence, and the metal-insulator transition is not de-

 

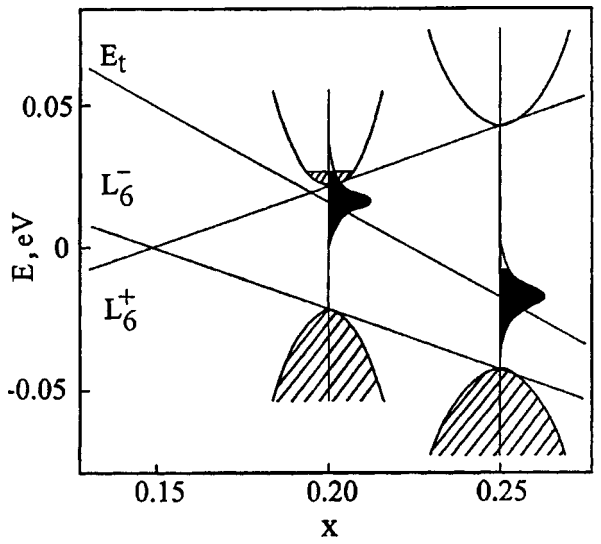


FIG. 1. Energy spectrum of electron-irradiated $Pb_{1-x}Sn_xSe$ alloys with an inverse spectrum.

tected in the range of fluences investigated. With consideration of the energy diagram shown in Fig. 1, it can be assumed that the radiation-defect band in $Pb_{1-x}Sn_xSe$ ($x=0.2$), which is located in the band gap near the bottom of the conduction band $L_6^*$, has a substantial width and strongly overlaps the conduction band, forming a single band of allowed states. Just this circumstance, as well as the high initial electron concentrations in the samples, probably precluded reaching the metal-insulator transition during irradiation in the range of fluences investigated.

To determine the defect production rate during irradiation, as well as the parameters of the radiation-defect band in the alloys investigated, the dependence of the electron concentration at $T=4.2$ K on fluence was calculated in the present work within the previously proposed model of the energy spectrum of an alloy.[2] It was assumed in performing the calculations that the sum of the electron concentrations in the conduction band $n(\Phi)$ and in the radiation-defect band $n_t(\Phi)$ during irradiation is equal to the initial electron concentration in the sample $n_0$:

$$n_0=n(\Phi)+n_t(\Phi), \quad n_t(\Phi)=\int_{-\infty}^{E_F} g_t(E)\,dE, \tag{1}$$

where $g_t(E)$ is the density-of-states function in the radiation-defect band, and $E_F$ is the Fermi energy, which was calculated within Dimmock's model[4] with the dispersion-law parameters given in Ref. 5.

TABLE I. Parameters of the $Pb_{1-x}Sn_xSe$ samples investigated at $T=4.2$ K.

| Sample | $x$ | Type | $\rho\cdot10^4$, $\Omega\cdot$cm | $\lvert R_H\rvert$, cm$^3$/C | $N\cdot10^{-17}$, cm$^{-3}$ | $\mu_H\cdot10^{-5}$, cm$^2$/V·s |
|---|---|---|---|---|---|---|
| W-4 | 0.2 | *n* | 4.4 | 2.3 | 26.7 | 0.053 |
| W-14 | 0.2 | *n* | 4.9 | 2.7 | 22.9 | 0.056 |
| W-3 | 0.25 | *n* | 17.6 | 13.4 | 4.7 | 0.076 |
| W-6 | 0.25 | *n* | 13.9 | 15.4 | 4.1 | 0.111 |

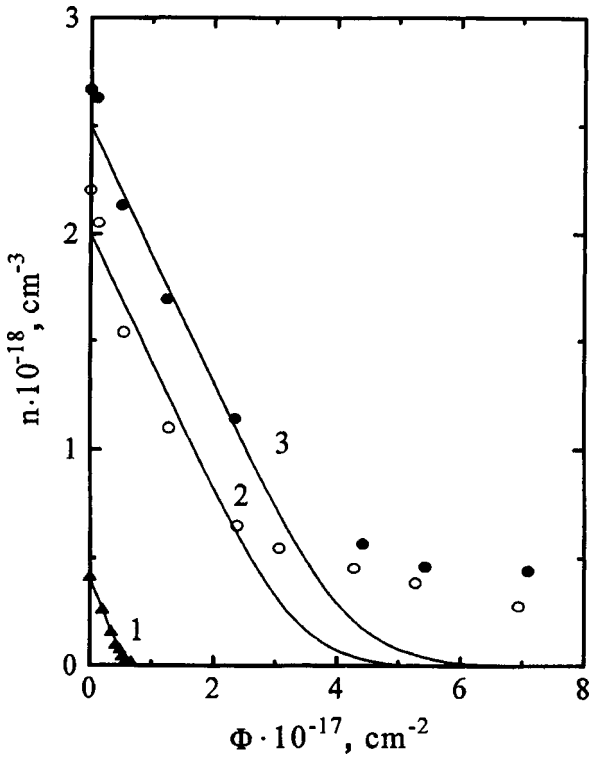


FIG. 2. Dependence of the electron concentration in $n$-$Pb_{1-x}Sn_xSe$ ($x=0.25$ and 0.2) at $T=4.2$ K on fluence. Solid lines — calculation with the parameters listed in Table II. Samples: *1* — W-6, *2* — W-14, *3* — W-4.

In the first stage of the calculations it was also assumed that the radiation-defect production rate $dN_D/d\Phi$ does not depend on fluence, that the total capacity of the radiation-defect band depends linearly on fluence, i.e., $N_t=\Phi(dN_t/d\Phi)$, and that the density-of-states function in the radiation-defect band $g_t(E)$ can be approximated by a Gaussian curve:

$$g_t(E)=\frac{N_t}{\sigma\sqrt{2\pi}}\exp\left[-\frac{(E-E_t)^2}{2\sigma^2}\right], \tag{2}$$

where $\sigma$ is the width of the radiation-defect band.

The preliminary calculations showed that variation of the model parameters ($n_0$, $dN_t/d\Phi$, $E_t$, and $\sigma$) does not permit achieving satisfactory agreement between the theoretical and experimental $n(\Phi)$ curves for the samples with $x=0.2$. In addition, an independent determination of the numerical values of all the parameters of the radiation-defect band in $Pb_{1-x}Sn_xSe$ ($x=0.2$ and 0.25) turned out to be extremely difficult because of the low sensitivity of the dependence of the electron concentration on fluence to the parameters $E_t$ and $\sigma$. Therefore, when the results of calculations and experimental data were compared, the position of the middle of the radiation-defect band $E_t$ relative to the bottom of the conduction was calculated in accordance with the formula[2] $E_t=L_6^-+(87-250)\cdot x$ meV, the characteristic value of the resonance band width $\sigma$ ($\sigma\approx18$ meV) for electron-irradiated $Pb_{1-x}Sn_xSe$ alloys ($0.07\leqslant x\leqslant0.34$) was taken, and only the defect production rate $dN_t/d\Phi$ and the initial electron concentration $n_0$ were varied.

TABLE II. Parameters of the defect formation model for electron-irradiated $Pb_{1-x}Sn_xSe$ alloys with $N_t=\Phi\cdot dN_t/d\Phi$.

| No. | Sample | $x$ | $E_c-E_t$, meV | $\sigma$, meV | $n_0$, $cm^{-3}$ | $dN_t/d\Phi$, $cm^{-1}$ |
|---|---|---|---|---|---|---|
| 1 | W-6 | 0.25 | 60 | 18 | $4.0\times10^{17}$ | 6.0 |
| 2 | W-14 | 0.20 | 6 | 18 | $2.0\times10^{18}$ | 6.0 |
| 3 | W-4 | 0.20 | 6 | 18 | $2.0\times10^{18}$ | 6.0 |

The theoretical plots of $n(\Phi)$ thus obtained are depicted by the solid lines in Fig. 2, and the parameters of the model for each of the samples investigated are listed in Table II. The defect production rate during irradiation was the same for all the samples, but while the agreement between theory and experiment can be considered satisfactory for the sample with $x=0.25$, the theoretical $n(\Phi)$ curves for the samples with $x=0.2$ deviate significantly from the experimental points at low fluences and suggest the existence of a transition to the insulator state in the range of fluences investigated.

### 3. MODEL OF DEFECT FORMATION DURING ELECTRON IRRADIATION

An analysis of the theoretical $n(\Phi)$ curves with variation of the model parameters showed that the theoretical and experimental data can be reconciled only if it is assumed that the radiation-defect production rate decreases with increasing fluence.

The phenomenon of a decrease in the defect production rate during electron and $\gamma$ irradiation is well known in classical Ge and Si semiconductors and is associated with the formation of complexes of the primary radiation defects (vacancies) with impurity atoms in them. For example, in germanium doped with group-V impurities the formation of radiation defects during $\gamma$ and electron irradiation is described as a consecutive-parallel reaction of vacancies ($V$) with donor impurity atoms ($D$) and donor+vacancy complexes ($DV$):[6–10]

$$D+V\xrightarrow{K_1}DV, \quad DV+V\xrightarrow{K_2}DVV, \tag{3}$$

where $K_1$ and $K_2$ are the rate constants of the reactions resulting in the formation of donor+vacancy and donor +2 vacancies complexes, respectively.

In this case $K_1>K_2$, and the accumulation of electrically neutral $DV$ complexes is dominant at first (before $n-p$ conversion). As the fluence is increased further, the concentration of $DV$ complexes as the intermediate product decreases, and the concentration of $DVV$ complexes increases and tends to a limiting value equal to the concentration of the donor impurity. In the initial stage the dominant defect formation mechanism is the formation of $DV$ complexes. At this point the defect production rate decreases with increasing fluence as a result of the decrease in the concentration of electrically active donors, and the electron concentration $n(\Phi)$ decreases according to an exponential law (see the inset in Fig. 3):

$$n(\Phi)=n_0\exp(-K\cdot\Phi/n_0), \tag{4}$$

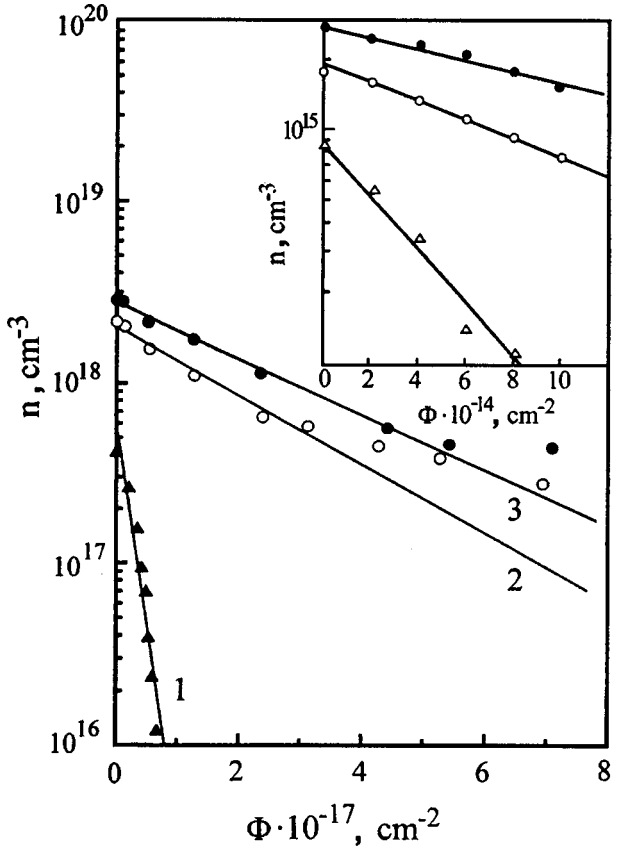


FIG. 3. Dependence of the electron concentration in $n$-$Pb_{1-x}Sn_xSe$ ($x=0.25$ and 0.2) and in antimony-doped Ge[10] (inset) on electron flux. Samples: *1* — W-6, *2* — W-14, *3* — W-4.

$$dn/d\Phi=-K\exp(-K\cdot\Phi/n_0), \tag{5}$$

$$N_{DV}(\Phi)=N_D(1-\exp(-K\cdot\Phi/N_D)), \tag{6}$$

$$dN_{DV}/d\Phi=K\exp(-K\cdot\Phi/N_D), \tag{7}$$

where $K$ is the initial rate of decrease in the electron concentration (the initial defect production rate), $N_D$ is the concentration of donors, and $N_{DV}$ is the concentration of $DV$ complexes.

Plotting the experimental data for the electron concentration in electron-irradiated samples of $Pb_{1-x}Sn_xSe$ ($x=0.2$ and 0.25) in logarithmic coordinates gave curves, whose initial segments, where the Fermi level is still fairly high in the conduction band (Fig. 1), are described well by straight lines (Fig. 3). Just as in the case of germanium doped by group-V donors, the slope of the straight lines increases with decreasing initial electron concentrations in the sample, in correspondence to the approximately identical initial rates of decrease in the electron concentration during irradiation for all the samples. The obvious similarity among the $n(\Phi)$ curves shown in Fig. 3 allows us to presume that the principal defect formation mechanism in $Pb_{1-x}Sn_xSe$ alloys is the formation of complexes of the primary radiation defects with the structural defects characteristic of the unirradiated crystals. This circumstance allows us to calculate the $n(\Phi)$ curves using dependences of the radiation-defect density and production rate on fluence in forms similar to (6) and (7):

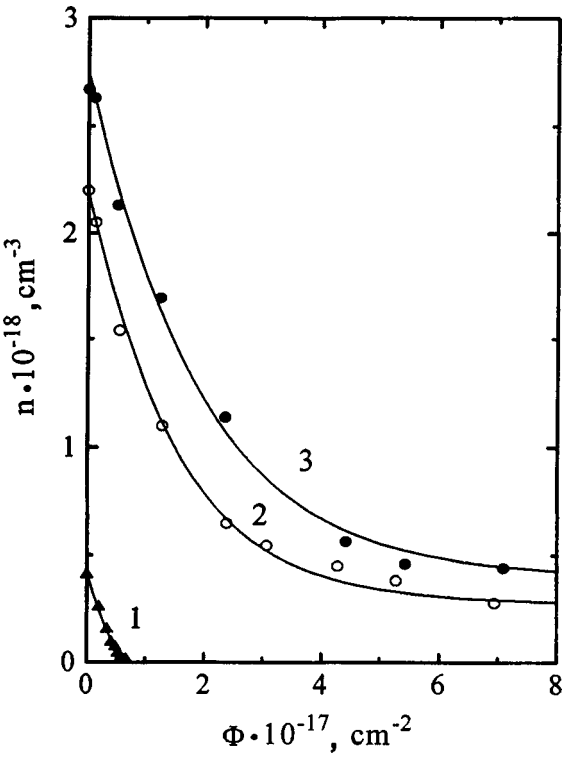


FIG. 4. Dependence of the electron concentration in $n$-$Pb_{1-x}Sn_xSe$ ($x=0.25$ and 0.2) at $T=4.2$ K on fluence. Solid lines — calculation with the parameters listed in Table III. Samples: *1* — W-6, *2* — W-14, *3* — W-4.

$$N_t(\Phi)=N_d(1-\exp(-K\cdot\Phi/N_d)), \tag{8}$$

$$dN_t/d\Phi=K\exp(-K\cdot\Phi/N_d), \tag{9}$$

where $N_d$ is the concentration of the structural defects characteristic of the as-grown crystals and $K$ is the initial defect production rate.

Variation of the parameters $K$ and $N_d$ enabled us to obtain satisfactory agreement between theory and experiment within the model of the energy spectrum of $Pb_{1-x}Sn_xSe$ alloys in Fig. 1 for all the samples investigated (Fig. 4). The parameters of the model for each of the samples are listed in Table III.

TABLE III. Parameters of the defect formation model for electron-irradiated $Pb_{1-x}Sn_xSe$ alloys with $N_t=N_d(1-\exp(-K\cdot\Phi/N_d))$.

| No. | Sample | $x$ | $E_c-E_t$, meV | $\sigma$, meV | $n_0$, $cm^{-3}$ | $K$, $cm^{-1}$ | $N_d$, $cm^{-3}$ |
|---|---|---|---|---|---|---|---|
| 1 | W-6 | 0.25 | 60 | 18 | $4.20\times10^{17}$ | 10.1 | $6.5\times10^{17}$ |
| 2 | W-14 | 0.20 | 6 | 18 | $2.19\times10^{18}$ | 12.0 | $2.1\times10^{18}$ |
| 3 | W-4 | 0.20 | 6 | 18 | $2.75\times10^{18}$ | 12.0 | $2.5\times10^{18}$ |

In conclusion, we note that the concrete microscopic structure of the complexes formed during electron irradiation of the $Pb_{1-x}Sn_xSe$ alloys investigated is still not clear. However, taking into account that electron irradiation leads to the formation of an unfilled radiation-defect band at $E_t$ and a decrease in the free-electron concentration with a high initial rate $dn/d\Phi\approx10\ cm^{-1}$, we can assume that the complexes have an acceptor character and contain selenium vacancies (in the free state a selenium vacancy is a source of two electrons). The analogs of the donor impurity atoms in Ge in the case of undoped $Pb_{1-x}Sn_xSe$ alloys can include any structural defects, i.e., atoms of an unmonitored impurity (for example, oxygen), dislocations, and even vacancies which existed in the as-grown unirradiated crystals.

## CONCLUSION

Thus, a decrease in the defect production rate with increasing fluence has been discovered in the present work during the high-dose electron irradiation of $n$-$Pb_{1-x}Sn_nSe$ ($x=0.2$ and 0.25). The experimental plots of the electron concentration in the alloys investigated as a function of fluence have been compared with the theoretical curves within a model of the energy spectrum of electron-irradiated $Pb_{1-x}Sn_xSe$ alloys, and the principal parameters of the model have been determined. A model of defect formation during the electron irradiation of alloys, which presumes the formation of complexes of the primary radiation defects with structural defects characteristic of the as-grown unirradiated crystals, has been proposed.

We thank A. M. Musalitin for irradiating the samples investigated with fast electrons.

This work was financially supported by the Russian Fund for Fundamental Research (Grants 96-02-18325 and 96-15-96500).

[1] E. P. Skipetrov, V. P. Dubkov, and B. B. Kovalev, Semicond. Sci. Technol. **4**, 831 (1989).
[2] N. B. Brandt and E. P. Skipetrov, Fiz. Nizk. Temp. **22**, 870 (1996) [Low Temp. Phys. **22**, 665 (1996)].
[3] E. P. Skipetrov, Solid State Commun. **69**, 1053 (1989).
[4] J. O. Dimmock, in *The Physics of Semimetals and Narrow Gap Semiconductors*, edited by D. L. Carter and R. T. Bate (Pergamon Press, New York, 1971), p. 319.
[5] N. B. Brandt, Ya. G. Ponomarev, and E. P. Skipetrov, Fiz. Tverd. Tela (Leningrad) **29**, 3233 (1987) [Sov. Phys. Solid State **29**, 1856 (1987)].
[6] N. A. Vitovskiĭ, M. Maksimov, and T. V. Mashovets, Fiz. Tekh. Poluprovodn. **4**, 2276 (1970) [Sov. Phys. Semicond. **4**, 1960 (1971)].
[7] L. S. Smirnov, V. F. Stas', and V. V. Khaĭnovskaya, Fiz. Tekh. Poluprovodn. **5**, 85 (1971) [Sov. Phys. Semicond. **5**, 70 (1971)].
[8] V. D. Tkachev and V. I. Urenev, Fiz. Tekh. Poluprovodn. **5**, 1516 (1971) [Sov. Phys. Semicond. **5**, 1324 (1972)].
[9] T. V. Mashovets, V. V. Emtsev, and S. N. Abdurakhmanova, Fiz. Tekh. Poluprovodn. **8**, 96 (1974) [Sov. Phys. Semicond. **8**, 59 (1974)].
[10] V. F. Stas', in *Physical Processes in Irradiated Semiconductors* [in Russian], L. S. Smirnov [Ed.], Nauka, Novosibirsk (1977), Chap. 4, p. 112.

Translated by P. Shelnitz

# Influence of oxygen on the ion-beam synthesis of silicon carbide buried layers in silicon

V. V. Artamanov, M. Ya. Valakh, N. I. Klyuĭ, V. P. Mel'nik, A. B. Romanyuk, B. N. Romanyuk, and V. A. Yukhimchuk

*Institute of Semiconductor Physics, Ukrainian National Academy of Sciences, 252028 Kiev, Ukraine*
(Submitted March 16, 1998; accepted for publication April 2, 1998)
Fiz. Tekh. Poluprovodn. **32**, 1414–1419 (December 1998)

The properties of silicon structures with silicon carbide (SiC) buried layers produced by high-dose carbon implantation followed by a high-temperature anneal are investigated by Raman and infrared spectroscopy. The influence of the coimplantation of oxygen on the features of SiC buried layer formation is also studied. It is shown that in identical implantation and post-implantation annealing regimes a SiC buried layer forms more efficiently in CZ Si wafers or in Si (CZ or FZ) subjected to the coimplantation of oxygen. Thus, oxygen promotes SiC layer formation as a result of the formation of $SiO_x$ precipitates and accommodation of the volume change in the region where the SiC phase forms. Carbon segregation and the formation of an amorphous carbon film on the SiC grain boundaries are also discovered. © *1998 American Institute of Physics.* [S1063-7826(98)00212-9]

## 1. INTRODUCTION

Silicon carbide (SiC) is unquestionably one of the most promising materials in modern electronics. Silicon carbide is a wide-gap semiconductor (its gap width varies from 2.3 to 3.3 eV, depending on polytype) and exhibits high thermal, radiation, and chemical stability.[1,2] Along with the possibility of altering the type of conduction and the mobility of its charge carriers, these properties determine the areas for the practical application of SiC: from light-emitting diodes to high-temperature high-speed transistors.[2–4]

One promising method for synthesizing SiC is the high-dose implantation of oxygen ions in silicon.[5–9] Along with a low degree of contamination and comparatively low synthesis temperatures, this method makes it possible to create a SiC layer at a required depth by varying the energy of the implanted ions. Silicon structures with a SiC buried layer formed by ion implantation can serve as SOI (silicon-on-insulator) structures, which have definite advantages over the conventional structures with a $SiO_2$ buried layer obtained by SIMOX (separation by implanted oxygen).[10] The primary advantages are the significantly higher radiation stability and thermal conductivity of a SiC buried layer, which enable devices to function under more severe conditions. The promising nature of the use of SiC layers in Si formed by ion implantation as substrates for the subsequent deposition of SiC epitaxial films or diamondlike films has been reported in several publications.[6,11] On the other hand, a SiC buried layer obtained under definite conditions can serve as a stop layer for the etching of silicon in a technology used to produce various sensors.[8]

Most of the studies devoted to the investigation of the ion-beam synthesis of SiC buried layers focused on the influence of the implantation and postimplantation annealing temperatures, the energy and dose of the implanted ions, and the substrate orientation on the properties of the layer obtained.[5–8]

We previously demonstrated the significant stimulating effect of impurity carbon on the formation of a $SiO_2$ buried layer in silicon.[12] Conversely, oxygen influences the formation of SiC layers.[9]

In this context the purpose of the present work was to investigate the influence of oxygen on SiC buried layer formation in silicon during high-dose carbon implantation as a function of the postimplantation annealing conditions.

## 2. EXPERIMENT

Wafers of *p*-Si(100) grown by the float-zone technique (FZ Si) and Czochralski silicon (CZ Si) were investigated. The oxygen concentration in the as-grown FZ Si and CZ Si wafers was $\leqslant 10^{16}$ and $6\times10^{17}$ cm$^{-3}$, respectively. The Si wafers were implanted by 125 keV $C^+$ ions at a dose of $4.3\times10^{17}$ cm$^{-2}$. The ion-beam current density did not exceed 2 $\mu$A/cm$^2$. During implantation, the wafers were additionally heated on their rear side to 500 °C by halogen lamps. Some wafers were coimplanted by 150 keV $O^+$ ions at a dose of $2\times10^{16}$ cm$^{-2}$. After implantation, the wafers were subjected to a high-temperature anneal at 1180 or 1250 °C for 4 h in an argon atmosphere.

The infrared (IR) absorption spectra were measured on an IFS-113v Fourier spectrometer with a spectral resolution of 2 cm$^{-1}$. The Raman spectra were measured using an automated system based on a DFS-24 spectrometer. A cooled FÉU-136 photomultiplier operating in the photon-counting mode served as the detector. The spectra were excited by an argon laser ($\lambda = 474.4$, 487.9, 496.5, and 514.5 nm). To avoid heating the sample during the recording of the Raman spectra, the laser radiation was focused on the sample by a cylindrical lens, and the total power of the exciting radiation

 

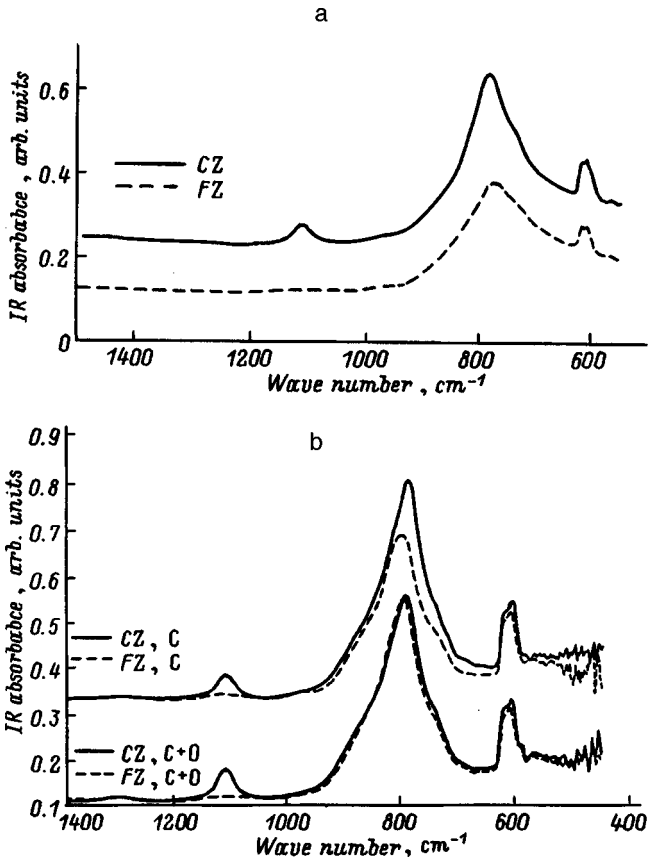


FIG. 1. IR absorption spectra of FZ Si (*1*) and CZ Si (*2*) wafers: a — after $C^+$ implantation without annealing; b — after implantation by $C^+$ ions and coimplantation by $C^+$ and $O^+$ ions followed by annealing at $T=1250\,^\circ$C.

did not exceed 100 mW. All the measurements were performed at room temperature.

### 3. RESULTS AND DISCUSSION

Figure 1a presents the IR absorption spectra of FZ Si and CZ Si wafers after the implantation of carbon atoms. The CZ Si samples display three characteristic bands at 600, 800, and 1100 $cm^{-1}$. The band at 600 $cm^{-1}$ corresponds to vibrations of Si–C bonds, whose carbon atom is found in a substitutional position in the silicon lattice. The band at 1100 $cm^{-1}$ is characteristic of oxygen-containing Si and corresponds to vibrations of Si–O–Si bonds. The presence of the band at 800 $cm^{-1}$, which is characteristic of Si–C bonds in the silicon carbide lattice, attests to the formation of a SiC buried layer right in the implantation process. We note that the spectrum of an implanted FZ Si wafer is similar as a whole to the one just described, but the band at 1100 $cm^{-1}$ is essentially absent due to the low concentration of oxygen in the as-grown wafer. In addition, the intensity of the band at 800 $cm^{-1}$ is smaller than for CZ Si.

Annealing the implanted structures at $T=1250\,^\circ$C leads to a sharp increase in the intensity and narrowing of the band at 800 $cm^{-1}$, attesting to an increase in the content of the SiC phase and its crystallization (Fig. 1b). More efficient formation of the SiC phase takes place in the CZ Si wafers, as is manifested by the significant increase in absorption at 800 $cm^{-1}$ in comparison to the FZ Si wafers. The relative content of the crystalline phase of SiC is also increased. In fact, decomposition of the band at 800 $cm^{-1}$ into two elementary bands corresponding to SiC in the amorphous and crystalline states[13] gives the following values for the ratio between the integrated intensities of the ''amorphous'' and ''crystalline'' bands: $I_a/I_c=2.9$ for CZ Si and 5.13 for FZ Si, respectively.

The results obtained can be interpreted within the following model. It is known that the synthesis of SiC layers in a Si matrix should be accompanied by a considerable decrease in the crystal volume in the region where the SiC phase forms (by 48%).[7] On the other hand, the formation of precipitates or a phase of $SiO_2$ in Si is accompanied by an increase in the crystal volume.[14] For example, in the case of the formation of a continuous $SiO_2$ buried layer, the volume should increase by 2.25 fold.[6,14] Clearly, when another phase forms in Si, processes which permit minimization of the free energy of the system are thermodynamically more advantageous. When SiC buried layers are synthesized in Si, this situation is realized for CZ Si wafers containing a large quantity of oxygen in the as-grown state. During the implantation and annealing of the CZ Si wafers, the $SiO_2$ precipitates forming in the region for formation of the SiC phase permit accommodation of the volume change and a decrease in the free energy of the system. More efficient formation of the SiC phase occurs as a result. In this case, the interstitial silicon atoms ($Si_i$) produced upon replacement of a Si unit cell by a $\beta$-SiC unit cell[6,7] interact with oxygen atoms in the free volume created to form $SiO_x$ precipitates. During the postimplantation anneal, the dimensions of the $SiO_x$ precipitates increase, and the excess oxygen is pushed out onto the boundaries of the SiC layer formed.[9] This model is supported by the fact the formation of a SiC phase is more efficient in oxygen-containing silicon already immediately after implantation (Fig. 1a). We note that since a SiC buried layer also forms in oxygen-free silicon, the model proposed in Refs. 6 and 7 is most likely operating in this case. In this model, as a result of the interaction of interstitial Si atoms with arriving C atoms in the free volume formed, one Si unit cell is replaced by two $\beta$-SiC cells. As a result, the change (increase) in volume should amount to only 3.25%.[6,7]

The contributions of the mechanisms described above to the formation of a SiC phase should depend significantly on the oxygen concentration and should be controlled by the relation between the diffusion coefficients or oxygen and carbon and the critical radii of the $SiO_2$ and SiC precipitates.

In order to test the proposed model, experiments were carried out to study the influence of the coimplantation of oxygen (before annealing) on the efficiency of the formation of a SiC phase in FZ Si and CZ Si wafers.

The IR absorption spectra of structures annealed at $T=1250\,^\circ$C after the coimplantation of oxygen are shown in Fig. 1b. As we see, there are essentially no differences in the shape, width, and intensity of the band at 800 $cm^{-1}$ for CZ Si and FZ Si wafers in this case, and the parameters of the band at 800 $cm^{-1}$ are close to the corresponding values for CZ Si wafers without the coimplantation of oxygen (Fig. 1b). Thus, the coimplantation of $O^+$ ions stimulates the for-

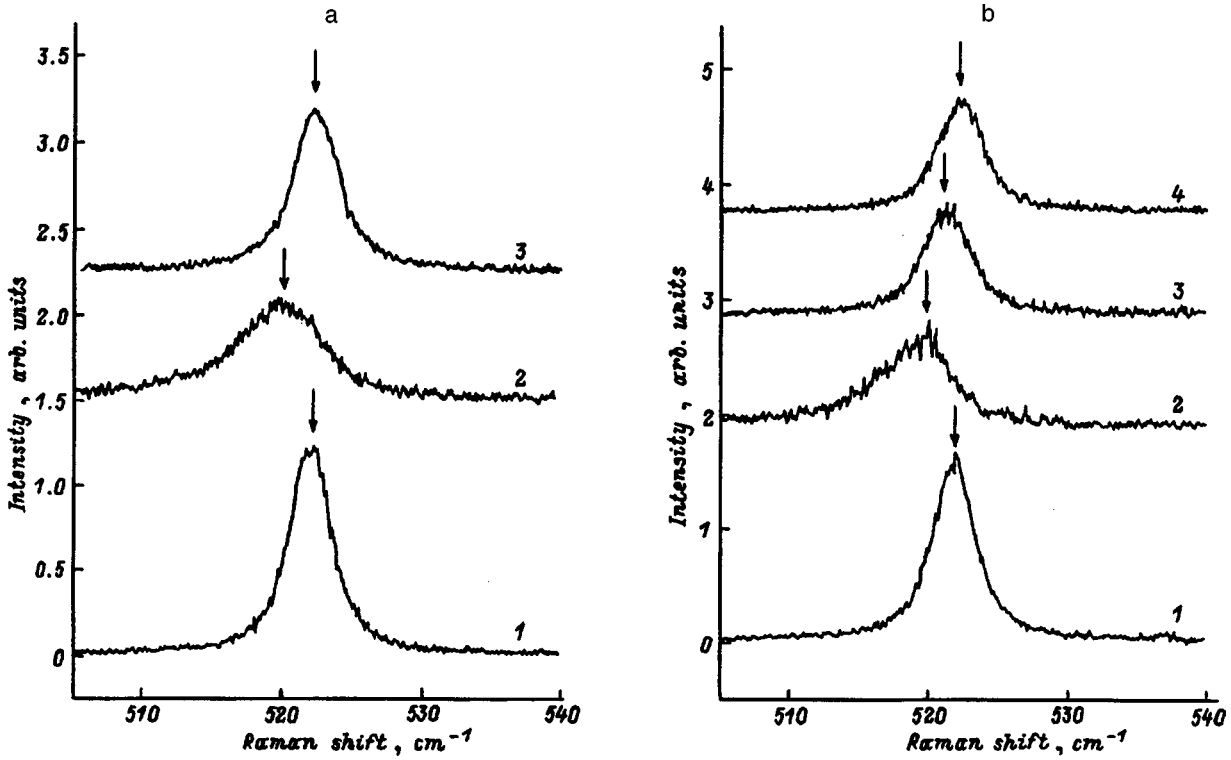


FIG. 2. Raman spectra of CZ Si (a) and FZ Si (b) wafers: *1* — as-grown samples, *2* — after implantation of $C^+$ ions, *3* — after implantation of $C^+$ ions and annealing at $T=1250$°C, *4* — after coimplantation of $C^+$ and $O^+$ and annealing at $T=1250$ °C.

mation of a SiC phase in FZ Si wafers, in support of the model proposed above.

It is noteworthy that no changes were observed in the IR transmission spectra of FZ Si wafers after the coimplantation of oxygen and an anneal at $T=1180$ °C. Thus, the postimplantation anneal temperature is the most important parameter determining the kinetics of SiC buried layer formation. The dimensions of the $SiO_x$ precipitates are clearly small for lower anneal temperatures[14] and do not permit compensation of the volume change in the region where the SiC phase forms.

An important characteristic of silicon structures with SiC buried layers is the presence of internal mechanical stresses in them. An investigation of these stresses, especially their spatial distribution, can provide important information for understanding the mechanisms underlying SiC buried layer formation. A picture of the processes leading to structural reorganization in the buried layer can be derived from the magnitude and sign of the mechanical stresses. We investigated the distribution of the mechanical stresses in structures with a SiC buried layer using Raman scattering. Figure 2 presents the Raman spectra of as-grown samples of FZ Si and CZ Si, as well as structures subjected to implantation by $C^+$ ions and a high-temperature postimplantation anneal. The spectra of the as-grown samples (curves *1*) exhibit a band at $\sim 522$ cm$^{-1}$, which is typical of Si and corresponds to scattering by long-wavelength Brillouin-zone-center optical phonons. A red shift and broadening of this band are observed after implantation as a result of structural disordering (curves *2*). The postimplantation anneal, which partially restores the structure of the implanted layer, leads to narrowing and reverse displacement of the band under discussion in the Raman spectrum (curves *3*). As a whole, the form of the Raman spectra for the as-grown, implanted, and annealed samples of FZ Si and CZ Si is similar. The only differences are the small red shift of the band for FZ Si and the blue shift for CZ Si relative to the original spectrum. These shifts are evidence of the presence of tensile stresses in an FZ Si wafer and compressive stresses in a CZ Si wafer after SiC buried layer formation. These findings can be explained in the following manner on the basis of the model proposed above. In an FZ Si wafer tensile stresses appear in the SiC layer itself as a result of the decrease in volume in the region where the SiC phase forms. As a result, the near-surface Si overlayer is also subjected to tensile stresses. In CZ Si wafers the formation of $SiO_x$ precipitates in the region where the SiC phase forms leads to overcompensation of the tensile stresses and the appearance of compressive stresses in both the SiC layer and in the near-surface Si layer. This conclusion is supported by the results of investigations of the spatial (with respect to depth in the sample) distribution of the mechanical stresses. In this case the Raman spectra of structures subjected to implantation and annealing were measured with excitation by laser radiation at a different wavelength. The thickness of the layer tested as a function of the absorption coefficient of Si was $d \propto 1/2\alpha$, where $\alpha$ is the absorption coefficient for the exciting radiation. The magnitude and sign of the mechanical stresses were estimated from the shift of the band at 522 cm$^{-1}$ using the known formula[15]

$$\sigma\ [\mathrm{Pa}] = -2.49\times 10^8 \Delta\nu, \tag{1}$$

where $\Delta\nu$ is the shift of the Raman band in cm$^{-1}$.

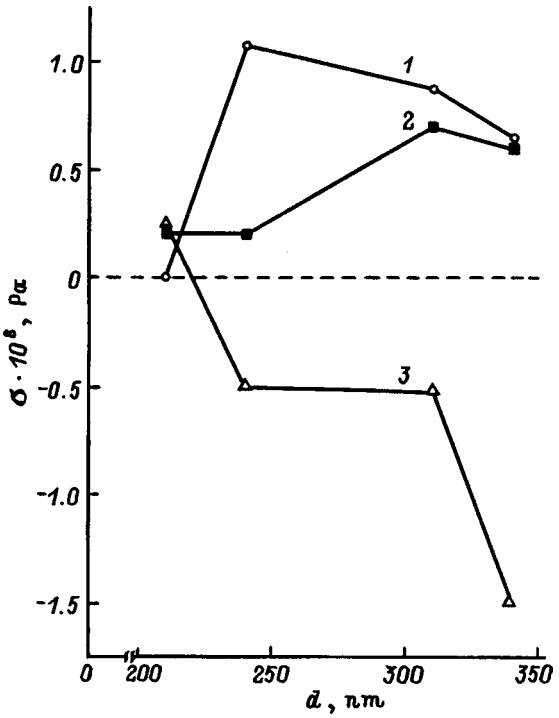


FIG. 3. Spatial distribution of mechanical stresses in structures with a SiC buried layer after annealing at $T=1250\,^{\circ}$C: *1* — $C^+$-implanted CZ Si, *2* — $C^+$-implanted FZ Si, *3* — $C^+/O^+$-implanted FZ Si.

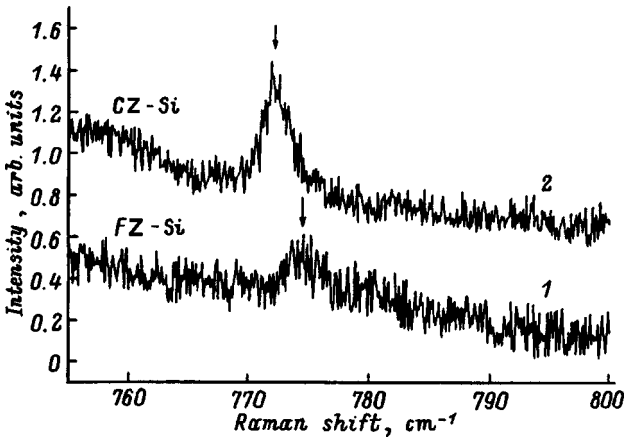


FIG. 4. Spectra of structures with a SiC layer after removal of the near-surface Si film: *1* — FZ Si, *2* — CZ Si.

The results obtained are presented in Fig. 3. It is seen that compressive stresses are observed for the CZ Si wafer with a SiC buried layer over essentially the entire region tested down to $d\approx 350$ nm. At the same time, the stresses in the FZ Si wafer are tensile and increase sharply as we approach the region where the SiC layer forms. We note that the mean projected range and rms straggling of carbon atoms in silicon at the implantation energy used are 330 and 70 nm, respectively.

As was noted above, the coimplantation of $O^+$ ions in an FZ Si wafer before the high-temperature anneal stimulates the formation of a SiC phase (Fig. 1b). In this case the Raman spectrum (Fig. 2b, curve *4*) and the spatial distribution of the mechanical stresses in such a structure become similar to those observed for CZ Si (Fig. 3, curve *2*). The precipitation of implanted oxygen in the regions for nucleation and growth of the SiC layer, which leads to overcompensation of the tensile stresses and the appearance of compressive stresses, clearly also takes place here.

It should be noted that the Raman spectra of the samples of both types (both CZ Si and FZ Si) recorded after the implantation of $C^+$ ions and after annealing did not contain the bands at 760–800 and 965–975 $cm^{-1}$ which correspond to scattering by TO and LO phonons in SiC.[16,17] This is due primarily to the substantial absorption of the laser radiation in the near-surface Si layer. In addition, the small cross section for scattering by phonons in SiC should be taken into account. After removal of the near-surface Si layer in a polishing etch, the Raman spectra of $C^+$-implanted and annealed samples of CZ Si and FZ Si displayed a clearly expressed band in the range 770–780 $cm^{-1}$ (Fig. 4). We stress that the implantation and annealing regimes which we employed correspond completely to the conditions for the formation of an effective SiC stop layer during the etching of silicon.[8] Thus, the signal observed at 770–780 $cm^{-1}$ was produced by a silicon carbide layer and corresponds to TO phonons.[16,17] The bands in the Raman spectra of the CZ Si and FZ Si samples are at $\sim$772 and $\sim$774 $cm^{-1}$, respectively. The Raman spectra were not investigated in the region of SiC LO phonons (965–975 $cm^{-1}$) because of the juxtaposition of a second-order Si scattering band. As can be seen from the spectra in Fig. 4, the wave numbers of the Raman bands are considerably lower than the values for the TO phonon in the spectrum of $3C$-SiC (796 $cm^{-1}$, Refs. 16 and 17) and approximate the position of one of the TO peaks in the Raman spectrum of $6H$-Si.[16] At the same time, the peaks that we observed cannot be assigned to $6H$-SiC for the following reasons. For one thing, according to the x-ray diffraction data, the SiC layer that we synthesized had a microcrystalline structure and consisted of $\beta$-SiC grains. In addition, according to the data in Ref. 6, inclusions or precipitates of $6H$-SiC can form in a structure with a SiC buried layer only in the near-surface Si layer. As we have already noted, this layer was removed in a polishing etch, as was confirmed by the results of an Auger analysis (which are not presented).

In our opinion, the observed red shift of the band corresponding to the $\beta$-SiC TO phonon can be explained in the following manner. According to data from transmission electron microscopy, the microcrystallites in the SiC layer that we synthesized measured $\sim 10-20$ nm. When SiC particles are of such size, the band at 796 $cm^{-1}$ undergoes a considerable red shift.[17] Sasaki *et al.*[17] explained this shift within a model that takes into account the structural imperfection of the near-surface layer of small SiC particles, which leads to ''softening'' of the TO phonon. In our opinion, the observed red shift of the band being analyzed can also be associated with the presence of considerable mechanical stresses on a SiC-microcrystallite/carbon-film interface. The formation of an amorphous carbon film on the grain boundaries in the SiC layer is evidenced by the Raman spectra measured in the range 1300–1550 $cm^{-1}$, which are shown in Fig. 5. We note

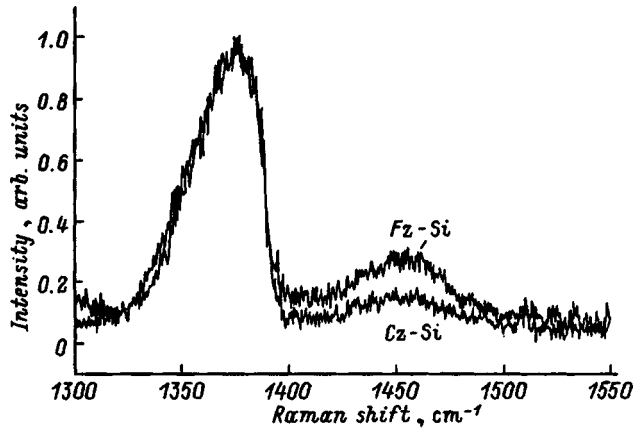


FIG. 5. Raman spectra of structures with a SiC layer after removal of the near-surface Si film in the region for the manifestation of C–C bonds.

that these spectra were also measured on samples with a near-surface Si layer removed by etching. The Raman spectra shown in Fig. 5 clearly display two bands at $\sim$1370 and 1460 $cm^{-1}$. These bands are close in wave number to the *D* (''disordered'') and *G* (''graphitic'') bands in the Raman spectra of amorphous carbon films.[18] Thus, it can be concluded that the synthesis of SiC buried layers is accompanied by the segregation of carbon on the boundaries of the SiC microcrystallites with the formation of an amorphous carbon film. The presence of such a film will clearly prevent the growth and coalescence of SiC particles. The differences between the Raman spectra of the CZ Si and FZ Si samples in the region 1300–1350 $cm^{-1}$ (Fig. 5) are noteworthy in this context. While the *D* bands of both samples essentially coincide, the *G* band of the FZ Si sample is much more intense than the corresponding band for CZ Si. This is evidence of the following. First, more carbon atoms reach the grain boundaries and form a carbon film during the formation of the SiC layer in FZ Si wafers. Second, the greater intensity of the *G* band for FZ Si indicates a greater content of the graphitic phase, which is the thermodynamically most stable allotropic form of carbon. These two factors will impede the efficient growth of a SiC layer. In fact, as can be seen from Fig. 4, the intensity of the band for scattering by SiC TO phonons is much higher in the Raman spectrum of the CZ Si sample than in that of the FZ Si sample. In addition, as has been noted repeatedly above, these differences are clearly displayed in the IR absorption spectra of CZ Si and FZ Si wafers without the coimplantation of oxygen (Fig. 1b).

## 4. CONCLUSION

1. During the ion-beam synthesis of SiC buried layers in Si, oxygen promotes formation of the SiC phase as a result of the formation of $SiO_x$ precipitates and accommodation of the free volume created. Overcompensation of the tensile mechanical stresses and the appearance of compressive stresses in the near-surface silicon layer are observed during this process.

2. The coimplantation of oxygen ions in oxygen-free silicon (FZ Si) permits the creation of conditions for the formation of a SiC phase similar to those in CZ Si.

3. The formation of a SiC buried layer is accompanied by the segregation of carbon followed by the formation of an amorphous carbon film on the SiC grain boundaries. The formation of an *a*-C film is one of the factors preventing the coalescence of SiC precipitates.

[1] G. L. Garris, *Properties of Silicon Carbide*, INSPEC, London (1995).
[2] G. Pensl and T. Troffer, Solid State Phenom. **45–48**, 115 (1996).
[3] P. A. Ivanov and V. E. Chelnokov, Semicond. Sci. Technol. **7**, 863 (1992).
[4] J. W. Palmour, J. A. Edmond, H. S. Kong, and C. H. Carter Jr., Physica B **185**, 461 (1993).
[5] L. T. Canham, M. R. Dyball, and K. G. Barraclough, Mater. Sci. Eng., B **4**, 951 (1990).
[6] K. J. Reeson, J. Stoemenos, and P. L. F. Hemment, Thin Solid Films **191**, 147 (1990).
[7] A. Nejim, P. L. F. Hemment, and J. Stoemenos, Appl. Phys. Lett. **66**, 2646 (1995).
[8] C. Serre, A. Perez-Rodriguez, and A. Romano-Rodriguez, in *Proceedings of the International Conference on Ion Implantation Technology, Catania, 1994* (Elsevier, Amsterdam, 1995), p. 32.
[9] N. I. Klyui, D. Kruger, B. N. Romanyuk, V. G. Litovchenko, and H. Richter, Solid State Phenom. **47–48**, 211 (1996).
[10] A. Auberton-Herve, A. Witkower, and B. Aspar, Nucl. Instrum. Methods Phys. Res. B **96**, 420 (1995).
[11] L. T. Canham, K. G. Barnaclough, and D. J. Roberts, Appl. Phys. Lett. **51**, 1509 (1987).
[12] B. N. Romanyuk, V. P. Mel'nik, R. I. Marchenko, and N. I. Klyuĭ, Poverkhnost', No. 1, 83 (1993).
[13] P. A. Aleksandrov, E. K. Baranova, A. E. Gorodetskiĭ, K. D. Demakov, O. G. Kutukova, and S. G. Shemardov, Fiz. Tekh. Poluprovodn. **22**, 731 (1988) [Sov. Phys. Semicond. **22**, 455 (1988)].
[14] S. L. Ellingboe and M. C. Ridgway, Mater. Sci. Eng., B **29**, 29 (1995).
[15] J. Takahashi and T. Makino, J. Appl. Phys. **63**, 87 (1988).
[16] H. Okumura, E. Sakuma, J. H. Lee, H. Mukaida, S. Misawa, K. Endo, and S. Yishida, J. Appl. Phys. **61**, 1134 (1987).
[17] Y. Sasaki, Y. Nishima, M. Sato, and K. Okumura, Phys. Rev. B **40**, 17 621 (1989).
[18] M. Yoshikawa, Mater. Sci. Forum **52&53**, 365 (1989).

Translated by P. Shelnitz

# Model of the redistribution of erbium during the solid-phase epitaxial crystallization of silicon

O. V. Aleksandrov, Yu. A. Nikolaev, and N. A. Sobolev

*A. F. Ioffe Physicotechnical Institute, Russian Academy of Sciences, 194021 St. Petersburg, Russia*
(Submitted April 22, 1998; accepted for publication April 27, 1998)
Fiz. Tekh. Poluprovodn. **32**, 1420–1423 (December 1998)

A quantitative model of the redistribution of rare-earth-ion impurities during the solid-phase epitaxial crystallization of Si layers amorphized by implantation is developed. The parameters of the model include the segregation coefficient $k$ and the width of the transition layer. The movement of the crystallization front toward the surface is accompanied by an increase in the segregation coefficient at a rate which can be characterized by the ratio of the thickness of the recrystallization layer to the width of the transition layer. The increase in $k$ is attributed to defect accumulation in the transition layer. In the case of a thin Er-containing amorphous layer, the segregation coefficient does not reach $k=1$, because the impurity is driven back toward the surface. In the case of a thicker Er-containing layer, the segregation coefficient exceeds $k=1$ and prevents the accumulation of impurity atoms near the surface. © *1998 American Institute of Physics.* [S1063-7826(98)00312-3]

The fabrication of light-emitting structures from rare-earth-doped silicon is of current interest.[1] The implantation of rare-earth (RE) ions at doses exceeding the amorphization dose followed by an anneal, during which restoration of the crystal structure takes place according to the mechanism of solid-phase epitaxy (SPE) is employed to raise the concentration of optically active centers.[2,3] The SPE process is accompanied by redistribution of the implanted impurity as a consequence of the segregation and trapping processes occurring on the moving single-crystal/amorphous-layer ($c/a$) interface. The character of this redistribution depends on the implantation conditions (energy, dose, temperature, and target orientation) and the annealing conditions (energy supply method, temperature, and duration) but is determined primarily by the type of impurity.[3,4] Slowly diffusing dopants with a high solubility in single-crystal silicon, such as B, P, As, and Sb, scarcely undergo redistribution, and the segregation coefficient $k\approx 1$. Rapidly diffusing transition-metal impurities with a low solubility in $c$-Si, such as Au, Ag, and Cu, are characterized by driving of the impurity back ($k\ll 1$) with the formation of a concentration peak in the amorphous phase ahead of the crystallization front, which leads to termination of the SPE process at high concentrations. A different type of behavior is observed for In and Ga impurities, which are completely trapped in Si at low concentrations ($k\approx 1$) and form narrow segregation peaks that move together with the crystallization front toward the crystal surface at large concentrations ($k<1$). A further increase in concentration can be accompanied by liquid-phase crystallization.

The behavior of impurities of the rare-earth elements Er and Pr in Si differs significantly from that of the impurities cited above.[4,5] At small amorphizing implantation doses only a small part of the impurity passes into the crystal ($k\ll 1$). At higher doses the crystallization process is characterized by enhancement of the trapping of Er by the recrystallized layer ($k$ increases from 0.01 to 0.2) accompanied by accumulation of the impurity near the surface. Finally, at implantation doses at which the concentration of Er trapped by the recrystallized layer exceeds a certain critical value, termination of the SPE crystallization process with twin formation takes place.[6] This critical value decreases with annealing temperature from $1.2\times 10^{20}$ cm$^{-3}$ at 600 °C to $6\times 10^{19}$ cm$^{-3}$ at 900 °C. Polman *et al.*[4,5] showed that the increase in the segregation coefficient of Er with increasing implantation dose is not associated with variation of the SPE crystallization rate. This allowed us to conclude that segregation is controlled by equilibrium thermodynamic processes, rather than by kinetic trapping. Within the qualitative phenomenological model that they proposed, the variation of $k$ is attributed to the presence of traps for RE ions in $a$-Si. An abrupt change in $k$ occurs when the traps are filled. At this point the amount of impurity in the concentration peak becomes higher than $6\times 10^{13}$ cm$^{-2}$, which corresponds to a volume density equal to $3\times 10^{20}$ cm$^{-3}$. The proposed model does not provide an explanation for the results of the experiments in Refs. 7–9, in which there was no accumulation of Er near the surface.

The purpose of the present work is to develop a quantitative model of the segregation of rare-earth-ion impurities during the SPE crystallization of amorphized silicon layers.

The SPE crystallization of amorphized silicon is observed already at fairly low annealing temperatures (450 − 500 °C), at which the diffusion processes in both the crystal and the amorphous layer are negligibly weak. According to the current ideas regarding the mechanism of SPE,[2,3] the SPE crystallization rate is limited by the diffusion of matrix atoms in a thin transition layer, in which the amorphous phase transforms into the crystalline phase. It was shown in Refs. 4 and 5 that the diffusion coefficient of Er impurity ions is more than three orders of magnitude higher in the

 

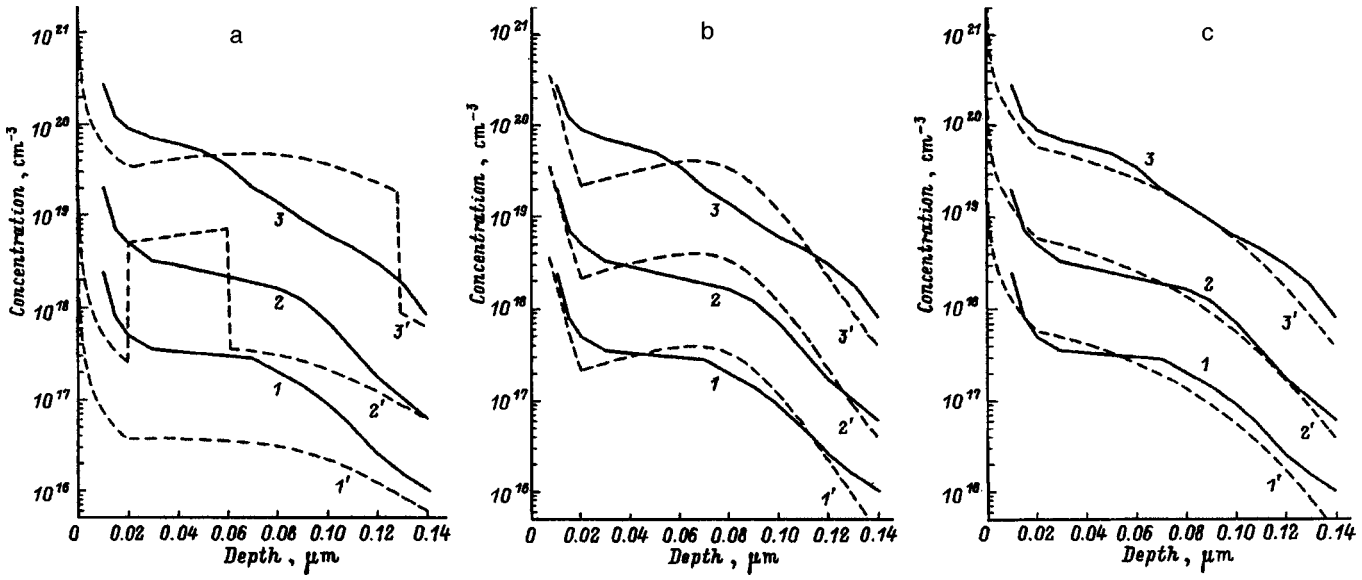


FIG. 1. Concentration profiles of Er in Si(100) after ion implantation at $E=250$ keV and annealing (600 °C, 15 min). Curves *1–3* (in a–c) — experiment in Ref. 5, implantation dose, cm$^{-2}$: *1* — $7\times10^{12}$, *2* — $7\times10^{13}$, *3* — $7\times10^{14}$; curves *1′–3′* — calculation: a — $k=k(Q)$; b — $k=k(C)$ for $C_i=1\times10^{18}$ cm$^{-3}$ (*1′*), $1\times10^{19}$ cm$^{-3}$ (*2′*), and $1\times10^{20}$ cm$^{-3}$ (*3′*); c — $k=k(x)$ for $k_0=0.01$, $k_s=2.5$, and $L=80$ nm.

*a*-Si layer with a thickness of about 10 nm near the SPE crystallization front than in the remainder of the amorphous layer. We suggest that this transition layer can be regarded as an analog of the molten zone in the case of liquid-phase crystallization, where the diffusion coefficient of an impurity is much higher in the liquid phase than in the solid phase. However, the known equations of the theory of liquid-phase crystallization[10,11] cannot be used to describe SPE, since the segregation coefficient varies during motion of the SPE crystallization front. The inhomogeneous initial distribution of the impurity after ion implantation must also be taken into account.

The variation of the concentration of the impurity in the transition layer $C_a(y)$ during SPE crystallization is determined from the detailed balance of the impurity between the transition layer, the amorphous phase, and the crystalline phase and is described by the differential equation

$$dC_a(y)/dy=(C_0(y)-kC_a(y))/L, \tag{1}$$

where $y=x_a-x$ is the current thickness of the recrystallized layer measured from the initial boundary of the amorphous layer $x_a$, $x$ is the current coordinate measured from the sample surface, $C_0(y)$ is the initial distribution of the impurity in the amorphous layer before recrystallization, and $L$ is the width of the transition layer. The boundary condition for Eq. (1) has the form

$$C_a(0)=\left[\int_0^L C_0(y)\,dy\right]\Big/ L. \tag{2}$$

Equation (1) is valid at $x\geqslant L$. When the crystallization front approaches the surface to within a distance equal to the width of the transition layer $L$, zone crystallization gives way to directed crystallization. The variation of the impurity concentration in the transition layer at $x\leqslant L$ is described in this case by the equation

$$dC_a(z)/dz=(1-k)C_a(z)/(L-z), \tag{3}$$

where $z=L-x$ is the current thickness of the recrystallized layer measured from a point at a distance $x=L$ from the surface. The boundary condition for Eq. (3) is the solution of Eq. (1) for $x=L$:

$$C_a(0)=C_a(x_a-L). \tag{4}$$

In both crystallization variants segregation is assumed to be an equilibrium process, and the concentration of the impurity in the recrystallized layer is defined as

$$C(x)=kC_a(x). \tag{5}$$

The problem (1)–(5) with the segregation coefficient $k$, which varies during movement of the SPE crystallization front, was solved numerically by a finite-difference method.

The experimental results of Ref. 5 were analyzed. In that study Er ions with an energy $E=250$ keV were implanted at various doses in an amorphized silicon layer of thickness $x_a=0.35\,\mu$m, which was created by the preliminary implantation of $Si^+$ ions. In the calculations the original distribution profile of Er was described by a Gaussian distribution with the parameters $R_p=0.102\,\mu$m and $\Delta R_p=0.027\,\mu$m.[12] The concentration profiles were calculated for a segregation coefficient specified in accordance with the phenomenological model in Refs. 4 and 5 by the amount of the impurity in the transition layer ahead of the crystallization front: $k=0.01$ when $Q_a<Q_i$, and $k=0.2$ when $Q_a\geqslant Q_i$, where $Q_i=6\times10^{13}$ cm$^{-2}$. As can be seen from Fig. 1a, calculated curves *1′–3′* give a very rough approximation of experimental distributions *1–3*.

Various monotonic dependences of the segregation coefficient on the impurity concentration in the transition layer, viz., linear, power-law, and exponential dependences, were

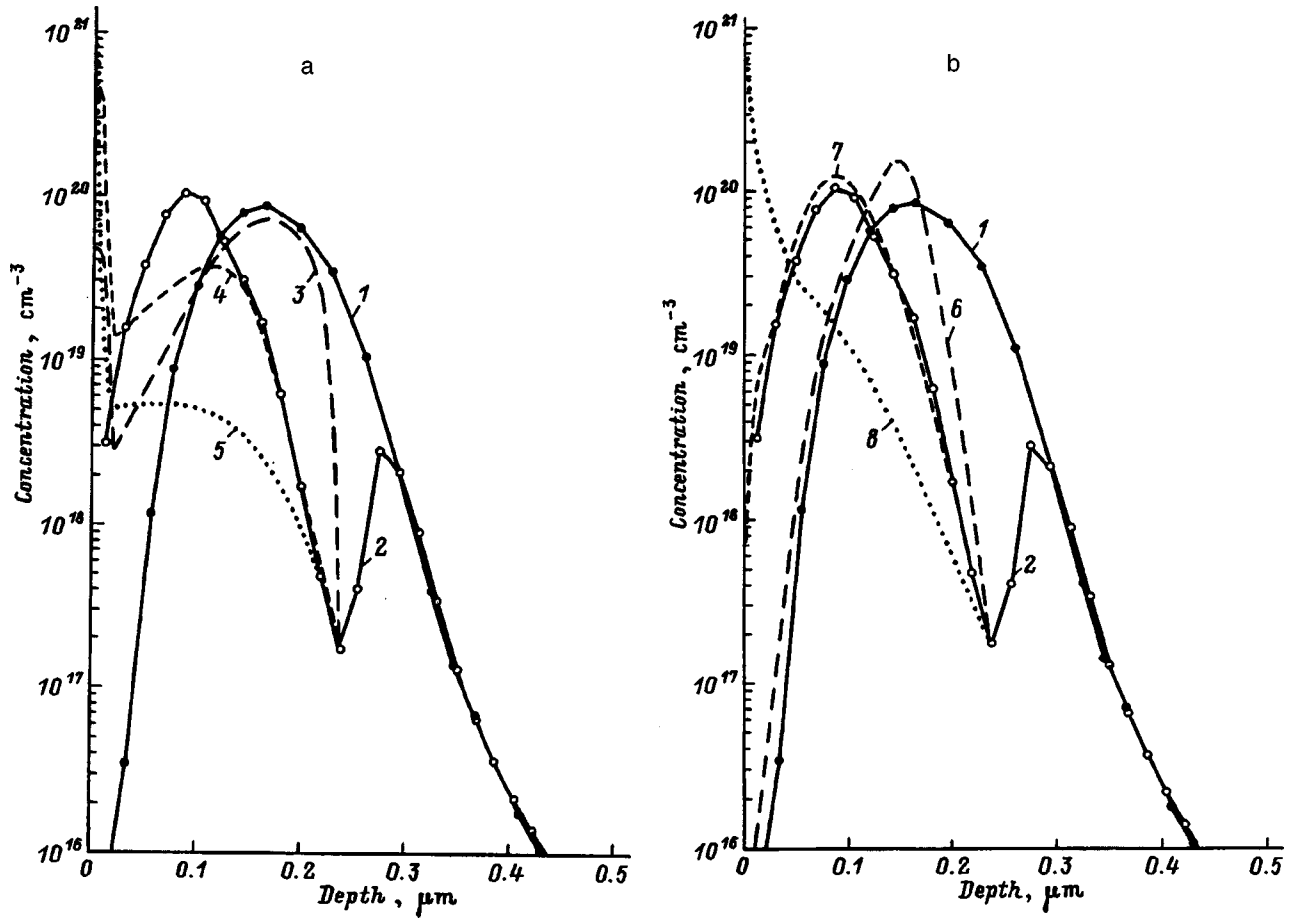


FIG. 2. Concentration profiles of Er in Si(100) after ion implantation at $E=500$ keV and a dose $Q=8\times10^{14}$ cm$^{-2}$ before (*1*) and after (*2*) annealing. *1, 2* — experiment in Ref. 9; *3–5* — calculation with $k=k(C)$ for $C_i=1\times10^{19}$ cm$^{-3}$ (*3*), $1\times10^{20}$ cm$^{-3}$ (*4*), and $1\times10^{21}$ cm$^{-3}$ (*5*); *6–8* — calculation with $k=k(x)$ for $k_0=0.005$, $k_s=2.5$, and various values of $L$, nm: *6* — 15, *7* — 27, *8* — 50.

tested as possibilities for the next approximation instead of the stepwise form of $k(Q_a)$. The best dependence had the form

$$k(C_a)=k_0\exp(C_a/C_i), \tag{6}$$

where $k_0$ is the initial value of the segregation coefficient at $x=x_a$, $k_0=0.01$, and $C_i$ is the impurity concentration near which the increase in the segregation coefficient begins ($C_i=Q_i/L$). The values of $C_i$ were selected so as to achieve the most satisfactory agreement between the calculation and experimental curves *1–3* and, as is important, were different for different implantation doses (Fig. 1b, curves *1′–3′*).

The dependence (6) was also used to simulate the concentration profiles of Er implanted in silicon at $E=500$ keV (the dose was $8\times10^{14}$ cm$^{-2}$, and $x_a=0.235$ $\mu$m) after an anneal (620 °C, 1 h) from Ref. 9. Figure 2a presents the experimental and calculated concentration profiles of Er for various values of $C_i$. As is seen from the figure, satisfactory agreement with the experimental profile is achieved only in the initial stage of SPE crystallization for $C_i=1\times10^{20}$ cm$^{-3}$. A concentration peak, which is not observed experimentally, forms near the surface at all values of $C_i$. The appearance of a near-surface concentration peak in this case is a consequence of the decrease in the impurity concentration in the transition layer and, accordingly, of the decrease in the concentration-dependent segregation coefficient to $k<1$ as the SPE crystallization front approaches the surface. Thus, the concentration dependence of the segregation coefficient does not permit a satisfactory description of the experimental concentration profiles of Er in Si after crystallization of the implanted layer. This is manifested by the absence of either $Q_i$ or $C_i$ for different implantation doses at $E=250$ keV (Figs. 1a and 1b), by the appearance of a false near-surface concentration peak for $E=500$ keV (Fig. 2a), and by the considerable deviation of the calculated distributions from the experimental curves.

An alternative possibility for describing the $C(x)$ profiles in the recrystallized layer is the coordinate dependence of the segregation coefficient $k=k(x)$. Various forms of $k(x)$ were tested, and the best dependence had the form

$$k(x)=k_0k_s/[k_0+(k_s-k_0)\exp(-(x_a-x)/L)], \tag{7}$$

where $k_s$ is the maximum value of the segregation coefficient.

The results of the calculation of the concentration profiles in the recrystallized layer with $k=k(x)$ of the form (7) for various values of $L$ and the experimental conditions in Ref. 9 are shown in Fig. 2b (curves *6–8*). A comparison of the calculated and experimental curves reveals that the best fit is achieved for the parameter values $k_0=0.005$, $k_s=2.5$,

and $L=27$ nm. Concentration profiles calculated for $k=k(x)$ defined by (7) for the experimental conditions in Ref. 5 and various implantation doses are plotted in Fig. 1c (curves $1'-3'$). The calculated curves for $k_0=0.01$, $k_s=2.5$, and $L=80$ nm are in satisfactory agreement with the experimental plots, i.e., if the initial thickness of the amorphized layer is fixed, the width of the transition layer $L$ does not depend on the dose of the implanted impurity. The experimental concentration profiles of Er in silicon layers after implantation at 250 and 500 keV and SPE crystallization at 600 and 620 °C, respectively, are described satisfactorily by a model with the coordinate dependence $k(x)$ of the form (7). The values of the segregation coefficient increase as the crystallization front advances. In the case of a thin Er-containing *a*-Si layer ($E=250$ keV) the maximum value of the segregation coefficient does not reach $k=1$. This accounts for the accumulation of Er near the surface (Fig. 1). In the case of a thick Er-containing *a*-Si layer ($E=500$ keV) the segregation coefficient becomes greater than unity. Such unusually high values of $k$ cause a decrease in the concentration of Er near the surface (Fig. 2). The cause of the increase in $k$ may be defect accumulation in the transition layer, which promote the trapping of RE ions by the epitaxially recrystallized single-crystal layer. Such defects can be either structural defects or atoms of residual impurities such as oxygen and carbon atoms. In particular, it was shown in Ref. 5 that the additional introduction of oxygen atoms leads to an increase in the trapping of Er in the recrystallized silicon layer.

Thus, a quantitative model of the redistribution of rare-earth-ion impurities during the SPE crystallization of a silicon layer amorphized by ion implantation has been developed. The model satisfactorily describes the experimental concentration profiles of an impurity if the segregation coefficient increases as the crystallization front advances toward the surface. The increase in $k$ can be caused by the accumulation of defects that promote the trapping of RE atoms in the silicon transition layer.

We thank A. V. Shestakov for performing the implantation and Yu. A. Kudryavtsev for measuring the concentration profiles.

This work was partially supported by the International Science and Technology Center (ISTC, Grant 168), the U.S. Civilian Research and Development Foundation for the Independent States of the Former Soviet Union (CRDF, Grant 235), and the Russian Fund for Fundamental Research (Grant 96-02-17901).

[1] N. A. Sobolev, Fiz. Tekh. Poluprovodn. **29**, 1153 (1995) [Semiconductors **29**, 595 (1995)].
[2] A. F. Vyatkin, Poverkhnost' No. 4, 5 (1991).
[3] G. L. Olson and J. A. Roth, in *Handbook of Crystal Growth, Vol. 3: Thin Films and Epitaxy*, edited by D. T. J. Hurle (Elsevier, Amsterdam–New York, 1994), p. 257.
[4] J. S. Custer, A. Polman, and H. M. van Pinxteren, J. Appl. Phys. **75**, 2809 (1994).
[5] A. Polman, J. S. Custer, P. M. Zagwijn, A. M. Molenbroek, and P. F. A. Alkemade, J. Appl. Phys. **81**, 150 (1997).
[6] A. Polman, J. S. Custer, E. Snoeks, and G. N. van den Hoven, Appl. Phys. Lett. **62**, 507 (1993).
[7] D. Moutonnet, H. L'Haridon, P. N. Favennec, M. Salvi, and M. Gauneau, Mater. Sci. Eng., B **4**, 75 (1989).
[8] W. P. Gillin, Zhang Jingping, and B. J. Sealy, Solid State Commun. **77**, 907 (1991).
[9] N. A. Sobolev, A. M. Emel'yanov, Yu. A. Kudryavtsev, R. N. Kyutt, M. I. Makovijchuk, Yu. A. Nikolaev, E. O. Parshin, V. I. Sakharov, I. T. Serenkov, E. I. Shek, and K. F. Shtel'makh, Solid State Phenom. **57–58**, 213 (1997).
[10] W. R. Runyan, *Silicon Semiconductor Technology* (McGraw-Hill, New York, 1965; Metallurgiya, Moscow, 1969).
[11] Yu. M. Tairov and V. F. Tsvetkov, *Technology of Semiconductor and Insulating Materials* [in Russian], Vysshaya Shkola, Moscow (1990).
[12] A. F. Burenkov, F. F. Komarov, M. A. Kumakhov, and M. M. Temkin, *Spatial Distributions of Energy Released in Atomic Collision Cascades in Solids* [in Russian], Énergoatomizdat, Moscow (1985).

Translated by P. Shelnitz

## ELECTRONIC AND OPTICAL PROPERTIES OF SEMICONDUCTORS

# Density-of-states anomaly and tunneling conductance of Au/*p*-$GaAs_{0.94}Sb_{0.06}$ contacts near the metal–insulator transition

T. Yu. Allen, Kh. G. Nazhmudinov, and T. A. Polyanskaya

*A. F. Ioffe Physicotechnical Institute, Russian Academy of Sciences, 194021 St. Petersburg, Russia*
(Submitted July 1, 1998; accepted for publication July 1, 1998)
Fiz. Tekh. Poluprovodn. **32**, 1424–1431 (December 1998)

The tunneling-current anomaly in Au/*p*-$GaAs_{0.94}Sb_{0.06}$ contacts at zero bias voltage ($V\to 0$) is investigated. Epitaxial layers of the solid solution $GaAs_{0.94}Sb_{0.06}$ are doped with germanium and have a conductivity close to that at the metal-insulator transition. The square-root dependence of the differential conductance $G(V)=(dV/dI)^{-1}$ at small values of $eV>kT$ TT predicted by the Al'tshuler–Aronov theory of quantum corrections to the density of states at the Fermi level in disordered conductors is observed. Satisfactory agreement between the experimental data and theory is observed at hole densities ($p$) in the layers greater than the critical density for the metal-insulator transition $p_c$, but the relative magnitude of the anomaly is sharply smaller at $p<p_c$. This confirms the specificity of the condition $k_F l\geqslant 1$ (instead of $k_F l\gg 1$) for applicability of the theory for the density-of-states anomaly appearing as a result of electron-electron interactions in a three dimensional electron gas.
 [S1063-7826(98)00412-8]

### 1. INTRODUCTION

An investigation of the tunneling conductance of a contact with a metal provides a direct measure of the density of states of the electron gas in the material in the barrier contact with the metal. Tunneling-current anomalies at zero bias voltage ($V\to 0$) were observed experimentally long ago in various types of barrier structures and reported in numerous publications.[1] However, despite the availability of complete experimental facts, a satisfactorily convincing theoretical explanation was not provided for this effect for a long time (see, for example, Chap. 27 in Ref. 1). The development of the theory of Fermi liquids for disordered systems of charge carriers[2–4] permitted reevaluation of many previously known experimental data on low-temperature phenomena in disordered conductors, including the tunneling-current anomaly at $V\to 0$. It was shown that the wave functions of electrons of similar energy are strongly correlated in space in such systems.[5] The diffusion of electron-density fluctuations in a field of lattice defects leads to significant enhancement of the electron-electron ($ee$) interaction.[1)] As a result, a singularity $\delta\nu$ in the single-particle density of states appears at the Fermi level $\nu_F=(m_\nu^* k_F/\pi\hbar^2)$, where $k_F$ is the wave vector of a charge carrier with the Fermi energy. The correction to the density of states at $T\to 0$ has the form (see, for example, Ref. 3, p. 29):

$$\delta\nu=\frac{\lambda_\nu|\varepsilon|^{1/2}}{4\sqrt{2}\,\pi^2(\hbar D)^{3/2}}. \tag{1}$$

Here $\lambda_\nu$ is a constant, which is determined by the character of the $ee$ interaction,[3,4] $\varepsilon\ll\hbar/\tau$ is the quasiparticle energy measured from the Fermi level $\varepsilon_F$, $\tau$ is the momentum relaxation time,

$$D=\frac{\sigma}{e^2(dp/d\varepsilon_F)} \tag{2}$$

is the diffusion coefficient, $\sigma$ is the conductivity, $p$ is the charge-carrier concentration, and $dp/d\varepsilon_F=\nu_F$.

For our investigations it is important that the theory of the density-of-states anomaly for a three-dimensional conductor is valid even if

$$\hbar/\tau\leqslant\varepsilon_F \tag{3}$$

(see Ref. 3, p. 31), while the ordinary condition for the applicability of theories of quantum corrections is

$$k_F l=2\varepsilon_F\tau/\hbar\gg 1. \tag{3a}$$

The condition (3) permits the analysis of data obtained near the metal-insulator transition on the metal side. When the interaction in the diffusive channel of $ee$ interactions is taken into account, $\lambda_\nu$ is a sum of two terms:

$$\lambda_\nu=\lambda_\nu^{(j=0)}+\frac{3}{2}\lambda_\nu^{(j=1)}. \tag{4}$$

The first of them is always equal to

$$\lambda_\nu^{(j=0)}=2$$

and describes the interaction of quasiparticles with a total spin $j=0$. The second term

 

$$\lambda_\nu^{(j=1)} = -4\left( \sqrt{1+\frac{F}{2}} - 1 \right) \tag{5}$$

corresponds to the interaction of quasiparticles with a total spin $j=1$. Here $F$ is the amplitude of the $ee$ interaction and can vary as a function of the band structure, the presence of paramagnetic impurities, the occurrence of interactions with phonons, etc. In the three-dimensional case this quantity can be defined in terms of $y=2k_F R_S$ as[3]

$$F = \frac{\ln(1+y^2)}{y^2}. \tag{6}$$

Here $R_S$ is the screening radius:

$$R_S = \frac{\chi}{4\pi e^2 (dp/d\varepsilon_F)}, \tag{7}$$

where $\chi$ is the dielectric constant.

The singularity in the density of states (1) leads to an anomaly in the tunneling conductance $G(V)=dI/dV$ (at small values of the bias voltage $V$) relative to the value determined by the ordinary density of states $\nu_F$. As a result, the quantity $\Delta G(V)=G(V)-G(0)$ equals

$$\frac{\Delta G(V)}{G(0)} = \frac{1}{4kT}\int_{-\infty}^{\infty} d\varepsilon \, \frac{\delta\nu(\varepsilon,T)}{\nu_0} \times \left( \frac{1}{\cosh^2 \dfrac{\varepsilon - eV}{2kT}} + \frac{1}{\cosh^2 \dfrac{\varepsilon + eV}{2kT}} \right),$$

i.e., it varies proportionally to $(eV/kT)^2$ when $|eV| \ll kT$, and it takes the following form[5] when $|eV| \gg kT$:

$$\frac{\Delta G(V)}{G(0)} = \frac{\delta\nu(|\varepsilon \cong eV|)}{\nu_F} = \frac{\lambda_\nu |eV|^{1/2}}{4\sqrt{2}\pi^2 (\hbar D)^{3/2} \nu_F}. \tag{8}$$

The theory of the tunneling anomaly[5] was tested on contacts of metals with films of granular Al (Ref. 7) and Ga (Ref. 8), with both three-dimensional and quasi-two-dimensional $In_2O_3$ films,[9] and with films of $Ga_{1-x}Au_x$ (Ref. 10) and $Nb_xSi_{1-x}$ (Ref. 11) solid solutions. Some studies[7,11] were performed in the vicinity of the metal-insulator transition. In all cases, in accordance with (8), a square-root dependence of the tunneling conductance $\Delta G$ on the bias voltage $V$ was observed, the proportionality coefficient

$$\alpha = \frac{\Delta G(V)}{G(0)|V|^{1/2}} \propto \lambda_\nu \sqrt{\rho^3 \nu_F} \tag{9}$$

depended on the resistivity of the film as $\rho^\eta$. It is noteworthy that in metals $\nu_F$ scarcely changes in response to the introduction of impurities or defects, whose presence influences only $\tau$, i.e., $\rho$, but not the carrier concentration. In this case we should have $\eta = 3/2$, but $\eta \cong 1$ was obtained in the experimental studies in which the dependence of $\alpha$ on $\rho$ was determined.[7,11]

Heavily doped superconductors have metallic conduction when $\varepsilon_F \gg kT$, and it should be expected that the tunneling anomaly for a Schottky barrier on a heavily doped semiconductor is of the same nature. There have been several experimental studies of the tunneling differential conductance of Schottky barriers fabricated (before the theory of quantum corrections appeared) on a fairly close analog of our material, viz., *p*-type GaAs (see, for example, Refs. 12–16). For example, performing measurements on GaAs doped with Zn and Cd (Pd served as the electrode), Mora *et al.*[12] discovered that the magnitude of the tunneling anomaly increases rapidly with increasing resistivity of *p*-GaAs and that its full width at half-maximum has a minimum in the vicinity of the metal-insulator transition (they used the position of this minimum to estimate the critical hole density at the transition point $p_c \cong 2\times 10^{18}$ cm$^{-3}$). In Refs. 13 and 16 the differential conductance of Au/*p*-GaAs Schottky barriers was analyzed for the purpose of determining the ''density-of-states tails'' in accordance with the theory in Ref. 6.

In Ref. 17 we reported the results of an investigation of the differential resistance of Au/*p*-$GaAs_{1-x}Sb_x$ structures fabricated on conducting *p*-GaAs substrates. We observed a square-root dependence of the tunneling conductance on voltage at $V \to 0$, but we were unable to measure the resistivity of the layer on which the Schottky barrier was fabricated in order to analyze $\alpha(\rho)$ in the form (9). Therefore, we made another attempt to test the theory in Ref. 5 on Au/*p*-$GaAs_{0.94}Sb_{0.06}$ Schottky barriers, setting up the experiment so that the value of the resistivity of the $GaAs_{0.94}Sb_{0.06}\langle Ge\rangle$ layer would be known.

## 2. EXPERIMENTAL METHOD AND DISCUSSION

Unlike the investigations described in Ref. 17 for Au/*p*-$GaAs_{1-x}Sb_x$ ($0.02 < x < 0.125$) contacts, in the present work the $GaAs_{0.94}Sb_{0.06}$ layers were grown in two variants simultaneously [in one technological experiment: on substrates of semiconducting GaAs to measure the resistivity $\rho$ and on *p*-GaAs substrates with a hole density $(0.5-1)\times 10^{19}$ cm$^{-3}$ to measure the tunneling conductance]. The methods for preparing $GaAs_{1-x}Sb_x$ epilayers doped with Ge (from 0.5 to 2 wt. %) were described in detail in Ref. 17, and the method for creating Schottky barriers was described in Ref. 18. In the present work, as in Ref. 17, we used Au/$GaAs_{0.94}Sb_{0.06}$ contacts with a diameter $\varnothing = 0.25$ mm. According to estimates made on our structures,[19] the thickness of the layer of the native oxide separating the Au film and the layer of the solid solution did not exceed 30 Å. The results of an investigation of the barrier height $\varphi_b$ in Au/$GaAs_{1-x}Sb_x$ structures ($0.02 < x < 0.125$) for layers with both *n*- and *p*-type conduction (based on the spectral dependence of the photoresponse) were presented in Ref. 20, and the results of a study of the electrophysical properties and low-temperature galvanomagnetic effects in *p*-$GaAs_{0.94}Sb_{0.06}$ were presented in Refs. 21–23.

The zero-bias anomalies in the tunneling conductance were investigated at helium temperature. When the temperature was raised, the form of the differential resistance curve changed, and the anomaly became less pronounced, vanishing entirely at $T \geqslant 60$ K.[18] The tunneling anomalies were measured on samples with a hole density equal to $(2-5)\times 10^{18}$ cm$^{-3}$, i.e., samples close to the metal-insulator tran-

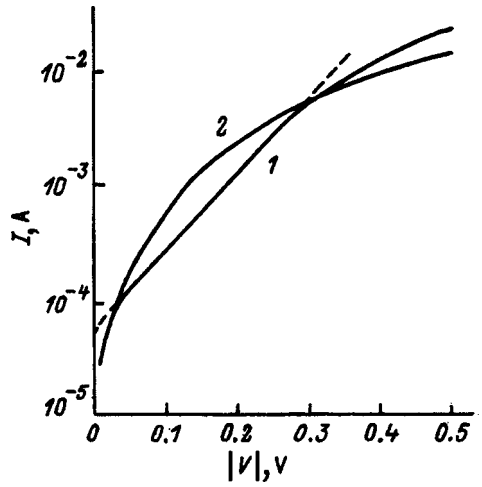


FIG. 1. Typical current-voltage characteristic of a Au/$p$-$GaAs_{1-x}Sb_x$ tunnel contact at $T=4.2$ K. Applied voltage: *1* — $V>0$, *2* — $V<0$. The dashed straight line denotes a segment of the plot of $I/I_0=\exp(eV/E_{00})$.

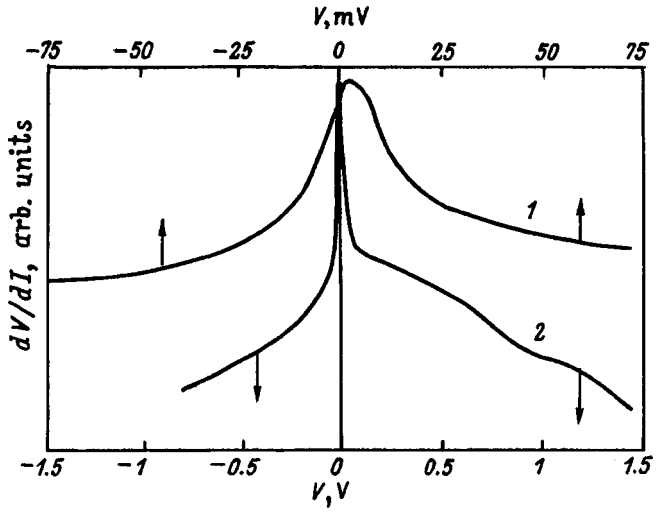


FIG. 3. Dependence of the differential resistance $R(V)$ on the bias voltage $V$ at $T=4.2$ K for structure 1 (see Table I). The values of $V$ for curve *1* correspond to the upper scale, and the values for curve *2* correspond to the lower scale.

sition. At hole densities less than $2\times10^{18}$ cm$^{-3}$ the resistance of the tunnel contact was so high that we were unable to measure its differential resistance.

Figure 1 shows a typical current-voltage characteristic (IVC) of the contacts investigated at $T=4.2$ K. It is seen that inversion of the IVC (greater values for the reverse currents than for the forward currents) occurs at voltages less than 0.15 V in accordance with Wilson's theory.[24] The forward branch of the IVC at large bias voltages obeys the dependence characteristic of a tunneling current[25]

$$I/I_0\propto\exp(eV/E_{00}), \tag{10}$$

where

$$E_{00}=\frac{\hbar}{2}\left[\frac{e^2(N_A-N_D)}{\chi m_{lh}^*}\right]^{1/2}, \tag{11}$$

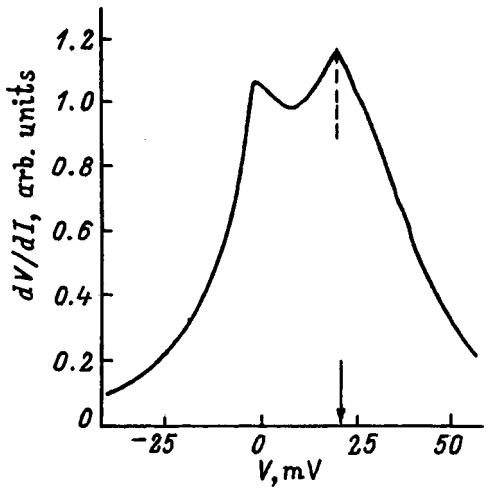


FIG. 2. Dependence of the differential resistance $R(V)=dV/dI$ on the bias voltage $V$ at $T=4.2$ K for the same contact as in Fig. 1. The arrow points to the voltage $V_{max}$ corresponding to the differential resistance maximum on the forward branch of the current-voltage characteristic.

$\chi=13$ is the dielectric constant of $GaAs_{0.94}Sb_{0.06}$ (the method for estimating $\chi$ was described in Ref. 23), and $m_{lh}^*=0.082m_0$ is the light-hole mass, since tunneling occurs from that band. The slope of the dashed straight line in Fig. 1 gives $E_{00}\cong41$ meV. A calculation using formula (11) gives $E_{00}\cong40.2$ meV if

$$N_A-N_D\cong p_r(T=295\ \text{K})=1/eR_H=5\times10^{18}\ \text{cm}^{-3}, \tag{12}$$

where $R_H$ is the Hall coefficient in a magnetic field $H\to0$ at $T=295$ K.

Figure 2 presents the dependence of the differential resistance on applied bias voltage $R(V)=dV/dI=1/G(V)$ for the same sample at $T=4.2$ K. Both the peak on the $R(V)$ curve at $V\to0$ (the zero-bias anomaly) and the maximum of $R(V)$ at the bias voltage $V=V_{max}\cong23$ meV are clearly seen.

Conley and Mahan[25] showed that the characteristic features of the $R(V)$ curves for any semiconductor, particularly the value of $eV_{max}$ (in comparison to $\varepsilon_F$) and the ''width'' of the $R(V)$ curve, i.e., the sharpness of the maximum $R(V_{max})$, are determined by the parameters $\varepsilon_F/E_{00}$ and $\varphi_b/E_g$. A fairly sharp peak can appear in the region of $R(V_{max})$ at $V_{max}=\varepsilon_F$, if the relations $\varphi_b/E_g\geqslant1/2$ and $\varepsilon_F/E_{00}<1$ hold for the specific material. If $\varphi_b/E_g\geqslant1/2$, but $\varepsilon_F/E_{00}\gg1$, a ''diffuse'' differential resistance maximum should be observed. Let us estimate these parameters for our structures. The gap width $E_g$ for $GaAs_{1-x}Sb_x$ at $T\leqslant77$ K varies from 1.52 to 1.3 eV in the composition range $0\leqslant x<0.13$, and $E_g\cong1.4$ eV when $x=0.06$. The barrier height $\varphi_{bp}$ for our structures on a $p$-type material equals $(0.82\pm0.06)$ eV at $T=77$ K.[20] As a result, $\varphi_{bp}/E_g\cong0.6$, and the ratio

$$\frac{\varepsilon_F}{E_{00}}=1.96\times10^{-4}\sqrt{\chi\left(\frac{m_{lh}^*m_0}{(m_v^*)^2}\right)(n[\text{cm}^{-3}])^{1/3}} \tag{13}$$

varies in the range from 0.4 to 0.6 as the hole density varies in the range $10^{18}<p<10^{19}$ cm$^{-3}$. The value for the density-of-states effective mass $m_v^*=0.473m_0$ and the value for the

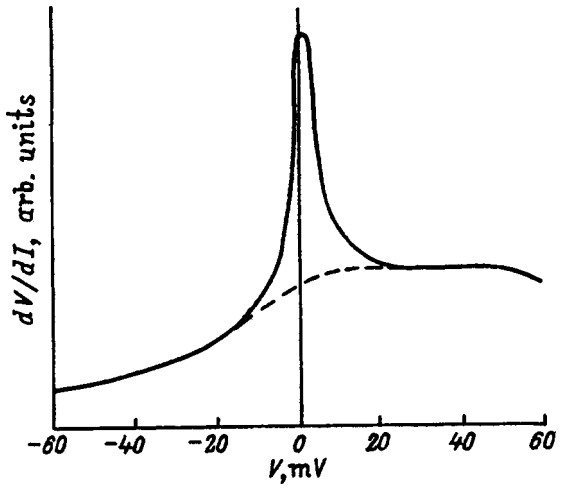


FIG. 4. Dependence of the differential resistance $R(V)$ on the bias voltage $V$ at $T=4.2$ K for structure 3 (see Table I). The dashed curve corresponds to $R_N(V)$, which is specified by the ''normal'' density of states.

light-hole mass $m_{lh}^*=0.082m_0$ were taken in (13). For $GaAs_{1-x}Sb_x$ with $n$-type conductivity $\varphi_{bn}/E_g\cong 0.7$ [$\varphi_{bh}\cong 1$ eV at 4.2 K (Ref. 20)], and the value of $\varepsilon_F/E_{00}$ is 2.5 times greater for the same carrier densities.

In accordance with these estimates, we observed a broad (diffuse) band on the $R(V)$ curve with a maximum at $V_{\max}=\varepsilon_F$ [with a weak surge in $R(V)$ at $V\to 0$] for contacts on a solid solution with $n$-type conduction.[18] The contacts on $p$-$GaAs_{1-x}Sb_x$ clearly display a peak at $V=V_{\max}$, and the value of $V_{\max}$ is, in fact, close to the values of $\varepsilon_F$ for $p\geqslant 5\times 10^{18}$ cm$^{-3}$, so that $V_{\max}\propto p^{2/3}$. The same phenomena were also noted in Ref. 16 for Au/$p$-GaAs contacts at $p>10^{19}$ cm$^{-3}$. As the hole density decreases and the metal-insulator transition is approached, the peak on the $R(V)$ curve at $V\to 0$ becomes increasingly sharp, and the amplitude of the zero-bias anomaly becomes comparable to or greater than $R(V_{\max})$, so that it is impossible to determine $V_{\max}$ (see Figs. 3–5 and Ref. 17).

TABLE I. Principal characteristics of epilayers of the solid solution $GaAs_{0.94}Sb_{0.06}$ doped with Ge.

| Sample | Ge content, at. % | Layer thickness, $\mu$m | $T=4.2$ K: $\rho$, $10^{-2}\Omega\cdot$cm | $T=295$ K: $p=1/eR_H$, $10^{18}$ cm$^{-3}$ |
|---|---|---|---|---|
| 1 | 0.5 | 18 | 14 | 2.3 |
| 2 | 0.5 | 19 | 7.6 | 2.6 |
| 5 | 0.65 | 20 | 6.5 | 2.8 |
| 3 | 0.7 | 20 | 4.7 | 3.4 |
| 4 | 0.75 | 26 | 6.8 | 2.7 |
| 6 | 0.85 | 24 | 4.4 | 3.7 |
| 7 | 1.0 | 14 | 3.6 | 4.2 |
| 8 | 2.0 | 16 | 2.6 | 5.0 |

Figures 3–5 show the $R(V)$ curves for a series of samples, whose parameters are listed in Table I, and Fig. 6 presents the relative amplitude of the anomaly relative to the ''background'' value $R_N(V\to 0)$:[2)]

$$A(V)=\frac{R(V)-R_N(V)}{R_N(0)}.$$

The background (relative to the anomaly) dependence $[R_N(V)]$ is associated with the ''normal'' density of states $\nu_F$ and was determined ''by sight'' (see the dashed line in Fig. 4). Because of the small width of the zero-bias anomaly in the samples investigated, determining $R_N(V)$ in this way should not introduce a large error. Figure 6 shows the features of $A(V)$ previously noted in Ref. 18, viz., the increase in $A$ with decreasing acceptor concentration and the ''asymmetry'' of the $A(V)$ curve, which stems from the displace-

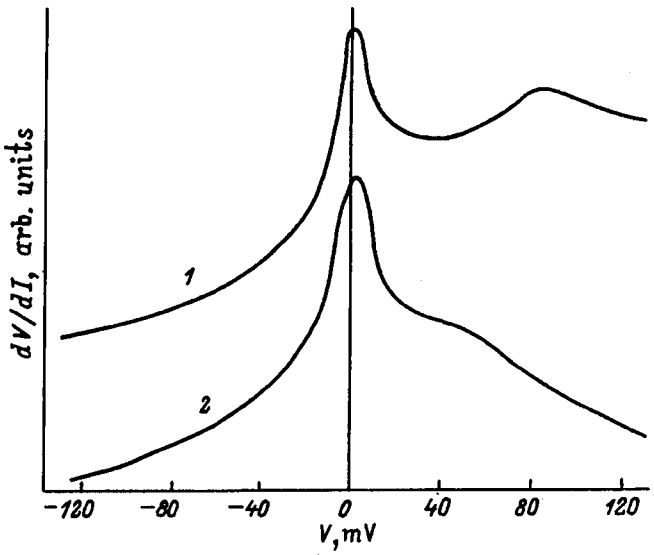


FIG. 5. Dependence of the differential resistance $R(V)$ on the bias voltage $V$ at $T=4.2$ K for structures 8 (curve *1*) and 7 (curve *2*). The numbers of the samples are the same as in Table I.

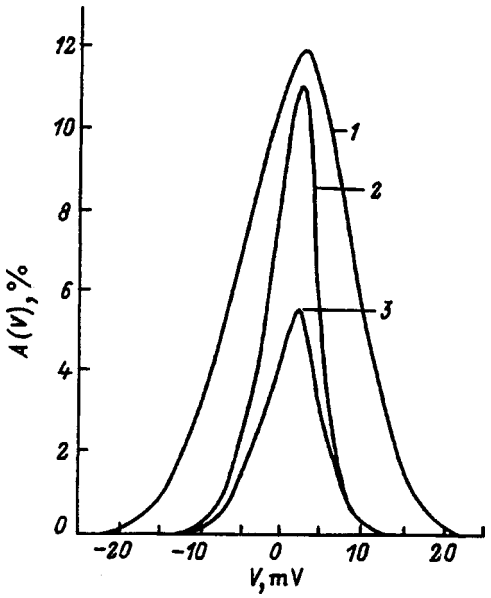


FIG. 6. Relative amplitude of the zero-bias anomaly extracted from the dependence of $R_N$ on $V$ specified by the ''normal'' density of states for contacts fabricated on $p$-$GaAs_{0.94}Sb_{0.06}$ layers with various Ge concentrations, at. %: *1* — 0.2, *2* — 1, *3* — 2.

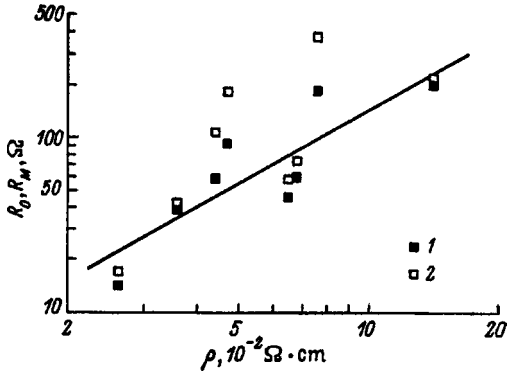


FIG. 7. Differential resistance $R(V)=(dI/dV)^{-1}$ at $V=0$ and $V=\delta V$ as a function of the resistivity of the $p$-$GaAs_{0.94}Sb_{0.06}$ layer at $T=4.2$ K: *1* — $R_0=R(V=0)$, *2* — $R_M=R(V=\delta V)$.

ment of the position of the maximum of $A(V)$ from $V=0$ toward forward biases by the small quantity $\delta V$. The values of $R_0 \equiv R(V=0)$ and $R_M \equiv R(\delta V)$ are plotted as functions of the resistivity $\rho$ at $T=4.2$ K in Fig. 7. If the large spread of the experimental data is taken into account, the distribution of $R_0=f(\rho)$ can be described by the power law

$$R_0 \propto \rho_0^m, \tag{14}$$

where $m=1.4\pm0.4$ (see the line in Fig. 7).

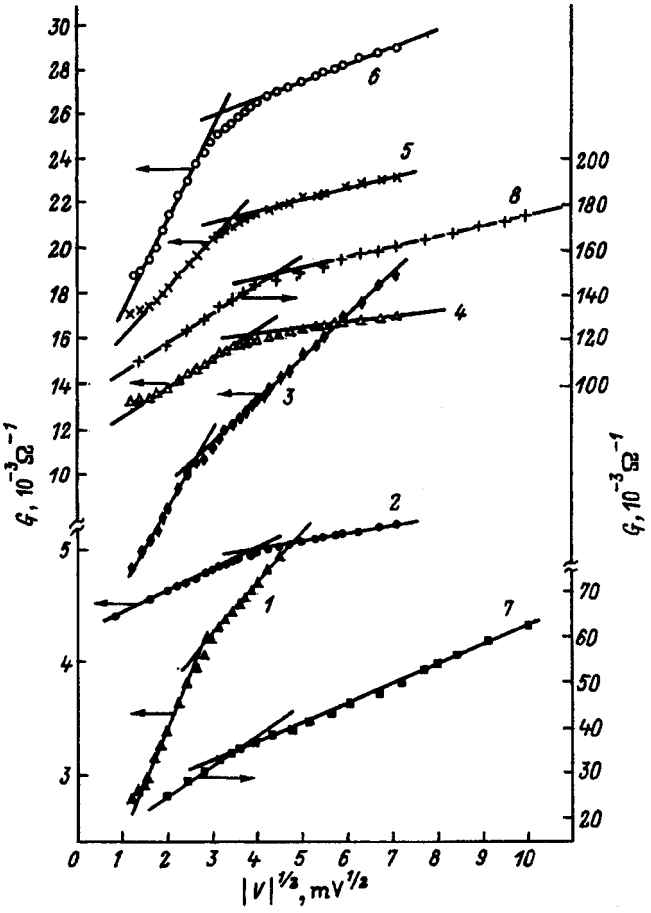


FIG. 8. Differential conductance $G=dI/dV$ under a reverse-bias voltage as a function of $\sqrt{|V|}$ at $T=4.2$ K. The numbers on the curves correspond to the numbers of the samples in Table I.

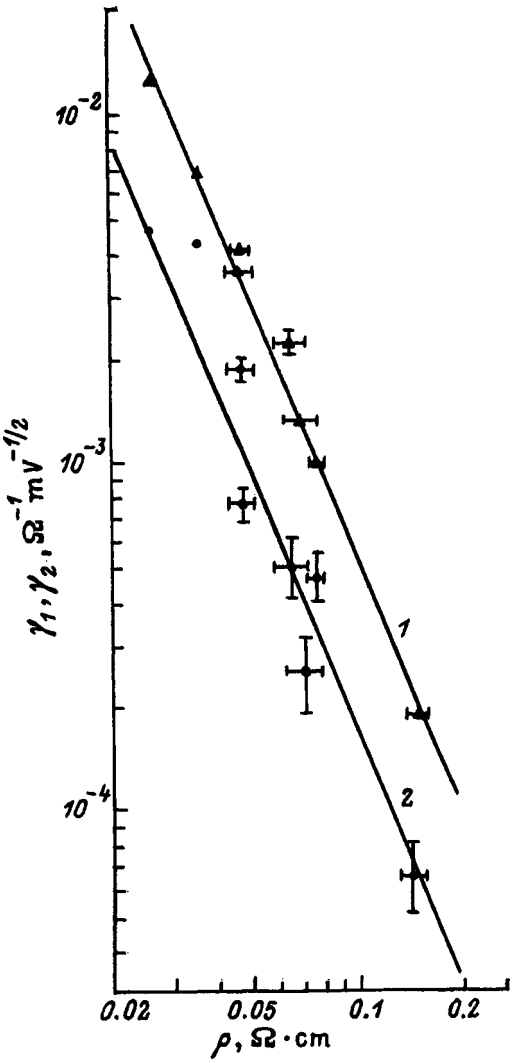


FIG. 9. Values of $\gamma_1$ (*1*) and $\gamma_2$ (*2*) [slopes of the linear segments of the $G(\sqrt{V})$ curves in Fig. 7] as functions of the resistivity of the $p$-$GaAs_{0.94}Sb_{0.06}$ layer at $T=4.2$ K.

Figure 8 presents plots of the differential conductance $G(V)=dI/dV$ as a function of $\sqrt{|V|}$ at small reverse-bias voltages for several samples. There are two segments with different slopes $\gamma_1$ and $\gamma_2$, which are defined as

$$\gamma=\alpha G(0)=\frac{\Delta G(V)}{|V|^{1/2}}.$$

The voltage corresponding to the change in slope was determined from the point of intersection of the straight lines and lies in the range from 7 to 19 mV. Plots of the dependence of $\gamma_1$ and $\gamma_2$ on the resistivity $\rho$ of the epilayers are shown in Fig. 9. Within the experimental error

$$\gamma_1, \gamma_2 \propto \rho^{-5/2}.$$

Let us now compare our experimental results with the theory in Ref. 5. Figure 10 presents the values of

$$\gamma_1 R_0=\frac{\Delta G(V)}{G(0)|V|^{1/2}}$$

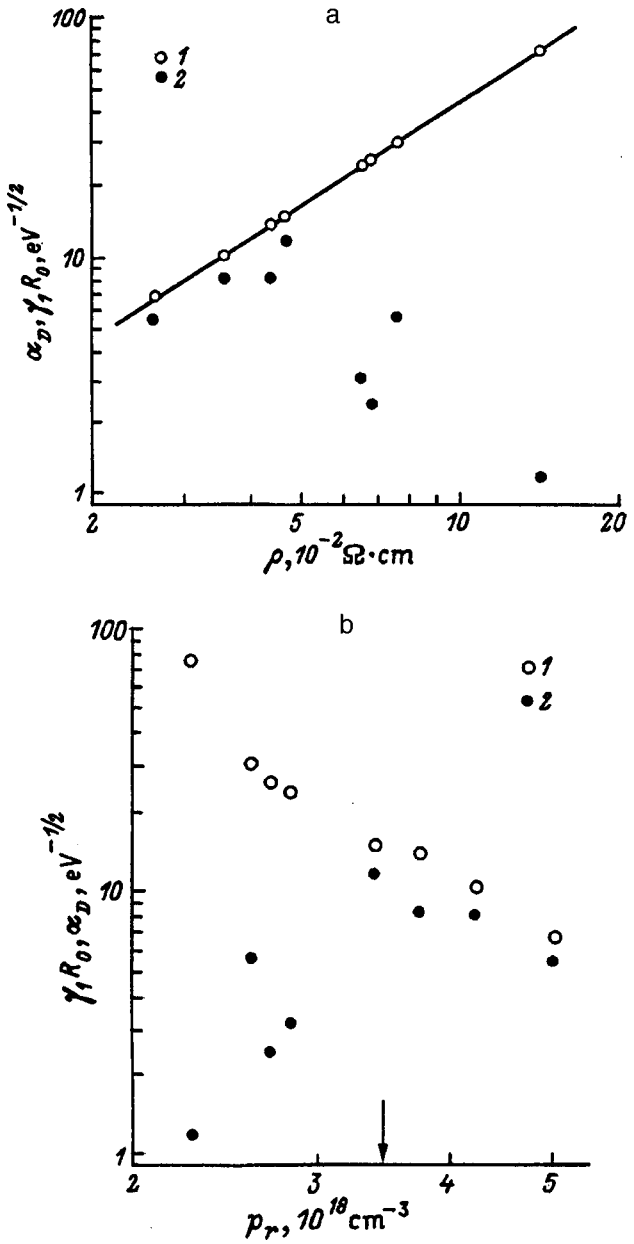


FIG. 10. Experimental values (*1*) of $\gamma_1 R_0 = (\Delta G(V)/\Delta(eV)^{1/2})/G(0)$ at $T = 4.2$ K and calculated values of $\alpha_D$ (*2*) as functions of the resistivity $\rho$ at $T = 4.2$ K (the straight line corresponds to $\alpha_D \sim \rho^{\eta}$, where $\eta = 1.43 \pm 0.01$) (a) and the carrier concentration $p_r \cong N_A - N_D$ measured at $T = 295$ K (b). The arrow points to the concentration corresponding to the metal-insulator transition.

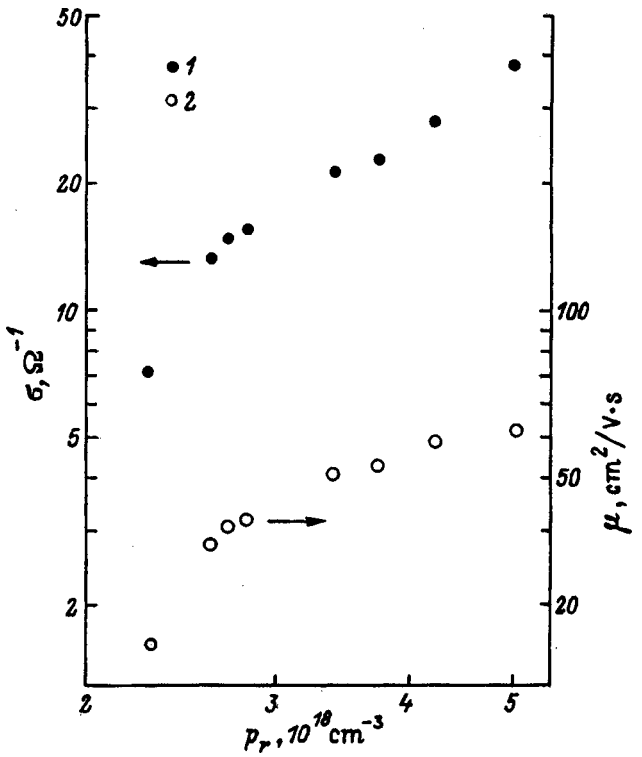


FIG. 11. Conductivity ($\sigma$) and Hall mobility ($\mu$) of $p$-$GaAs_{0.94}Sb_{0.06}$ measured at $T = 4.2$ K as functions of $p_r \cong N_A - N_D$.

as a function of the resistivity of the epilayer [the values of $\gamma_1$ and $R_0 = 1/G(0)$ are shown in Figs. 8 and 7, respectively], as well as the values of

$$\alpha_D = \frac{\lambda_\nu}{8}\sqrt{\frac{2m_\nu k_F}{\hbar^2}}\left(\frac{e^2}{\pi^2\hbar}\rho\right)^{3/2},$$

which were calculated on the basis of the transport characteristics of the epilayers (Fig. 11), and the values of the constant $\lambda_\nu$ of the *ee* interactions in the diffusive channel, which were calculated on the basis of (4)–(7). It can be seen from Fig. 10 that the theoretical values of $\alpha_D$ are close to the experimental values of $\gamma_1 R_0$ only for samples with a small resistivity. The dependence $\alpha_D = f(\rho)$ is described by a power function with the exponent $\eta = 1.43 \pm 0.01$ (the line in Fig. 10a). The value of $\eta$ differs from the theoretical value of 3/2 because $\lambda_\nu$ and $\nu_F$ depend on the hole density. The same data are presented in Fig. 10b as a function of the concentration $N_A - N_D \cong p_r$. It can be seen that the experimental ($\gamma_1 R_0$) and theoretical ($\alpha_D$) values of the coefficients begin to diverge dramatically when $N_a - N_D$ becomes less than the critical density for the metal-insulator transition estimated in Ref. 23, i.e., when $p_r < p_c \cong 3.6 \times 10^{18}$ cm$^{-3}$.

The satisfactory agreement between the experimental values of $\gamma_1 R_0$ and their theoretical equivalents $\alpha_D$ in the hole density range considered should be noted, since the value of $k_F l$ for the layers investigated on the metal side of the transition ($3.4 \times 10^{18} \leqslant p_r \leqslant 5 \times 10^{18}$ cm$^{-3}$) varies from 0.6 to 1. This finding confirms the validity of the special condition (2), under which the theory of the density-of-states anomaly in a three-dimensional conductor is applicable.[3]

## 3. CONCLUSION

We have discovered that the tunneling conductance of Au/$p$-$GaAs_{0.94}Sb_{0.06}$ Schottky barriers at small bias voltages (the *zero-bias anomaly*) is proportional to the square root of the voltage and that the slope of the linear segment is in satisfactory agreement with the theory of quantum corrections to the density of states,[5] but only for hole densities $p > p_c$, where $p_c \cong 3.6 \times 10^{18}$ cm$^{-3}$ is the critical density for the metal-insulator transition in $p$-$GaAs_{0.94}Sb_{0.06}$.

It was stated in the first publications on quantum corrections, for example, Ref. 26, that the density-of-states anomaly specified by the *ee* interaction increases in disor-

dered conductors as the metal-insulator transition is approached, vanishing entirely on the insulator side of the transition due to the formation of a Coulomb gap in the density of states. Just such a situation is illustrated in Fig. 10b. The arguments put forward in Ref. 26 were confirmed in Ref. 27, where the correction $\delta\nu$ was calculated for a three-dimensional electron gas without any assumptions regarding weak disorder of the electron subsystem, i.e., without the condition (3a). It is noted only that renormalization of the amplitude of the *ee* interaction (6) and the diffusion coefficient (2) should occur in systems with strong disorder.

Thus, the zero-bias anomaly in the tunneling conductance at Schottky barriers can be attributed to the Al'tshuler–Aronov anomaly in the density of states caused by features of the *ee* interaction inherent to a disordered electron gas. An analysis of the results of an experiment performed on barriers to $p$-$GaAs_{0.94}Sb_{0.06}$ layers with $k_F l \cong 1$ also confirms the specificity of the cut-off requirement for applicability of the theory of the density-of-states anomaly in a three-dimensional gas, which does not impose the condition of weak disorder $k_F l \gg 1$.

We wish to express our thanks to V. N. Karyaev for preparing the samples. T. Yu. Allen thanks the American Association of University Women and the University of Chattanooga Foundation, and T. A. Polyanskaya thanks the Russian Fund for Fundamental Research (Grant 98-02-18396) for their support.

[1)]In a system of localized electrons, the same factor, i.e., inhomogeneity of the charge-density distribution, leads to the formation of a Coulomb gap.[6]

[2)]In Ref. 18 there was an error in the denominator in the expression for the experimental determination of $A(V)$ [see Eq. (4) in Ref. 18]. The correct expression is presented here.

[1] *Tunneling Phenomena in Solids*, edited by E. Burstein and S. Lundqvist (Plenum Press, New York, 1969; Mir, Moscow, 1973).
[2] B. L. Altshuler and A. G. Aronov, Physica B **126**, 314 (1984).
[3] B. L. Altshuler and A. G. Aronov, in *Electron Interactions in Disordered Systems*, Elsevier (1985), Chap. 1, p. 1.
[4] P. A. Lee and T. V. Ramakrishman, Rev. Mod. Phys. **57**, 287 (1985).
[5] B. L. Altshuler and A. G. Aronov, Solid State Commun. **30**, 115 (1979).
[6] B. I. Shklovskii and A. L. Efros, *Electronic Properties of Doped Semiconductors* (Springer-Verlag, Berlin, 1984; Nauka, Moscow, 1979).
[7] R. C. Dynes and J. P. Garno, Phys. Rev. Lett. **46**, 137 (1981).
[8] R. Sood, Phys. Rev. B **25**, 6064 (1982).
[9] Y. Imry and Z. Ovadyahu, Phys. Rev. Lett. **49**, 841 (1982).
[10] W. L. McMillan and J. Mochal, Phys. Rev. Lett. **46**, 556 (1981).
[11] G. Hertel, D. J. Bishop, E. G. Spencer, J. M. Rowell, and R. C. Dynes, Phys. Rev. Lett. **50**, 743 (1971).
[12] N. A. Mora, S. Bermon, and J. J. Loferski, Phys. Rev. Lett. **27**, 664 (1971).
[13] G. Mahan and J. W. Conley, Appl. Phys. Lett. **11**, 29 (1967).
[14] N. A. Mora, S. Bermon, and F. N. Pollak, Phys. Rev. Lett. **28**, 225 (1972).
[15] N. A. Mora, J. J. Loferski, and S. Bermon, in *Proceedings of the International Conference on Radiation, Damage, and Defects in Semiconductors*, Reading, Berkshire, England, 19–21 July 1972, Institute of Physics (1973), p. 103.
[16] K. P. Abdurakhmanov, Sh. Mirakhmedov, A. Tashabaev, and S. S. Khudaĭberdiev, Fiz. Tekh. Poluprovodn. **10**, 658 (1976) [Sov. Phys. Semicond. **10**, 393 (1976)].
[17] T. Yu. Allen, T. A. Polyanskaya, Kh. G. Nazhmudinov, and I. G. Savel'ev, Fiz. Tekh. Poluprovodn. **32**, 579 (1998) [Semiconductors **32**, 517 (1998)].
[18] T. Yu. Allen, T. A. Polyanskaya, Kh. G. Nazhmudinov, S. G. Yastrebov, and I. G. Savel'ev, Fiz. Tekh. Poluprovodn. **32**, 574 (1998) [Semiconductors **32**, 513 (1998)].
[19] V. G. Karyaev, Kh. G. Nazhmudinov, M. V. Egorova, and I. G. Savel'ev, Fiz. Tekh. Poluprovodn. **20**, 1634 (1986) [Sov. Phys. Semicond. **20**, 1025 (1986)].
[20] L. V. Sharonova, T. A. Polyanskaya, Kh. G. Nazhmudinov, V. N. Karyaev, and L. A. Zaĭtseva, Fiz. Tekh. Poluprovodn. **22**, 93 (1988) [Sov. Phys. Semicond. **22**, 57 (1988)].
[21] T. Yu. Bil'gil'deeva, V. N. Karyaev, and T. A. Polyanskaya, Fiz. Tekh. Poluprovodn. **22**, 381 (1988) [Sov. Phys. Semicond. **22**, 235 (1988)].
[22] T. Yu. Bilgildeeva and T. A. Polyanskaya, Phys. Status Solidi B **149**, 649 (1988).
[23] T. Yu. Allen and T. A. Polyanskaya, Fiz. Tekh. Poluprovodn. **31**, 587 (1997) [Semiconductors **31**, 496 (1997)].
[24] A. H. Wilson Proc. R. Soc. London, Ser. A **136**, 487 (1932).
[25] J. Conley and G. Mahan, Phys. Rev. **161**, 681 (1967).
[26] W. L. McMillan and J. M. Mochel, Phys. Rev. Lett. **46**, 556 (1981).
[27] G. Vignale and W. Hanke, Phys. Rev. B **36**, 2924 (1987).

Translated by P. Shelnitz

# Kinetics of electric field screening in a space-charge region with a leakage channel and low-temperature conductance of surface channels in high-resistivity *n*-Si

N. I. Bochkareva and A. V. Klochkov

*A. F. Ioffe Physicotechnical Institute, Russian Academy of Sciences, 194021 St. Petersburg, Russia*
(Submitted July 7, 1998; accepted for publication July 8, 1998)
Fiz. Tekh. Poluprovodn. **32**, 1432–1438 (December 1998)

The kinetics of electric field screening in a space-charge region with a leakage channel is considered on the basis of an experimental study of the conductance of surface channels in *n*-Si. The characteristic times of the fast and slow stages of space-charge relaxation at the channel boundary after switching of the reverse bias are estimated. The proposed channel-current relaxation mechanism can account for the observed large radio-frequency conductance of surface channels in *n*-Si and the formation of capacitance relaxation spectra similar to those traditionally associated with the charge exchange of deep centers. The nature of the surface donor centers responsible for the formation of conducting layers at the $Si–SiO_2$ interface near 90 K is discussed.  [S1063-7826(98)00512-2]

**1**. The space-charge dynamics observed upon electric field screening in a semiconductor with a potential barrier, which are slow in comparison to Maxwellian relaxation, are usually associated with the presence of deep centers and their charge exchange. This approach has been developed in models of percolative conduction through drift barriers[1,2] and underlies the methods for identifying deep centers using barrier capacitance measurements.[3] However, the possibility of slow transient electrical processes associated with screening currents in a percolation or leakage channel was not analyzed. Thus, the insensitivity of deep-level transient spectroscopy toward surface leakage-current channels was postulated in Ref. 3. This hypothesis was based on a simplified model representation of a channel as an active resistance which shunts the barrier capacitance.[4] However, numerous difficulties in interpreting the experimental data, which point out, in particular, a relationship between the measured transient capacitance and reverse currents, were resolved only by adding elements to the model of the charge exchange of hypothetical deep centers (see, for example, Refs. 4 and 5). Nevertheless, the radio-frequency reactance[6] and the slow dynamics of the transient current[7] of leakage channels were noted back in the early studies, but their mechanisms were not elucidated. Temperature-dependent relaxation spectra were observed in Ge and Si and were associated with the transient currents of surface electronic leakage channels and their dependence on temperature and structural defect density.[8,9] In Ref. 9 an attempt was made to relate the increase in the screening time to size effects in the Debye length in a channel. When deep centers in real barrier structures are investigated by capacitance methods, the main contribution to the relaxation signal can be made by the transient reactive current of the surface leakage channel, rather than by the transient bias current caused by charge exchange of deep centers. As experiment has shown, leakage channels are manifested as characteristic features of the static, radio-frequency, and transient characteristics of barrier structures, making it possible to separate the effects of deep centers from the size effects in leakage channels. For this reason, we should study these features and examine a model of percolative conduction in a leakage channel.

The interest in this model is also due to some new experimental possibilities. The general laws discovered in Ge and Si, which dictate nonmonotonic variation of the surface electron density with temperature and a tendency for the formation of electron layers on the surface (at $T \simeq 90$ K), have been associated with oxygen- and hydrogen-containing donor complexes and variation of their electronegativity in the vicinity of ''characteristic'' temperatures.[8,9] In our opinion, the discovery of these general laws makes it possible to move forward in the study of the electronic properties of a semiconductor/oxide interface, particularly the mechanism of the formation of built-in charge in the oxide. This research can also provide new information pertaining to the mechanism of the influence of oxygen and hydrogen centers on the low-temperature conductivity of oxides with allowance for the important, but not yet thoroughly elucidated, role of various oxygen- and hydrogen-containing species existing in oxides in the mechanism underlying their conductivity and superconductivity.[10,11]

The purpose of the present work is to examine a qualitative model of percolative conduction in a leakage channel by studying the current response of surface channels in Schottky diodes on *n*-Si and to advance some hypotheses regarding the nature of the low-temperature surface donor centers on the basis of an analysis of the results.

**2**. The investigations were performed on high-resistivity *n*-Si with a resistivity $\rho = 2$ k$\Omega \cdot$cm. Silicon(100) wafers were oxidized in dry oxygen or a chlorine-containing atmosphere at 750 or 1050 °C for 1 h. In addition, near-surface oxidation-induced stacking faults (OSF's) with a penetration depth ($<1\mu$m), which is smaller than the equilibrium width of the space-charge layer ($w_0$), were introduced into some of the samples. The method for introducing the OSF's was de-

 

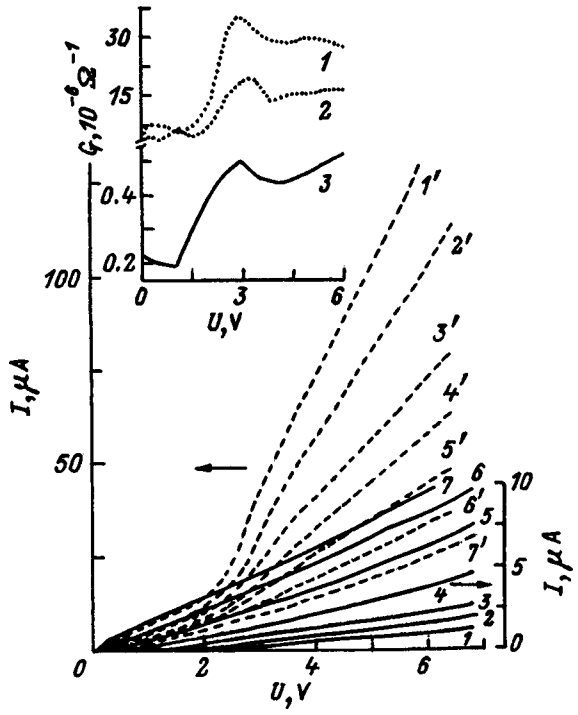


FIG. 1. Current-voltage characteristics of Schottky diodes on *n*-Si oxidized in dry oxygen (*1–7*) and in a chlorine-containing atmosphere (*1′–7′*). *T*, K: *1*, *1′* — 80; *2*, *2′* — 125; *3*, *3′* — 165; *4′* — 185; *4*, *5′* — 210; *5*, *6′* — 245; *6* — 282; *7*, *7′* — 300. The inset illustrates the character of the variation of the conductance (*G*) of the diodes with voltage at two temperatures *T*, K: *1* — 80, *2*, *3* — 165.

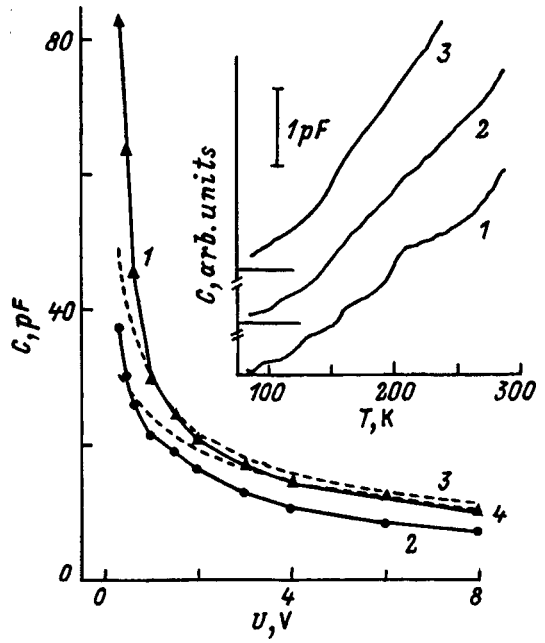


FIG. 2. Capacitance-voltage characteristics (*1*, *2*) and calculated barrier capacitance vs voltage curves (*3*, *4*). *T*, K: *1* — 300, *2* — 80. $\varphi_0$, eV: *3* — 0.15, *4* — 0.8. Inset — $C(T)$ curves for various values of the bias voltage *U*, V: *1* — 8, *2* — 4, *3* — 2.

scribed in Refs. 9 and 12. After the oxide layer was removed in HF, 3 mm diam Schottky barriers were created on the surface with OSF's by sputtering Au (in a vacuum), and ohmic contacts were formed on the rear surface by chemically depositing Ni.

**3**. The characteristic feature of the ''soft'' reverse current-voltage characteristics (IVC's) of the diodes investigated is a tendency for sublinearity in the voltage ranges $U<1-2$ V and $U>4-10$ V and superlinearity at intermediate voltages (Fig. 1). The leakage current was equal to $10^{-8}-10^{-5}$ A at 300 K and $U=1$ V. Either a decrease or an increase in the leakage current was observed during cooling, depending on the oxidation regime (Fig. 1).

Figure 2 compares the current-voltage characteristics (curves *1* and *2*) with the calculated plots of the barrier capacitance $C_g(U)$ for Schottky barriers of heights $\varphi_0=0.15$ and 0.8 eV (curves *3* and *4*). It is seen from the figure that at 300 K the measured capacitance $C>C_g$ at $U<1$ V and $C<C_g$ at $U>4$ V for all possible values of $\varphi_0$, while at 80 K $C<C_g$ at $U>0.4$ V.

The temperature dependences of the conductance at constant voltage $G(T)$, of the active component of the radio-frequency conductance $\tilde{G}(T)$, and of the capacitance $C(T)$ are reversible and have a nonmonotonic character (Figs. 2 and 3).

The transient-capacitance relaxation spectra observed in the samples with OSF's using transient capacitance spectroscopy[3] are presented in Fig. 4. It can be seen from Figs. 3 and 4 that peaks are observed in the spectra at the temperatures of the humps on the $C(T)$ curves. We note the identical nature of the spectra and $C(T)$ curves for samples of the same series and the absence of a direct relationship between the amplitudes of the spectral peaks and the value of the dc leakage current.

**4**. Let us discuss the results obtained after advancing some model arguments regarding the current response of a leakage channel to variation of the reverse voltage.

*A. Mechanism of the influence of a transverse electric field on the dc and ac current response of the leakage channel*. The observed IVC's have a form which is typical of short channels with Schottky gates in unipolar field-effect transistors. Such IVC's are attributed to variation of the width (*a*) and length (*L*) of the conducting region of the channel with variation of the voltage on the drain and with lowering of the internal barrier to electrons by a longitudinal electric field $E(x)$.[13–15] The character of the IVC is an indication of the existence of a leakage channel and allows us to postulate that the sources of the channels are potential wells in the barrier.[9]

When a current flows, the penetration of the field into a channel and the expansion of the depletion region inside it are determined by the distribution of the potential along the channel $U(x)$. The distribution of the potential $U(x)$ is influenced by the transverse electric field $E_y(x)$ appearing on the boundary between the channel and the depletion region in response to the abrupt change in the voltage *U*. A conception of the character of the influence of $E_y(x)$ can be obtained by examining the model of a symmetric channel with a short-circuited gate located in the plane of the source (Fig. 5a).

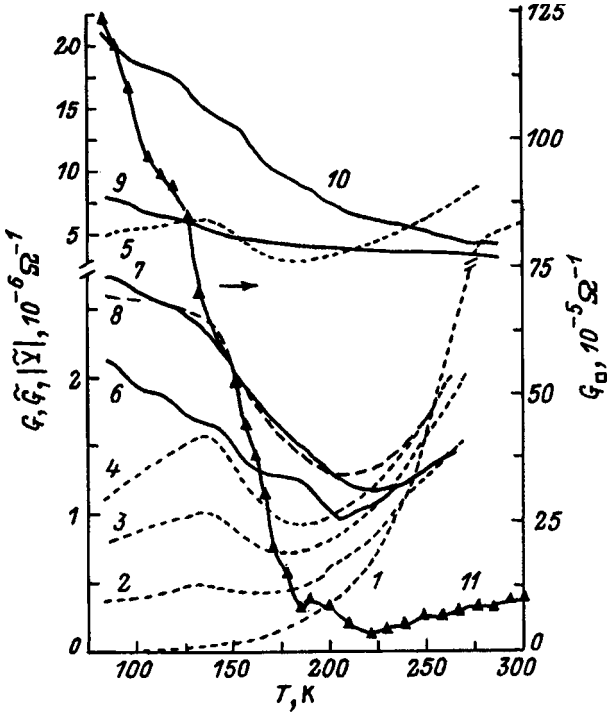


FIG. 3. Temperature dependence of the static conductance $G$ (*1*, *9*, *10*), the active radio-frequency conductance $\tilde{G}$ (*2–5*), and the modulus of the complex radio-frequency conductance $|\tilde{Y}|$ (*6–8*) of Au–*n*-Si diodes and the conductance per square $G_{\square}$ of an *n*-Si sample (*11*). The silicon surfaces were oxidized in dry oxygen (*1–8*, *11*) and in a chlorine-containing atmosphere (*9–10*) at two temperatures $T$, °C: *1–10* — 1050, *11* — 750. $U$, V: *1* — 0.1; *2*, *7* — 4; *3* — 2; *4*, *8–9* — 1; *5* — 0.3; *6* — 8; *10* — 7; *11* — 6. $\tilde{U}$, mV: *2–8* — 50; $f=160$ kHz.

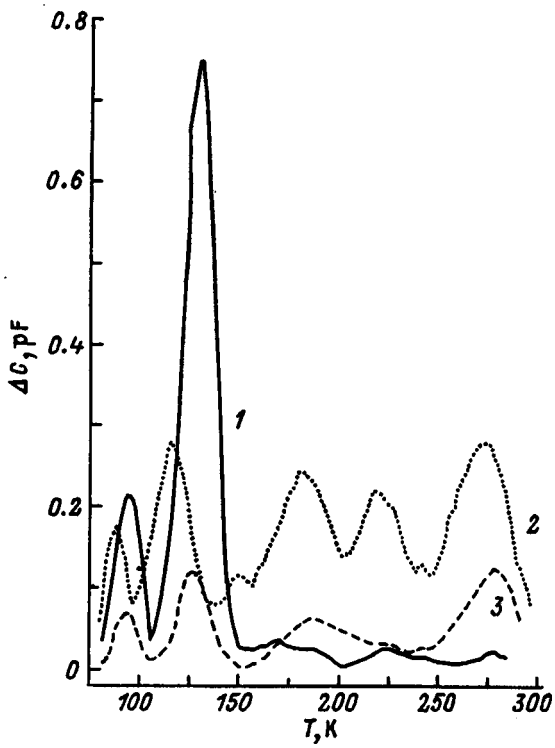


FIG. 4. Transient-capacitance relaxation spectra of Schottky diodes on *n*-Si oxidized in dry oxygen (*1*) and in a chlorine-containing atmosphere (*2*, *3*). Storage time of the samples before the measurements: *1–2* — 1 day, *3* — 4 months. Switching: 0.5→2.5 V; $t_1=2$ ms, $t_2=10$ ms, $f=160$ kHz, $\tilde{U}=50$ mV.

Since the longitudinal electric field in the Schottky layer $E_g(x)$ decreases linearly with the distance $x$ from the surface, i.e., since

$$E_g(x)=\left[-\frac{2(U+U_i)}{w}\right]\left(1-\frac{x}{w}\right),$$

($U_i$ is the diffusion potential, and $w$ is the depletion-layer width), a potential difference should appear between the channel and the space-charge region. It can be written in the form

$$U_g^*(x)=U_g(x)-IR(x),$$

where $I$ is the channel current, $R(x)$ is the channel resistance, and $U_g(x)$ is the distribution of the potential of the internal gate, i.e., the space-charge region adjacent to the channel:

$$U_g(x)=\left[\frac{2(U_i+U)}{w^2}\right]\left(wx-\frac{x^2}{2}\right).$$

For a field which is uniform across the channel width $E_0(x)=-U/w$, $U_0(x)=Ux/w$, and

$$U_{g0}^*(x)=U_g(x)-U_0(x)=2\left[\frac{(U_i+U)x}{w}\right]-\frac{(U_i+U)x^2}{w^2}-U_i.$$

The direction of the transverse field $E_y(x)$ is different in the source and drain regions. The estimate of $x_0$, i.e., the position of the apparent boundary between the source and drain regions, obtained from the condition $U_{g0}^*(x)=0$ gives $x_0=w_0$ for $U\ll U_i$ and $x_0=wU_i/U$ for $U\gg U_i$. When $E_y(x)$ is screened, the channel should narrow at the source (at $x_0>x>0$) and widen toward the drain as $1/E\propto(1-x/w)^{-1}$ in the region $w>x>x_0$. The character of the distribution of the longitudinal field $E(x)$ in the channel tends to approach the distribution of $E_g(x)$ in the depletion region.

These estimates permit drawing a conclusion regarding the causes of the nonlinearity of the channel IVC. The tendency for sublinearity of the IVC at small and large voltages can be attributed, respectively, to decreases in the width and increases in the length of the channel, as in a short channel.[13] The observed rise in the channel conductance at intermediate voltages can be attributed to the influence of the transverse field $E_y(x)$ on the channel width and to lateral current spreading. We note here that the superlinearity of the IVC in short channels is associated with lowering of the barrier in the space-charge region by the longitudinal electric field $E(x)$ and with an increase in the above-barrier current.[14,15] The weak temperature dependence of the channel current observed in the diodes investigated, as well as the reversal of the sign of the temperature coefficient of the channel conductance in some of the diodes, attest to the small magnitude of the above-barrier currents and support the conclusion that the transverse field influences the channel conductance.

When a radio-frequency probe voltage $\tilde{U}$ is applied, the channel width is modulated by the resultant transverse potential difference $\tilde{U}_g^*(x)$. This leads to a phase shift between

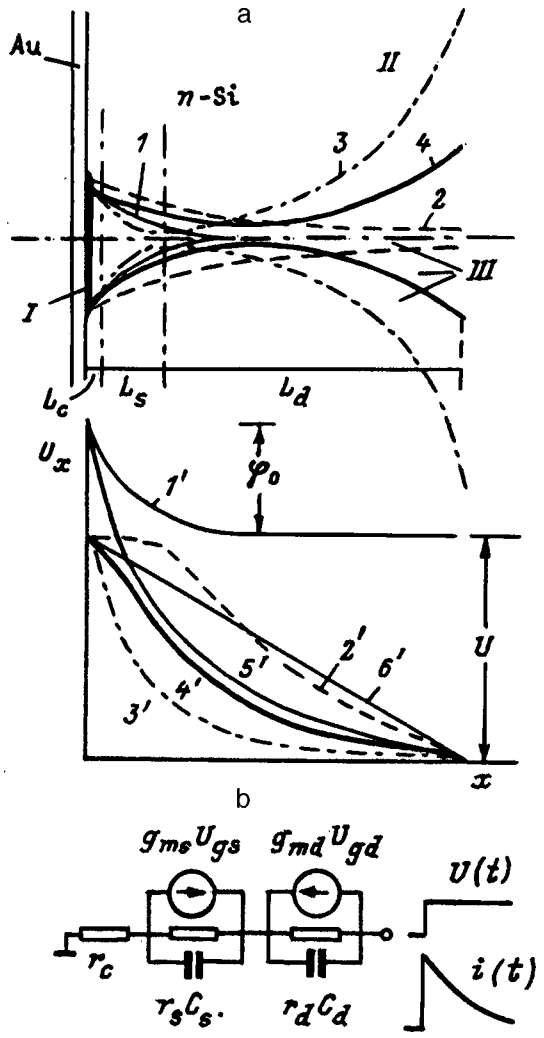


FIG. 5. Qualitative picture of the formation of a conducting channel in the space-charge region (a) upon the supply of a voltage step (*1–4*) and distribution of the potential along the channel (*1′–4′*), inside the space-charge region (*5′*), and in a channel that is uniform across its width (*6′*), b — approximate equivalent circuit of a channel. Fig. a: *I* — accumulation layer, *II* — space-charge region of the near-surface barrier, *III* — quasineutral region (channel). *1, 1′* — $t<0$; *2, 2′* — $t<t_f$; *3, 3′* — $\tau_f<t<\tau_s$; *4, 4′* — $t=\infty$.

the channel current and the voltage. The variation of the channel width in the narrow region ($a_s$) $\Delta a_s \approx \Delta w = w_0 \times \tilde{U}/(U_i+U)$ at small $U<U_i$ is comparable to the channel width at the source ($a_0$), i.e., $\Delta a_s \cong a_0$, and this is the reason for the large value of the active conductance $\tilde{G} \gg G$ (Fig. 3, curve *5*). As the voltage $U$ increases, the channel lengthens and becomes more uniform. The radio-frequency channel conductance approximates the dc conductance (Fig. 3, curves *1–4*).

The complex channel conductance $\tilde{Y}=\tilde{G}\pm j\tilde{B}$ and the reactive conductance can have either a capacitive ($+j\tilde{B}$) or inductive ($-j\tilde{B}$) character. The reactive channel current is summed in the external circuit with the bias current through the barrier capacitance $C_g$. The measured capacitance of the diode then equals $C=C_g\pm\tilde{B}/\omega$, where $\omega$ is the frequency of the probe voltage. At the small values of $U$ corresponding to the sublinear portion of the IVC, the voltage increment causes narrowing of the channel, the capacitive component of the reactive current dominates, and $C>C_g$ (Fig. 2). At values corresponding to the superlinear portion of the IVC the voltage increment increases the lateral current spreading, the channel current has an inductive character, and $C<C_g$ (Fig. 2).

*B. Screening of the transverse electric field upon instantaneous bias switching and transient channel leakage current.* Following a sudden increase in the reverse bias (for example, $0\rightarrow U$), the depletion region of the Schottky barrier expands during the Maxwellian relaxation time. The channel initially performs the role of a ''grounded'' screen, which prevents penetration of the edge field of the barrier into the quasineutral region at the source. The positive potential in the depletion region adjacent to the source region draws electrons into the near-boundary region. The channel tends to widen to $a(x)\approx a_0/(1-x/w)$ toward the drain (Fig. 5a).

As the lateral current spreading increases, the resistance of the drain region decreases, and the electric field is redistributed along the channel: it decreases at the drain and increases at the source. In addition, the effective potential $U_g^*(x)$ of the internal gate in the source region increases because of the ohmic voltage drop in the channel: $U_g^*(x)=U_g(x)-IR(x)$ [in the source region $U_g(x)<0$]. This leads to gradual narrowing of the channel at the source and a rise in the resistance of the source region. The current reaches a maximum and then begins to fall off. The resistance of the source region acts as an ''automatic-bias'' resistance, which increases with current.

Thus, following a pulsed increase in the voltage, the leakage channel at first screens the source region from penetration of the field, but the lateral current spreading is suppressed by the increase in the field at the source and the narrowing of the channel, and the current jump is followed by a slow decrease. These arguments are clearly also applicable to an asymmetric surface leakage channel on an open surface. A surface current spike associated with current spreading followed by narrowing of the channel should also be observed in the case where the surface charge density is insufficient for the formation of an accumulation layer, but the width of the depletion region on the surface is less than in the bulk, and the conditions for surface breakdown due to shock ionization or tunneling develop on the surface in the initial moment following bias switching.

In accordance with the foregoing arguments, the channel can be divided along its length into three regions by convention (Fig. 5a):

a source region of length $L_s(U)$, conductance $g_s(U_{gs},U_s)=\partial I_s/\partial U_s$ ($g_s\equiv 1/r_s$), and transconductance $g_{ms}(U_{gs},U_s)=\partial I_s/\partial U_{gs}$;

a drain region of length $L_d(U)$, conductance $g_d(U_{gd},U_d)=\partial I_d/\partial U_d$, ($g_d\equiv 1/r_d$), and transconductance $g_{md}(U_{gd},U_d)=\partial I_d/\partial U_{gd}$;

a near-contact region of length $L_c(U)$ and conductance $g_c(U_c)$, ($g_c\equiv 1/r_c$).

Here the voltage drops on these regions are denoted, respectively, by $U_s, U_d$, and $U_c$ ($U_s+U_d+U_c=U$) and the cur-

rents by $I_s$ and $I_d$ (in the channel $I_s=I_d=I$), and the potential of the internal gate is set equal to $U_{gs}=U_g(L_c)$ for the source region and $U_{gd}=U_g(L_s)$ for the drain region. Denoting the potential increments following the bias switching $U_0\rightarrow U_0+U$ for the source and drain regions by $\Delta U_s \equiv u_s, \Delta U_d \equiv u_d, \Delta U_{gs} \equiv u_{gs}$, and $\Delta U_{gd} \equiv u_{gd}$, for the channel-current increment in a steady-state regime we can write $i=g_s u_s+g_{ms}u_{gs}=g_d u_d+g_{md}u_{gd}$.

The approximate equivalent circuit of a channel can be depicted in the form of the *RC* circuit shown in Fig. 5b, where $C_s$ and $C_d$ are the capacitances of the source and drain regions, respectively. When $r_d<r_s$, the transient processes in such a circuit following the supply of a voltage step are similar to the processes in an aperiodic *RLC* circuit with losses. The current increment has the character of a spike, and the fast rise in current gives way to slow decay to the stationary value $i_\infty$. The transient characteristic for the case of a simplified approximation which takes into account only the passive elements of the *RC* circuit is described by the difference between two exponential functions, and the current increment is

$$i(t)-i_\infty \approx i_{s0}\exp\left(-\frac{t}{\tau_{s0}}\right)-i_{d0}\exp\left(-\frac{t}{\tau_{f0}}\right),$$

where $\tau_{f0}\cong r_c C^*$ for $C^*=C_s+C_d$ is the time constant of the fast stage of relaxation, $\tau_{s0}\cong r_d C^*$ is the time constant of the slow stage, and $i_{s0}$ and $i_{d0}$ are preexponential factors.[16]

Let us estimate the influence of the internal negative feedback in the channel on the characteristic current rise time and decay time, taking into account that the redistribution of the field upon current flow also causes variation of the effective potentials of the internal gates in the source ($U^*_{gs}$) and drain ($U^*_{gd}$) regions, which is accompanied by variation of the channel conductance with the characteristic times $\tau_{ms}=C_s/g_{ms}$ in the source region and $\tau_{md}=C_d/g_{md}$ in the drain region.[15,17] The influence of both the widening of the channel at the drain and the associated narrowing of the channel at the source on the current can be represented using the equivalent current generators $g_{ms}u_{gs}$ and $g_{md}u_{gd}$ with opposite phases (Fig. 5b).

Following an instantaneous voltage increase ($U\gg U_i$), in the initial stage of relaxation ($U_d>U_s$) the value of $U_d$ decreases in response to current spreading, so that $u_d\approx U-U_d(t)$. Since $g_{ms}\sim(U_s)^{1/2}$ and $g_{md}\sim(U_d)^{1/2}$ (Ref. 15), $g_{ms}u_{gs}\ll g_{md}u_{gd}$. Taking into account that $(r_s+r_c)^{-1}\approx g_s$, we can write the equation for the channel-current increment $i_f$ in the form

$$i_f=u_d g_s=g_{md}(u_{gd}-u_d)-C^*\frac{\partial u_d}{\partial t}-u_d g_d. \qquad (1)$$

Since $g_{s,d}$ and $g_{ms,md}$ depend on $u_d$, the relaxation of the current is nonexponential. Setting $r_s=r_0$ and $g_{md}=g_m$ ($g_m$ is the maximum value of $g_{md}$), for the initial stage of relaxation from (1) we obtain

$$i_f=\frac{g_m U}{1+g_m r_0}\left[1-\exp\left(-\frac{t}{\tau_f}\right)\right], \qquad (2)$$

$$\tau_f=\frac{r_0 C^*}{1+g_m r_0}. \qquad (3)$$

When the current spreads, the transconductance $g_{md}$ decreases, and $g_{ms}$ increases. The current rise gives way to decay when $g_{ms}u_{gs}>g_{md}u_{gd}$. The channel narrows at the drain, $U_d$ rises, the voltage on the source region $U_s$ decreases, and the channel widens in the source region. The channel-current increment $i_s=i_{\max}-i(t)$ can be written in the form

$$i_s=g_{ms}(u_{gs}-i_s r_c)-(u_d+i_s r_c)g_s.$$

Taking into account that $g_{ms}r_s=\mu$, where $\mu=\partial U/\partial U_{gs}$ is the voltage gain and $\mu u_{gs}\approx U$, we obtain

$$i_s=\frac{U-u_d}{r_s(1+g_{ms}r_c)}=C^*\frac{\partial u_d}{\partial t}. \qquad (4)$$

The current decay, like the rise, is nonexponential. Setting $r_s=r_{sm}$ and $r_c\approx r_0$ in the initial stage of decay and taking into account that $g_{ms}(U)\approx g_m$, for $i_s$ we obtain

$$i_s=i_\infty+(i_{\max}-i_\infty)\exp\left(-\frac{t}{\tau_s}\right), \qquad (5)$$

$$\tau_s=r_{sm}C^*(1+g_m r_0). \qquad (6)$$

Thus, it follows from (2)–(3) that the increase in the effective potential of the internal gate during the rise in current suppresses its growth. As a result, the current rise time decreases. The current spreading is accompanied by an increase in the resistance $r_s$. During the subsequent decay of the current, both $U_s$ and $r_s$ decrease simultaneously, compensating the decay of the current. As a result, as follows from (5) and (6), the current decays more slowly than in the absence of internal feedback. In addition, it can be seen from (2) that the greater is the conductance of the source $g_c$ and, thus, the greater is the initial current $i_f$, the more the resistance $r_s$ increases in the initial stage of relaxation ($r_s\sim i_{\max}\sim g_c$) and the more slowly the current decays.

This result corresponds to the general properties of a negative-feedback amplifier: an increase in the level of negative feedback expands the transmission band in the directions of both higher and lower frequencies. The level of negative feedback equals $1+\beta\mu_0(\omega)$, where $\mu_0(\omega)$ is the gain in the absence of feedback and $\beta$ is the feedback coefficient. For a channel $\beta=1$, and $\mu_0\approx g_m r_0$. The decrease in gain due to the effect of internal negative feedback leads (because of the constancy of the product of the gain and the transmission band) to a decrease in the characteristic current rise time $\tau_f$ by a factor of $1+\beta\mu_0=(1+g_m r_0)$ and to an increase in the characteristic time $\tau_s$ of the slow decay of the pulse plateau by a factor of $1+\beta\mu_0=(1+g_m r_0)$, in agreement with (3) and (6).

The observed correlation between the $\tilde{G}(T)$ and $C(T)$ curves provides evidence that $\omega\tau_f\cong 1$ ($\omega=2\pi f$, $f=160$ kHz). Hence, as an estimate of the time scale of the fast stage of recharging of the channel capacitance we can obtain $\tau_f\approx 10^{-6}$ s. Let us estimate the time of the slow relaxation stage. Taking into account that $g_m\cong g_c, g_c\sim a_0$, and $g_s\sim a_s$, we obtain

$$g_m r_0 \approx \frac{a_0}{a_s} \approx \frac{\tilde{G}}{G}.$$

Taking $\tilde{G}/G \leqslant 10^2$ and $r_{sm} \approx 10^6 - 10^7 \Omega$, from (3) and (6) we obtain $\tau_s \approx 10^6 \tau_f \leqslant 1$ s as an upper estimate. When $g_m r_0 > 1$, it follows from (2) that the current increment amounts to $i_f = U g_c$, and the value of the channel current reflects the conductance of the source. Hence it follows that the nonmonotonic character of $\tilde{G}(T)$ reflects the nonmonotonic character of the variation of the surface conductance with temperature.

When a probe signal $\tilde{U}$ is applied after switching of the voltage $U$, the inductive current at first increases rapidly (during a time $t \simeq \tau_f$) due to widening of the channel. In this stage the measured capacitance $C = C_g - \tilde{B}/\omega$, and $C < C_g$. As the active channel conductance slowly rises (during a time $t \approx \tau_s$), the inductive channel conductance decreases, and the measured capacitance slowly increases with the resultant formation of peaks in the relaxation spectra. Thus, the character of the relaxation of the measured capacitance as a result of the influence of the size effects on the Debye length in a leakage channel is similar to the character of the relaxation of the barrier capacitance upon the charge exchange of deep levels, which is usually regarded as the only cause of the formation of relaxation spectra in transient capacitance measurements.

We stress that the reactive channel current and, thus, the measured capacitance are determined by the modulation of the channel width by the probe and depleting voltages and depend on the transconductance of the channel, rather than on the dc conductance of the leakage channel. This accounts for the experimental fact that diodes with leakage currents differing by orders of magnitude exhibit identical temperature-induced capacitance jumps and relaxation spectra.

*C. Nature of the centers responsible for the nonmonotonic character of the surface conductance.* As can be seen from Fig. 3, the temperature dependence of the modulus of the complex conductance $|\tilde{Y}| = (G^2 + B^2)^{1/2}$ has a stepwise character and attests to an increase in the surface conductance upon cooling in the temperature range $T < 160$ K. Figure 3 also presents the results of measurements of the conductance per square $G_\square(T)$ in samples with ohmic contacts created on the surface of an *n*-Si wafer with OSF's. The figure reveals a correlation between the $\tilde{G}(T)$ and $G_\square(T)$ curves.

The analogous features of the $\tilde{G}(T)$ curves for Si and Ge (Ref. 8) were related in Ref. 9 to the variation of the surface free-electron density with temperature $n_s(T)$. The role of donor surface states can be performed by complexes containing three-coordinated oxygen atoms, whose donor activity is created by the orbitals of lone pairs.[18] Such complexes can contain oxygen atoms,[19] like the oxygen thermodonors described in Ref. 20, and they can contain hydrogen atoms[18] or molecules of adsorbed water.[21] The general laws governing the course of the $n_s(T)$ curves in Si and Ge can be understood, if we take into account the ability of oxygen- and hydrogen-containing centers to form a series of complexes which readjust their configuration at low temperatures. This conclusion is supported by the closeness of the temperatures at which the peaks of the relaxation spectra and the humps on the $\tilde{G}(T)$ curves are observed to the known temperatures for release of the rotational mobility of adsorption complexes containing oxygen atoms[19] and water molecules,[21,22] as well as defects in crystals with hydrogen bonds.[23] This allows us to relate the nonmonotonic character of the $n_s(T)$ curves to the variation of the electronegativity of the complexes upon readjustment of their configuration in the vicinity of the ''characteristic'' temperatures. The increase in $n_s$ upon cooling can be attributed to the ''freezing'' of a complex and its immobilization on a dangling Si bond, and the decrease in $n_s$ can be attributed to the restructuring of a defect in an energetically more favorable configuration with a smaller binding energy. In hydrogen-containing complexes this restructuring is associated with the tunneling of a proton along a weak hydrogen bond to a neighboring oxygen atom[23] and with the formation of weakly electronegative hydroxyl radicals according to the reversible reaction $H_2O + O \Leftrightarrow 2OH$ (Ref. 22). The relaxation peaks at $T > 150$ K in the spectra of samples oxidized in dry oxygen (Fig. 4, curve *1*) can be caused by complexes containing oxygen atoms and water molecules.[21,9] The small amplitudes of these peaks in the spectra following oxidation by chlorine (Fig. 4, curve *2*) can be associated with the small number of dangling bonds,[15] and the increase in their amplitudes during aging (curve *3*), which is accompanied by a decrease in $n_s$, can be associated with the formation of SiOH complexes with a strong chemical bond, an increase in the number of unpassivated dangling Si bonds, and the formation of stable complexes. We note that this model is consistent with the nonmonotonic temperature dependences of the density of dangling silicon and oxygen bonds in $SiO_2$ and on a $Si-SiO_2$ interface following postirradiation annealing in the range $77-300$ K which were observed in Ref. 24 using electron paramagnetic resonance and were associated with the presence of hydride and hydroxyl groups in the oxide. The character of the oscillations of the density of these defects with annealing and the attendant variation of the built-in charge in $SiO_2$ (Ref. 24) correspond to the character of the variation of the amplitudes of the peaks in the relaxation spectra during the aging of samples with OSF's, which can be attributed to the formation and structural transformation of complexes with hydrogen bonds upon annealing.

**5**. Thus, the kinetics of electric field screening in a barrier structure with a leakage channel is influenced by current spreading and negative feedback in the channel. The amplitude and rise time of the current pulse are restricted by the accumulation of space charge at the source due to current spreading and by a decrease in space charge at the drain. The decay of the current and the accumulation of space charge at the drain are slowed due to disappearance of the space charge at the source. The radio-frequency channel current can have either a capacitive or inductive character and make a contribution to the measured capacitance of the barrier structure. The slow relaxation of the surface leakage current

of Schottky barriers on *n*-Si with OSF's is manifested in the relaxation spectra, which reflect the nonmonotonic temperature dependence of the surface conductance, which is presumably caused by oxygen- and hydrogen-containing donor centers.

We thank the participants in the scientific seminar of the Laboratory of Nonequilibrium Processes in Semiconductors of the A. F. Ioffe Physicotechnical Institute of the Russian Academy of Sciences for discussing this work.

[1] V. B. Sandomirskiĭ, A. G. Zhdan, M. A. Messerer, and I. B. Gulyaev, Fiz. Tekh. Poluprovodn. **7**, 1314 (1973) [Sov. Phys. Semicond. **7**, 881 (1974)].
[2] A. Ya. Vinnikov, A. M. Meshkov, and V. N. Savushkin, Fiz. Tverd. Tela (Leningrad) **22**, 2989 (1980) [Sov. Phys. Solid State **22**, 1745 (1980)].
[3] D. V. Lang, J. Appl. Phys. **45**, 3023 (1974).
[4] G. L. Miller, D. V. Lang, and L. C. Kimerling, Annu. Rev. Mater. Sci., (1977).
[5] M. C. Chen, D. V. Lang, W. C. Dautremont-Smith, A. M. Sergent, and J. P. Harbison, Appl. Phys. Lett. **44**, 790 (1984).
[6] W. L. Brown, Phys. Rev. **91**, 518 (1953).
[7] Ya. A. Fedotov, *Principles of the Physics of Semiconductor Devices* [in Russian], Sov. Radio, Moscow (1970).
[8] N. I. Bochkareva, Fiz. Tekh. Poluprovodn. **25**, 537 (1991) [Sov. Phys. Semicond. **25**, 323 (1991)].
[9] N. I. Bochkareva and A. V. Klochkov, Fiz. Tekh. Poluprovodn. **32**, 82 (1998) [Semiconductors **32**, 71 (1998)].
[10] H. A. Blackstead and J. D. Dow, J. Supercond. **9**, 563 (1996).
[11] Yu. M. Baĭkov, S. E. Nikitin, Yu. P. Stepanov, and V. M. Egorov, Fiz. Tverd. Tela (St. Petersburg) **39**, 823 (1997) [Phys. Solid State **39**, 729 (1997)].
[12] J. Kaniewski, M. Kaniewska, and A. R. Peaker, Appl. Phys. Lett. **60**, 359 (1992).
[13] J. L. Morenza and D. Esteve, Solid-State Electron. **21**, 739 (1978).
[14] J. Nishizawa, T. Terasaki, and J. Shibata, IEEE Trans. Electron Devices **ED-22**, 185 (1975).
[15] A. Blicher, *Field-Effect and Bipolar Power Transistor Physics*, (Academic Press, New York 1981; Énergoatomizdat, Leningrad 1986).
[16] M. I. Kontorovich, *Operational Calculus and Processes in Electric Circuits* [in Russian], Sov. Radio, Moscow (1975).
[17] S. M. Sze, *Physics of Semiconductor Devices*, 2nd ed. (Wiley-Interscience, New York 1969; Mir, Moscow 1984).
[18] G. Lucovsky, in *Proceedings of the 23rd International Conference on the Physics of Semiconductors*, Berlin, Germany (1996), Vol. 2, p. 907.
[19] A. Spitzer and H. Luth, Surf. Sci. **118**, 121 (1982).
[20] V. D. Tkachev, L. F. Makarenko, V. P. Markevich, and L. I. Murin, Fiz. Tekh. Poluprovodn. **18**, 526 (1984) [Sov. Phys. Semicond. **18**, 324 (1984)].
[21] P. A. Thiel and T. E. Madey, Surf. Sci. Rep. **7**, 211 (1987).
[22] A. B. Anderson, Surf. Sci. **105**, 159 (1981).
[23] M. P. Tonkonogov, Usp. Fiz. Nauk **168**, 29 (1998) [Phys. Usp. **41**, 25 (1998)].
[24] D. L. Gricom, J. Appl. Phys. **58**, 2524 (1985).

Translated by P. Shelnitz

## SEMICONDUCTOR STRUCTURES, INTERFACES AND SURFACES

# Macroscopic ion traps at the silicon-oxide interface

S. G. Dmitriev and Yu. V. Markin

*Institute of Radio Engineering and Electronics, Russian Academy of Sciences, 141120 Fryazino, Russia*
(Submitted April 28, 1998; accepted for publication May 14, 1998)
Fiz. Tekh. Poluprovodn. **32**, 1439–1444 (December 1998)

The drift kinetics of the mobile charge in $SiO_2$ films, its capture on ion traps localized at the Si–$SiO_2$ interface, and ion emission from these traps are investigated by measuring the capacitance-voltage characteristics, the dynamic current-voltage characteristics, and the thermally stimulated depolarization current of the insulator. The current components (peaks) associated with the emission of particles trapped on the interface during thermofield treatment are isolated in an explicit form. The charge of the surface ions is shown to be neutralized mainly by Si electrons, and the field dependence of the ion emission currents is characterized by an anomalous Schottky effect associated with opening of the ion-trap potential by the external field. The relationship between these traps and the potential inhomogeneities, i.e., potential wells for mobile particles, on the interface under consideration is discussed. It is noted that the mobile ions in the insulator can be used for interface potential inhomogeneity diagnostics. © *1998 American Institute of Physics.* [S1063-7826(98)00612-7]

The mobile ionic charge $Q_m$ in the $SiO_2$ films in silicon metal-oxide-semiconductor (MOS) structures[1] can be captured on traps located at the interface during appropriate (polarizing or positive) thermofield treatment, which induces the displacement of $Q_m$ toward the Si–$SiO_2$ interface.[2] During a depolarizing (negative) thermofield treatment, the kinetics of the migration of the mobile charge are often assigned to the thermal emission of ions that were initially localized in these traps. In other words, at elevated temperatures (~200°C) the mobility of the ions is fairly high, and the transport of particles captured in traps through the thin insulator layer under the action of a field is limited by their emission from the traps. Just such an approach has been used for the most part in interpreting data from experimental investigations of the thermally stimulated depolarization (TSD) currents in Si-based MOS structures;[3–5] however, the nature of such interfacial traps has not been thoroughly established.

The investigation of TSD currents has revealed that the activation energy for the ion emission from traps depends on the electric field $\mathcal{E}$ applied to the $SiO_2$ film, and it has usually been assumed that the field dependence of the emission rate obeys a $\propto \exp(\alpha \mathcal{E}^{1/2}/kT)$ law,[6,7] where $\alpha$ is a proportionality factor, $k$ is Boltzmann's constant, and $T$ is the temperature. A similar dependence on $\mathcal{E}$ was also observed in investigations of the drift kinetics of $Q_m$ using dynamic current-voltage characteristics.[8,9] However, it was found that $\alpha > \alpha_0 = q^{3/2}[(\varkappa_2 - \varkappa_1)/\varkappa_1(\varkappa_1 + \varkappa_2)]^{1/2}$ ($q$ is an elementary charge, and $\varkappa_1$ and $\varkappa_2$ are the dielectric constants of the contacting media), where $\alpha_0$ corresponds to the field-induced lowering of the image-force potential barrier (the normal Schottky effect).

Another feature of the behavior of ions near the interface is their partial neutralization, but the mechanism of this passivation is still not entirely clear.[1,10] The neutralization of ions on the interface can occur as a result of their capture on surface traps followed by neutralization of the ionic charge by silicon electrons, and then this portion of the ions will play the role of sources of specific interface states, as was probably observed in Ref. 11.

Macroscopic dipole-charge formations on an inhomogeneous semiconductor-insulator interface were considered as a model of effective ion traps in Ref. 12. One characteristic feature of such traps is that they have a long-range potential, which leads to a strong field dependence of the emission rate of particles trapped in them in proportion (in weak fields) to $\exp(\alpha \mathcal{E}^{\gamma}/kT)$ $(1/2 < \gamma < 2/3)$ with $\alpha > \alpha_0$ (the anomalous Schottky effect).

A more complete study of the mechanism of the neutralization of mobile ions at the Si–$SiO_2$ interface requires isolating the current component caused by the deneutralization of particles in an explicit form. The solution of this problem is the subject of the present work, which examines ion emission from surface ion traps.

1. *Experimental results*. The experiments were performed on Al–$SiO_2$–Si(KÉF-4.5)–Al–*n*-Si MOS structures, which were fabricated by oxidizing the Si substrate in an atmosphere of dry oxygen. The thickness of the $SiO_2$ layer ($h$) was 0.2 $\mu$m, and the area of the structures was $S = 0.36 \times 10^{-2}$ cm$^2$. The measurements were performed at a constant temperature $T = 520$ K. The experiments were carried out in the following manner. At first positive thermofield treatment was performed: a polarizing potential $V_s = -10$ V was supplied to the semiconductor layer of the MOS capacitor, inducing the migration of the positively charged ions in $SiO_2$ toward the interface with Si. The sample was held at that value of $V_s$ until the polarization current dropped to

 

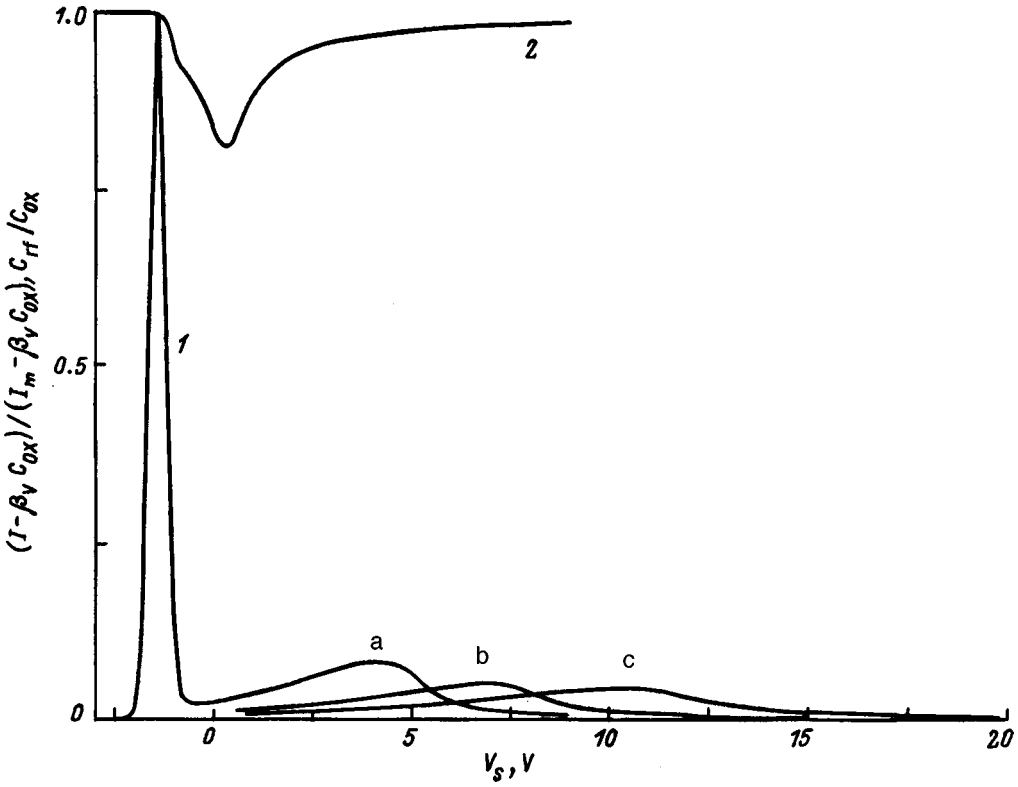


FIG. 1. Dynamic current-voltage (*1*) and capacitance-voltage (*2*) characteristics for MOS structures on *n*-Si. $\beta_v$, mV/s: a — 16, b — 55, c — 176. $I_m$, A: a — $10^{-10}$, b — $3.45\times10^{-10}$, c — $1.1\times10^{-9}$; $C_{ox}=62.2$ pF.

zero. After completion of the polarization process, the voltage $V_s$ was varied according to a linear law with the time $t$ toward depolarizing values. The dynamic current-voltage characteristic $I(V_s)$ and the ''radio-frequency'' (1 MHz) capacitance of the structure $C_{rf}(V_s)$ were recorded as $V_s$ was varied.

Figure 1 shows typical plots of $I(V_s)$ (curves *1*) and $C_{rf}(V_s)$ (curve *2*), which were obtained for various values of the sweep rate $\beta_V=dV_s/dt$. It is seen that the depolarization current has two peaks and that the maximum of the first of them is located at $V_{s0}=-1.4$ V, i.e., its position does not depend on the sweep rate of the bias voltage of the structure. This is evidence in support of a mechanism of quasiequilibrium ''overflow'' of ions from the Si–$SiO_2$ contact to the metallic electrode.[13] The effective surface concentration of ions found from the area of this current peak (relative to the $\beta_V C_{ox}$ level, where $C_{ox}$ is the geometric capacitance of the dielectric gap of the MOS structure) is $N_{m1}\approx5.9\times10^{12}$ $cm^{-2}$.

The position of the maximum of the second peak corresponds to inversion of the silicon near-surface charge (the electric field in the $SiO_2$ layer $\mathcal{E}_{ox}\sim V_s/h\geqslant10^5$ V/cm), and as $\beta_V$ increases, the peak is displaced toward larger depolarizing values of the potential $V_s$ (larger values of the field $\mathcal{E}_{ox}$). The concentration of ions here is $N_{m2}\approx2.8\times10^{12}$ $cm^{-2}$.

Unlike the depolarization current, the capacitance of the structure does not depend on $\beta_V$. In the initial region of the decrease in $C_{rf}(V_s)$, which corresponds to passage of the Si surface from an accumulation state to a depletion state as $V_s$ is varied, there is a feature, which reflects the drift of the ions (which cause the first current peak) from the Si–$SiO_2$ interface to the metallic electrode. In fact, in this case the rate of variation of the surface potential $\varphi_s'$ of the semiconductor relative to its bulk value (or the variation of $C_{rf}$) can be determined by both the rate of variation of the external voltage $V_s$ and the rate of ''departure'' of ions from the interface. As the positive ionic charge drains from the interface, the rate of variation of $\varphi_s'$ drops, and ultimately, after the current in the first peak drops to values of the order of $\beta_V C_{rf}$, the derivative $d\varphi_s'/dt$ is determined only by the variation of $V_s$.

2. *Drift kinetics of the mobile charge in* $SiO_2$. Let us now turn to the current peaks observed at higher values of $V_s$. Two cases are possible here: a) as $\mathcal{E}_{ox}$ is gradually increased, the current peak is caused by the drift of ions in the $SiO_2$ layer from the semiconductor-insulator interface to the gate of the MOS structure; b) the current peak reflects the emission of particles from surface ion traps stimulated by the external field.

Let us estimate the mobility of the ions causing the second peak under the assumption of a drift mechanism of current flow. In this case the characteristic time for ion drift through the $SiO_2$ layer $\tau_d=h/v_d=h/\mu_d\mathcal{E}_{ox}\sim h^2/\mu_d V_m\sim\Delta V_s/\beta_V$, i.e., $\mu_d\sim\beta_V h^2/V_m\Delta V_s$, where $V_d$ is the drift velocity of the ions, $\mu_d$ is their drift mobility, $V_m$ is the position of the maximum of the current peak, and $\Delta V_s$ is the full width at half-maximum (FWHM) of the peak. For example, for the values $\beta_V=5.5\times10^{-2}$ V/s, $V_m\approx6.95$ V, and $\Delta V_s\approx5.35$ V, which correspond to the condition for observation and the parameters of the second current peak (Fig. 1, curve *1*b), we find $\mu_d\approx5.92\times10^{-13}$ $cm^2/V\cdot s$. According to Ref. 14, the known species of mobile ions in $SiO_2$ have the following values under the present temperature regime

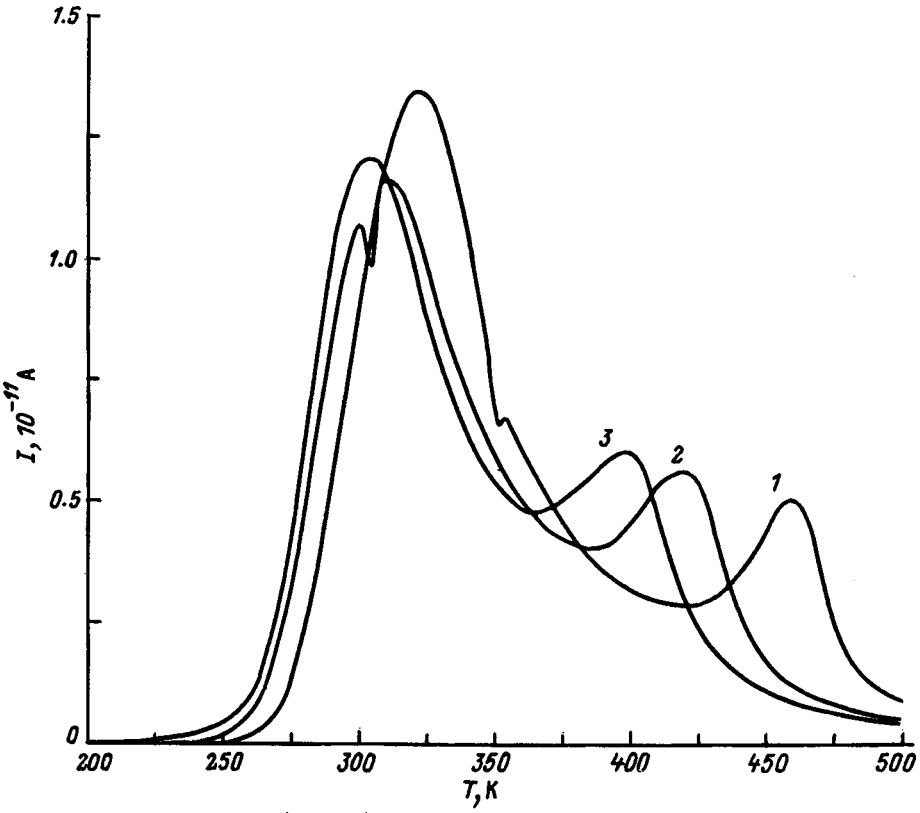


FIG. 2. TSD curves of an MOS structure for various values of the depolarization voltage $V_s$, V: *1* — 10, *2* — 20.36, *3* — 30.51. The temperature sweep rate is $\approx 0.3$ K/s.

($T=520$ K) for the measurements: $\mu_d=\mu_0\exp(-E_d/kT)$ ($E_d$ is the activation energy for ion drift): $\mu_d(\mathrm{Li}^+)=6.98\times10^{-8}$ cm$^2$/V·s, $\mu_d(\mathrm{Na}^+)=1.91\times10^{-8}$ cm$^2$/V·s, and $\mu_d(\mathrm{K}^+)=2.1\times10^{-13}$ cm$^2$/V·s. Thus, it can be presumed that the nature of the second current peak is governed by the drift of potassium ions through the $SiO_2$ layer.

In order to analyze this hypothesis, experiments involving measurement of the TSD currents of the structure under investigation were performed at various depolarization voltages (Fig. 2). Like the dynamic current-voltage characteristics, the TSD current has two peaks. Omitting the detailed analysis of the current peaks, we note that if the nature of the second peak is governed by the drift of $K^+$ through the $SiO_2$ film, the observed currents should not exceed $I_m=qSN_{m2}\mu_2(T_m)V_s/h^2$ ($T_m$ is the temperature at the maximum of the second current peak), i.e., $4\times10^{-13}$, $7\times10^{-14}$, and $2.4\times10^{-14}$ A for curves *1*, *2*, and *3*, respectively. The observed current values clearly exceed the values just listed (Fig. 2).

3. *Neutralization of ions at the* $Si-SiO_2$ *interface*. We next show that the group of ions considered, which are initially localized at the silicon-oxide interface, are in a neutral state. In fact, the condition that the mobile particles be in a charged state leads to the displacement of $C_{\mathrm{rf}}(V_s)$ along the voltage axis toward more positive values by $\sim V_s^*=4\pi qN_{m2}h/\varkappa_{\mathrm{ox}}=25.3$ V ($\varkappa_{\mathrm{ox}}$ is the dielectric constant of $SiO_2$), i.e., the minimum on the capacitance vs voltage curve should then be observed in the region of the second current peak. The position of the minimum of $C_{\mathrm{rf}}(V_s)$ at $V_s=0.35$ V clearly points out the neutral state of these particles. This circumstance, as well as the anomalously high values of the TSD currents, support using an emission model to describe the migration kinetics of the mobile charge causing the second peak on the dynamic current-voltage characteristics, the emission process being preceded by deneutralization of the mobile particles captured in traps.

4. *Field dependence of the rate of ion emission from interface traps*. The existence of a dependence of the position of the second current peak on the sweep rate $\beta_V$ indicates that emptying of the ion traps is stimulated by the field. Two models are usually utilized to interpret such a field dependence of the emptying rate: a) the ions are captured on negatively charged microscopic ion traps located near the interface, where the field stimulation of their emptying is caused by the Poole–Frenkel effect;[7,15] b) the ions are trapped on the interface by the surface image-force potential, they are neutralized by semiconductor electrons, and their emission in an electric field is specified by the normal Schottky effect.[6,8,9] We shall show that these models do not properly describe the results of our experiments.

The concentration of negatively charged microscopic ion traps near the $Si-SiO_2$ interface should be no smaller than $N_{m2}$. After a depolarizing thermofield treatment of the structure, such a negative charge should lead to displacement of the capacitance-voltage characteristic along the voltage axis by $\sim V_s^*$ in the negative direction. However, the minimum of the quasistatic capacitance-voltage characteristic measured at $T=300$ K after a negative thermofield treatment is observed at $V_s=+1.9$ V. Moreover, in the case of a homogeneous distribution of these traps throughout the oxide, some symmetry should be observed in the current peaks corresponding to the group of ions under consideration relative to the $V_s$ (or

$t$) axis for the forward and reverse bias voltage sweeping directions, but we did not observe such an effect. All this points to the absence of microscopic ion traps.

Let us perform the further analysis for the general case in which the probability of ion emission from a trap in the insulator is proportional to $\exp[-(E_0-\alpha\mathcal{E}^\gamma)/kT]$, where $\alpha\mathcal{E}^\gamma$ is the lowering of the emission barrier by the external field $\mathcal{E}$ ($\mathcal{E}$ is the absolute value of the field in the insulator at the interface with the semiconductor), the parameters $\alpha$ and $\gamma$ depend on the form of the potential and the nature of the trap model (see Ref. 12 and the accompanying text), and $E_0$ is the thermal ''ionization'' energy of a trap, which includes the energy needed for the deneutralization process. Therefore, the equation of the trap emptying kinetics in the absence of recapture has the form

$$\frac{dn_i}{dt}=-\nu n_i\exp\left[-\frac{E_0-\alpha\mathcal{E}^\gamma(t)}{kT}\right]$$

($n_i$ is the current concentration of trapped ions, and $\nu$ is the frequency factor), and its solution is

$$n_i=N_{m2}\exp\left\{-\frac{1}{\tau}\int_0^t\exp\left[\frac{\alpha\mathcal{E}^\gamma(t')}{kT}\right]dt'\right\},$$

where $\tau=\nu^{-1}\exp(E_0/kT)$ is the thermal lifetime of an ion in a trap. The absolute value of the ion emission current

$$I=-qS\frac{dn_i}{dt}=\frac{qSN_{m2}}{\tau}\exp\left\{\frac{\alpha\mathcal{E}^\gamma}{kT}-\frac{1}{\tau}\int_0^t\exp\left[\frac{\alpha\mathcal{E}^\gamma(t')}{kT}\right]dt'\right\}$$

as a function of $\mathcal{E}$ has a maximum at $\mathcal{E}=\mathcal{E}_m$, where $\mathcal{E}_m$ is defined by the equation

$$\alpha\gamma\mathcal{E}_m^{\gamma-1}\left(\frac{d\mathcal{E}}{dt}\right)_{\mathcal{E}=\mathcal{E}_m}=\frac{kT}{\tau}\exp\left(\frac{\alpha\mathcal{E}_m^\gamma}{kT}\right). \quad (1)$$

We note further that $d\mathcal{E}/dt=\beta_V/h$ under the conditions of the experiment. In fact, the maximum of the current peak under discussion corresponds to inversion-type band bending in silicon. In this case the potential $\varphi_s'=-(V_s-\varphi_s)$ of the Si surface calculated relative to the value in the bulk of the semiconductor satisfies the equation $\lambda(v_0-1)=\lambda^{-1}\exp(v_0)$ (Ref. 16), where $\varphi_s$ is the potential of the Si surface $v_0=q(V_s-\varphi_s)/kT$, $\lambda=N_d[(1+4n_{\rm in}^2/N_d^2)^{1/2}+1]/2n_{\rm in}$, $N_d$ is the concentration of the donor impurity, and $n_{\rm in}$ is the intrinsic carrier concentration in silicon. With the parameters used ($N_d=10^{15}$ cm$^{-3}$ and $T=520$ K) $\varphi_s'\approx-0.26$ V. The field $\mathcal{E}=(\varphi_s-V_0)/h$, where $V_0$ is the zero-field potential at the semiconductor-insulator interface (i.e., when $\varphi_s=V_0$, $\mathcal{E}=0$; for more information regarding $V_0$ see Ref. 17). Assuming that there is no accumulation of the total charge $Q_m$ in the bulk of the $SiO_2$ layer during the measurements of the dynamic current-voltage characteristics (i.e., that all the mobile ions are localized at the metal/$SiO_2$ interface in the voltage range corresponding to the second current peak) and allowing for the weak dependence of the inversion-type band bending in silicon on $V_s$, we have $dV_0/dt\approx0$, $d\varphi_s/dV_s\approx1$, and $d\mathcal{E}/dt\approx\beta_v/h$.

Thus, in the coordinates

$$x=\mathcal{E}_m^\gamma,\quad y=\ln(\beta_V\mathcal{E}_m^{\gamma-1}) \quad (2)$$

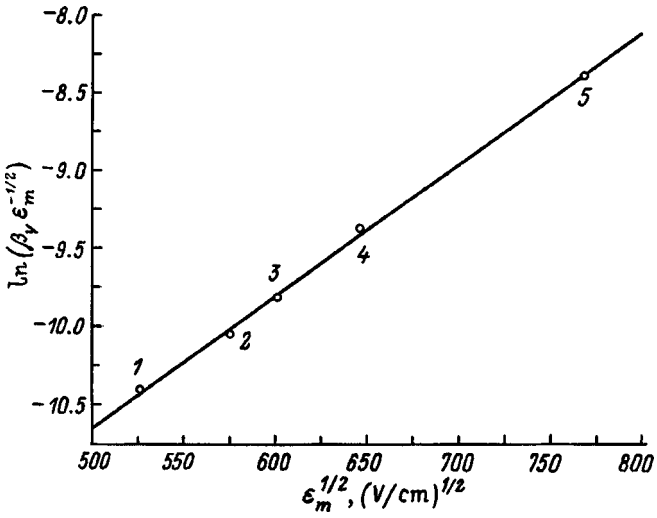


FIG. 3. Experimental plot in the coordinates (2) for $\gamma=1/2$.

Eq. (1) is a straight line with a slope $\alpha/kT$ relative to the $\mathcal{E}_m^\gamma$ axis. In other words, the form of Eq. (1) (for these coordinates) is self-similar relative to the nature of the field stimulation of the ion trap emptying rate, permitting its use to elucidate the mechanism of ion emission in an external field and to thereby investigate the nature of the interface ion traps.

5. *Mechanisms of the field emission of ions from interface traps*. In order to obtain the experimental dependences just indicated we must know the relationship between $\mathcal{E}_m$ and $V_s$. Taking into account the smallness of $\varphi_s'$ ($|\varphi_s'/V_s|\ll1$), we shall henceforth set $\varphi_s\approx V_s$. If, in addition, we take (as, for example, in Ref. 18) $V_{s0}$, i.e., the position of the maximum of the first current peak, as the value of $V_0$, we have $\mathcal{E}_m=(V_{sm}-V_{s0})/h$, where $V_{sm}$ is the position of the maximum of the second current peak on the dynamic current-voltage characteristics.

Let us next consider the possibility of the realization of the normal Schottky effect. Figure 3 shows the plot in the coordinates (2) for $\gamma=1/2$ obtained from the dynamic current-voltage characteristics measured with various values of $\beta_V$: *1* — 0.016, *2* — 0.025, *3* — 0.033, *4* — 0.055, *5* — 0.176 V/s. It is seen that this dependence is a straight line with a slope $\alpha/kT=8.48\times10^{-3}$ (V/cm)$^{-1/2}$. At the measurement temperature $T=520$ K we have $\alpha=6.085\times10^{-23}$C(V·cm)$^{1/2}$. The value for the normal Schottky effect is $\alpha_0=2.18\times10^{-23}$C(V·cm)$^{1/2}$, i.e., the value of $\alpha$ found is 2.8 times greater than $\alpha_0$. This finding points out the weak influence of the image-force potential.

On the other hand, the anomalous field dependences of the ion emission currents (the anomalous Schottky effect) indicate the presence of interface ion traps created by macroscopic dipole-charge formations.[12] In the case of charged ''circular'' (not excessively extended) spots $\gamma=1/2$, and $\alpha>\alpha_0$ by several fold, as was observed in our experiments. The total negative charge of these spots should then be no less than $qSN_{m2}$. However, such a value of the charge would lead to shifts of the capacitance-voltage characteristic after a negative thermofield treatment of the structure, which are not

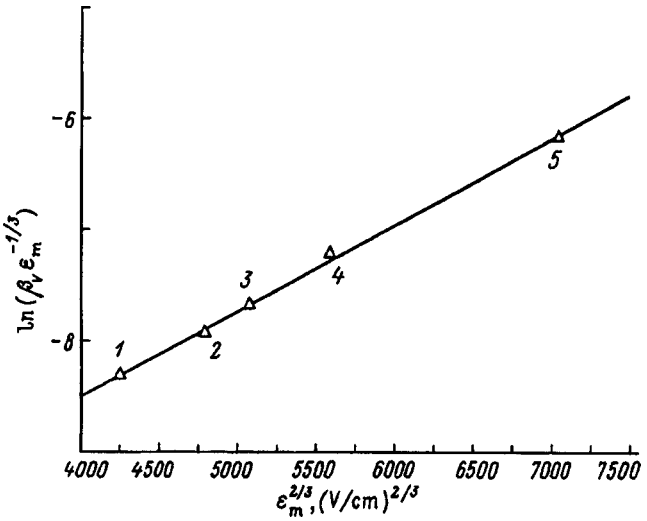


FIG. 4. Experimental plot in the coordinates (2) for $\gamma=2/3$.

observed experimentally (see Sec. 4). Therefore, the charge state of the macroscopic ion traps is neutral as a whole, pointing out the ''dipole'' nature of the surface potential inhomogeneities.

Figure 4 presents the plot in the coordinates (2) for $\gamma=2/3$, which corresponds to the case of dipole spots.[12] This dependence has the form of a straight line with the slope $\alpha/kT=7.78\times10^{-4}$ $(\mathrm{V/cm})^{-2/3}$.

According to Ref. 12, for a circular dipole spot (of radius $R$) $\alpha=3/2\{q^2[\varkappa_s/(\varkappa_{ox}+\varkappa_s)]\Delta\chi R^2\}^{1/3}$, where $\varkappa_s$ is the dielectric constant of silicon and $\Delta\chi$ is the dipole ion potential energy jump, and for the experimental value of $\alpha$ we find $R[\text{Å}]\approx41(0.1\ \text{eV}/\Delta\chi)^{1/2}$. We note that this relation provides an effective estimate of the parameters of dipole spots.

Thus, the conventional methods for treating the field dependences of ion currents,[6–9,15] in which a definite value of $\gamma$ is postulated at the onset (for example, $\gamma=1/2$ for the normal Schottky effect or the Poole–Frenkel effect) can lead, as we see, to errors in the interpretation of experimental results, and a more complicated analysis is needed to determine the emission mechanism and the parameters of interface ion traps.

A more detailed analysis requires data on the form and characteristic dimensions of the macroscopic charge and dipole spots, the statistical variability of their parameters, etc. However, the experimental methodical approach used in the present work has already enabled us to achieve the following results: the drift kinetics of $Q_m$ in the $SiO_2$ layer have been analyzed; it has been shown that some of the mobile ions are trapped on the $Si-SiO_2$ interface (on interface ion traps) with subsequent neutralization of their charge by electrons from the semiconductor; a field dependence of the emptying rate of these traps has been discovered; the possible mechanisms of the field-induced trap emptying have been analyzed on the basis of experimental data; a generalized theoretical analysis of field-induced trap emptying has been performed; generalized coordinates, in which the construction of experimental dependences reveals the nature of interface ion traps, have been proposed for application to the experimental method used; it has been shown that these traps are created by macroscopic dipole spots on the interface; and estimates of the effective values of the parameters of these inhomogeneities have been given.

We note in conclusion that experiments devised to investigate ion currents in the insulator can serve as an effective tool for studying the semiconductor-insulator interface and permit the performance of a unique kind of ''ion probing'' of macroscopic inhomogeneities on this boundary.

[1] A. P. Baraban, V. V. Bulavinov, and P. P. Konorov, *Electronics of* $SiO_2$ *Layers on Silicon* [in Russian], Izd. LGU, Leningrad (1988).
[2] V. N. Vertoprakhov, B. M. Kuchumov, and E. G. Sal'man, *Structure and Properties of* $Si/SiO_2/M$ *Structures* [in Russian], Nauka, Sib. Otd., Novosibirsk (1981).
[3] T. W. Hickmott, J. Appl. Phys. **46**, 2583 (1975).
[4] P. K. Nauta and M. W. Hillen, J. Appl. Phys. **49**, 2862 (1978).
[5] M. R. Boudry and J. P. Stagg, J. Appl. Phys. **50**, 942 (1979).
[6] J. P. Stagg and M. R. Boudry, J. Appl. Phys. **52**, 885 (1981).
[7] G. Greeuw and J. F. Verwey, Solid-State Electron. **28**, 509 (1985).
[8] A. G. Tangena, N. F. de Rooij, and J. Middelhoek, J. Appl. Phys. **49**, 5576 (1978).
[9] C. Nylander, M. Armgarth, and C. Svensson, J. Appl. Phys. **56**, 1177 (1984).
[10] T. Hino and K. Yamashita, J. Appl. Phys. **50**, 4879 (1979).
[11] J. G. Hwu, J. Z. Hwang, and Y. L. Chiou, Thin Solid Films **125**, 17 (1985).
[12] S. G. Dmitriev and Yu. V. Markin, Fiz. Tekh. Poluprovodn. **30**, 1231 (1996) [Semiconductors **30**, 649 (1996)].
[13] A. G. Tangena, J. Middelhoek, and N. F. de Rooij, J. Appl. Phys. **49**, 2876 (1978).
[14] G. Greeuw and J. F. Verwey, J. Appl. Phys. **56**, 2218 (1984).
[15] C. Choquet, C. Plossu, M. Berenguer, B. Balland, and G. Barbottin, Thin Solid Films **167**, 45 (1988).
[16] A. G. Zhdan and Yu. V. Markin, Fiz. Tekh. Poluprovodn. **28**, 756 (1994) [ Semiconductors **28**, 444 (1994)].
[17] S. M. Sze, *Physics of Semiconductor Devices*, 2nd ed. (Wiley-Interscience, New York, 1969; Mir, Moscow, 1984).
[18] M. W. Hillen, G. Greeuw, and J. F. Verwey, J. Appl. Phys. **50**, 4834 (1979).

Translated by P. Shelnitz

# Manifestations of the deneutralization of mobile charges in $SiO_2$ in the spectroscopy of the silicon-oxide interface

S. G. Dmitriev and Yu. V. Markin

*Institute of Radio Engineering and Electronics, Russian Academy of Sciences, 141120 Fryazino, Russia*
(Submitted March 16, 1998; accepted for publication April 23, 1998)
Fiz. Tekh. Poluprovodn. **32**, 1445–1449 (December 1998)

The total number of mobile ions in the oxide film in a Si-based MOS structure is determined by the conventional methods of recording capacitance-voltage and dynamic current-voltage characteristics. The fraction of ions in the neutral state at the $Si-SiO_2$ interface is determined. Spectroscopy of the interface reveals a peak of the effective density of interface states. It is shown that the number of states in this peak corresponds to the number of neutralized particles. The mechanism for neutralization of the mobile charge of ions is discussed.
 [S1063-7826(98)00712-1]

The mobile ionic charge ($Q_m$) in $SiO_2$ films on silicon[1–3] is one of the main causes of the instability of the electrophysical characteristics of Si-based MOS structures and devices based on them;[4] therefore, a fairly large amount of attention has been devoted to research on the kinetics of ion drift. It has been established that $Q_m$ is created by positively charged alkali-metal $Li^+$, $Na^+$, and $K^+$ ions, which become mobile at elevated temperatures ($\sim 200-300\,^\circ$C) in fields equal to $10^5-10^6$ V/cm.[1,2]

Several studies have been devoted to the influence of mobile ions on the spectrum of interface states at the $Si-SiO_2$ boundary.[5–8] It is shown that, unlike the $SiO_2$ bulk, where $Li^+$, $Na^+$, and $K^+$ ions create a high donor level relative to the bottom of the Si conduction band,[9] the ions localized at the interface modify the spectrum of interface states in an energy range which corresponds to the silicon band gap.

Another special feature of the behavior of ions near the interface is their partial neutralization, which is especially characteristic of the ''chlorine'' oxide;[1,10] however, the mechanism of such passivation is still not entirely clear.[1] In addition, there has been no comparison of the number of particles in the neutral state with the degree of modification of the spectrum of interface states.

The drift kinetics of $Q_m$ observed in thermally stimulated depolarization experiments[2,3,11–13] are often described using a model of surface ion traps, whose the emission current makes an additional (and sometimes decisive) contribution to the observed thermally stimulated depolarization currents. However, the emission mechanism itself and the nature of such interface traps have likewise not been established.

The structure of the potential induced by dipole (or charged) ''spots'' on an inhomogeneous semiconductor-insulator interface was considered in Ref. 14. It was shown that the potential wells appearing in this case can serve as effective traps for charged particles, especially for positive ions in the insulator.

In the present work the total number of ions migrating toward the $Si-SiO_2$ interface during thermofield treatment and the fraction of these ions which are in the neutral state are determined from the results of an experimental investigation of thermally stimulated depolarization currents, dynamic current-voltage characteristics,[2] and radio-frequency and quasistatic capacitance-voltage characteristics,[2,9] and the influence of the ions on the spectrum of interface states is analyzed on the basis of data from the spectroscopy of the silicon-oxide interface.

The experiments were performed on $Al-SiO_2-Si-Al$ MOS structures fabricated by oxidizing a substrate of *n*-Si(100) (KÉF-4.5) in an atmosphere of dry oxygen. The thickness of the $SiO_2$ layer was 0.104 $\mu$m, and the area of the structures was $S=0.25\times10^{-2}$ cm$^2$. The measurements were performed in the temperature range $200\leqslant T\leqslant 500$ K. The experimental procedure was as follows. The sample was first subjected to a depolarizing thermofield treatment: the structure was heated to $T=500$ K with the voltage $V_s=7$ V on the Si substrate and held at that temperature for 30 min. At the conclusion of the depolarization process, which induced the displacement of $Q_m$ to the metal-$SiO_2$ interface, the structure was cooled to $T=300$ K, and synchronous measurements of the radio-frequency and quasistatic capacitance-voltage characteristics were carried out (see the inset in Fig. 1). Next, the depolarization process was repeated, and the sample was subsequently cooled to $T=200$ K, at which the radio-frequency capacitance-voltage characteristic of the structure investigated was recorded with the variation of $V_s$ according to a linear law with respect to time at the rate $\beta_V=26$ mV/s. Then the structure was heated to $T=500$ K, at which the sample was held for 30 min under a polarizing bias $V_s=-10$ V. Such a thermofield treatment induced the migration of mobile positively charged ions toward the $Si-SiO_2$ interface. At the conclusion of the polarizing process, for the purpose of determining the number $N_m$ of mobile ions reaching the interface, the structure was cooled to $T=200$ K without altering the value of $V_s$, the radio-frequency capacitance-voltage characteristic was recorded, the sample was heated to $T=500$ K, and dynamic

 

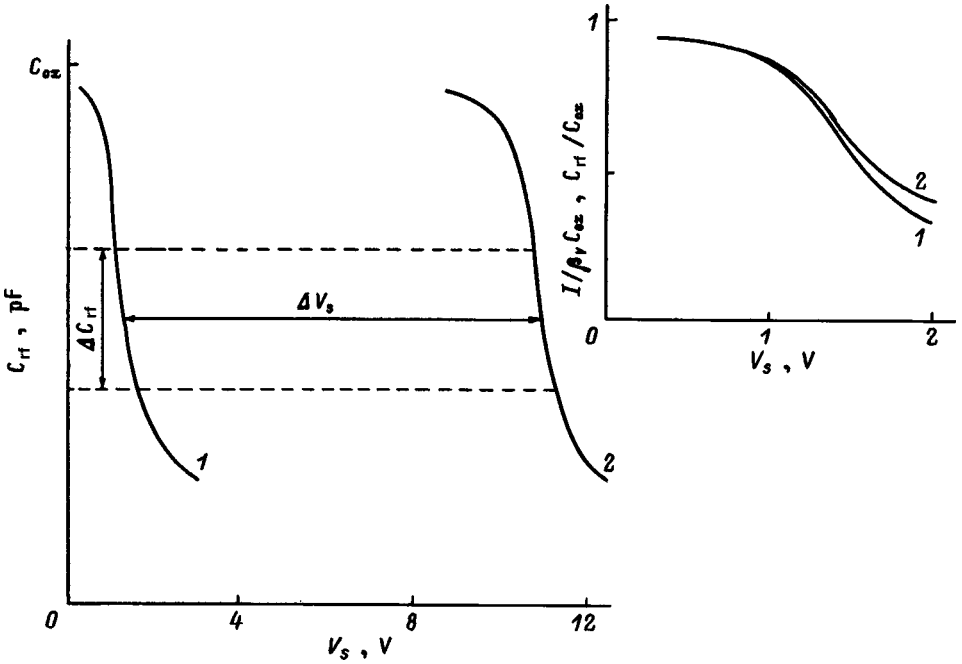


FIG. 1. Radio-frequency capacitance-voltage characteristics obtained before (*1*) and after (*2*) a polarizing treatment of the sample; $C_{ox}=83$ pF, $\Delta V_s=9.57$ V. Inset — radio-frequency (*1*) and quasistatic (*2*) capacitance-voltage characteristics before polarization of the structure; $\beta_V=1.6\times10^{-2}$ V/s.

current-voltage characteristics $[I(V_s)]$ were measured. Then a repeated thermofield treatment, which caused repeated migration of ions to the interface, was performed without variation of the conditions of the thermofield treatment on the structure under investigation, and then the sample was cooled to $T=200$ K. The constant bias voltage $V_s=7$ V was applied to the structure at that temperature, and the sample was heated at the rate $\beta_T=0.13$ K/s. The temperature dependences of the thermally stimulated depolarization current $I(T)$ and the radio-frequency capacitance $C_{\mathrm{rf}}(T)$ were recorded during the heating.

Figure 1 presents the experimental radio-frequency capacitance-voltage characteristics of the structure recorded before (curve *1*) and after (curve *2*) the polarizing thermofield treatment, and Fig. 2 shows the dynamic current-voltage characteristic. The effective (brought to the surface) concentration of mobile ions $N_m$ found from the area of the current peak on the dynamic current-voltage characteristic is $2.24\times10^{12}\mathrm{cm}^{-2}$. The shift $\Delta V_s$ of the radio-frequency capacitance-voltage characteristics, in turn, gives the value $N_m^*=2\times10^{12}\mathrm{cm}^{-2}$ (for the purpose of avoiding the influence of the fluctuation potential and other effects caused by the migration of ions toward the interface,[6] $\Delta V_s$ was found in the range of capacitance values $\Delta C_{\mathrm{rf}}$ in which the characteristics obtained before and after the thermofield treatment coincide if parallel displacement along the $V_s$ axis is added). Thus, the passivation parameter[1] $P=(N_m-N_m^*)/N_m\approx0.11$, and the number of neutral particles $N_0=2.4\times10^{11}\mathrm{cm}^{-2}$. In addition, the deneutralization process is reflected on the cur-

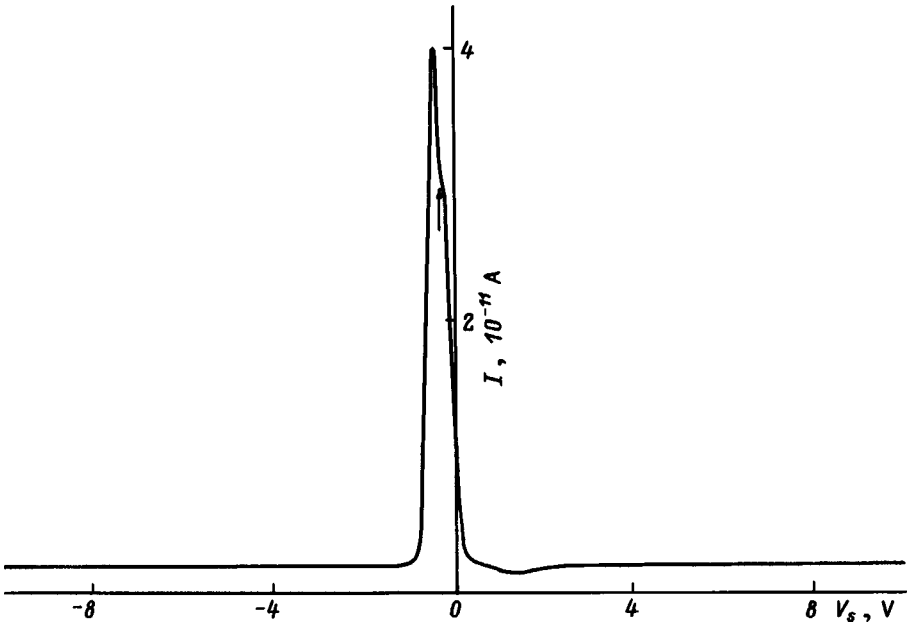


FIG. 2. Dynamic current-voltage characteristic of the structure studied. The arrow marks the feature on the $I(V_s)$ curve.

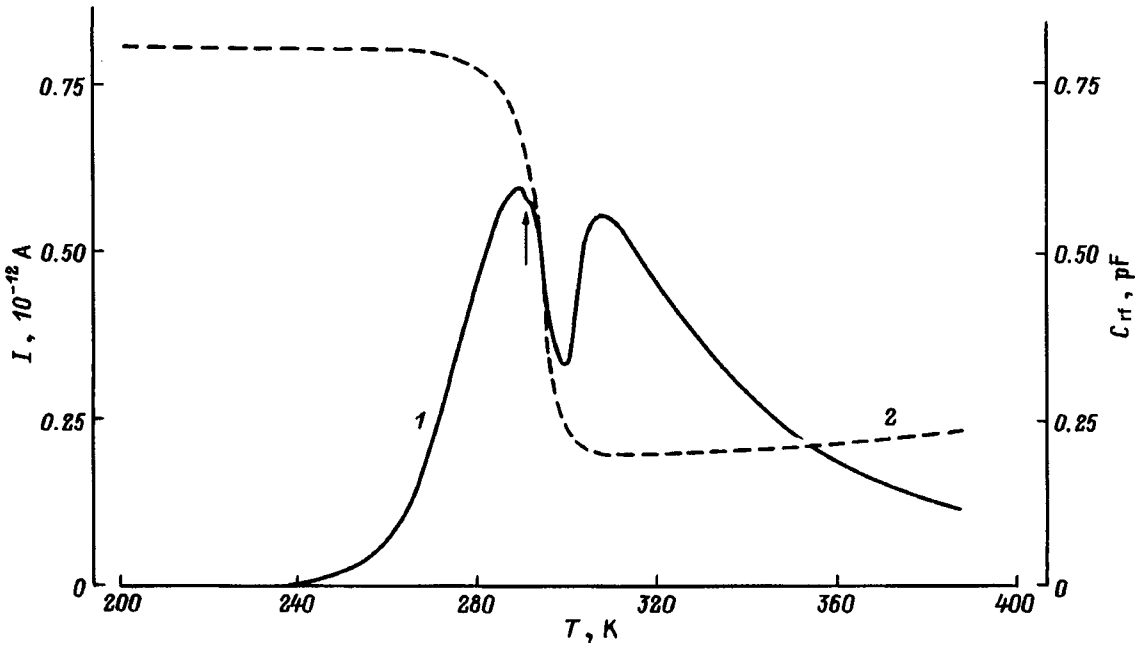


FIG. 3. Temperature dependence of the depolarization current (*1*) and the radio-frequency capacitance (*2*) of the structure studied. The arrow marks the feature on the $I(T)$ curve.

rent peak of the dynamic current-voltage characteristic in the form of a feature (which is marked by an arrow in Fig. 2) on the descending branch of $I(V_s)$, whose form indicates the ''opening'' of an additional ion current channel. This conclusion was tested in the following manner. The experiment preceding the measurements of the thermally stimulated depolarization currents was repeated for the purpose of finding the values of $N_m$ and $N_m^*$ again. If no deneutralization process occurred during the first measurements of $I(V_s)$, the new values of $N_m$ and $N_m^*$ should coincide ($N_m \approx N_m^*$), but the repeated cycle gave the former concentration values.

Figure 3 shows plots of $I(T)$ (curve *1*) and $C_{\rm rf}(T)$ (curve *2*). The current peak has a dip in the region where $C_{\rm rf}$ varies abruptly. It is due to relaxation of the semiconductor space-charge region during the thermally stimulated drift of ions from the $Si-SiO_2$ interface toward the metal.[15] In the initial portion of the dip on the $I(T)$ curve there is a feature (it is indicated by an arrow in Fig. 3), which can be assigned to the equilibrium charge exchange of a certain interface-state level at the semiconductor-insulator contact during the gradual increase in the depletion-inducing band bending in Si.

The component associated with the charge exchange of interface states can be isolated from the total current $I(T)$ by a procedure similar to the treatment of data obtained from synchronous measurements of the radio-frequency and quasistatic capacitance-voltage characteristics.[9] In the absence of the injection of mobile ions and other charges from $SiO_2$ into Si, $I(T)$ is equal to the current flowing from the semiconductor layer of the MOS capacitor: $I(T) = -\beta_T S d(\sigma_v + \sigma_{ss})/dT = \beta_T S(C_v + C_{ss}) d\varphi_s/dT$, where $\sigma_v$ is the charge density of the semiconductor space-charge region brought to the surface, $\sigma_{ss}$ is the electron charge density in interface states, $C_v = -d\sigma_v/d\varphi_s$ is the low-frequency capacitance of the semiconductor space-charge region, $C_{ss} = -d\sigma_{ss}/d\varphi_s = q^2 N_{ss}(F_s)$ is the capacitance associated with the equilibrium emptying of the interface states, $\varphi_s$ is the potential of the Si surface, $q$ is an elementary charge, $N_{ss}(F_s)$ is the density of interface states with a continuous energy distribution, $F_s$ is the Fermi level at the semiconductor surface, $F_s = F_0 - q\varphi_s$, $F_0 = -kT \ln(N_d/N_c)$, $k$ is Boltzmann's constant, $N_d$ is the dopant concentration in the Si substrate, and $N_c$ is the effective density of states in the semiconductor conduction band.

Having the experimental $C_{\rm rf}(T)$ curve and following the algorithm described in Ref. 9, we can find $C_v(T)$, $\varphi_s(T)$, the derivative $d\varphi_s/dT$ by numerical differentiation, and, thereby, the density of interface states $N_{ss}(F_s)$.

Figure 4 presents the spectrum of interface states $N_{ss}(F_s)$ obtained from $I(T)$ and $C_{\rm rf}(T)$ (curve *1*), as well as a plot of $N_{ss}(F_s)$ found from a treatment of the quasistatic and radio-frequency capacitance-voltage characteristics (curve *2*) according to the procedure described above with consideration of the replacements $\beta_T \to \beta_V$ and $T \to V_s$. It can be seen that the presence of ions at the $Si-SiO_2$ interface modifies the spectrum of interface states dramatically: apart from the increase in the density of states on the spectrum tail, which is caused both by the fluctuation potential[16] and by other effects,[6,7] there is also a peak at $F_s \approx 260$ meV. In addition, the number of states in the peak is $N_s \approx 3 \times 10^{11}\,{\rm cm}^{-2}$, which coincides to within 25% with the number of neutral particles $N_0$. Similar ''generation'' of a peak in the density of interface states was observed in Ref. 8, but no experiments have been performed to reveal the number of neutralized mobile ions, and there has not been any comparison with data from the spectroscopy of the $Si-SiO_2$ interface.

Thus, it can be concluded from the results of this work that the mobile ions found at the $Si-SiO_2$ interface are partially neutralized by trapping electrons from the semiconduc-

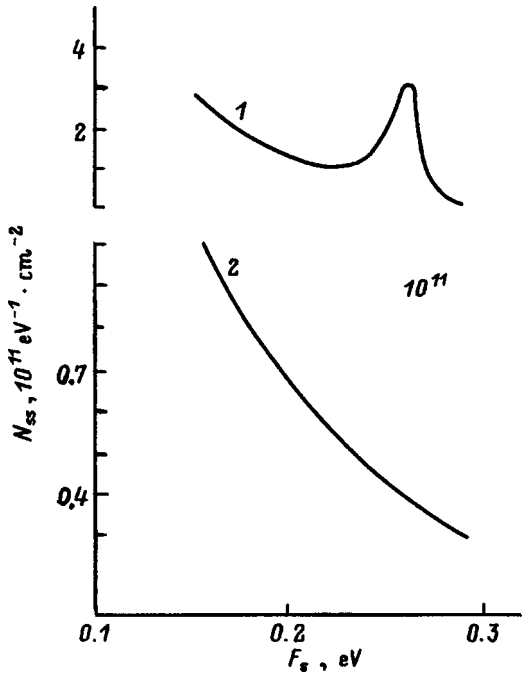


FIG. 4. Energy dependence of the density of interface electron states before (*2*) and after (*1*) a polarizing thermal treatment of the sample.

tor layer of the MOS structure. The drift of $Q_m$ toward the metallic electrode stimulated by the temperature or an electric field is accompanied by deneutralization of that portion of the ions, which is manifested in the form of features on the $I(T)$ and $I(V_s)$ curves. In addition, the spectroscopy of the interface performed by treating synchronously measured $I(T)$ and $C_{\rm rf}(T)$ curves reveals a monoenergetic peak in the effective density of interface states, in which the number of states corresponds to the number of neutral particles. This provides evidence that the kinetics of the deneutralization process are described by a single activation energy. In other words, a portion of the mobile ionic charge is neutralized initially by the capture of ions on interface traps (i.e., by the localization of ions at the $Si-SiO_2$ interface) with the subsequent trapping of electrons from the semiconductor on them.

A more complete study of the mechanism of the neutralization of mobile ions on the semiconductor-insulator interface requires isolating the component caused by deneutralization of the particles from the total current $I(T)$ [or $I(V_s)$]. The solution of this problem will be the subject of our next paper, in which we shall examine the emission of ions from surface ion traps.

Surface-charge formations were considered as a model of such traps in Ref. 14. One characteristic feature of such traps is that they have long-range Coulomb and/or dipole potentials, which leads to a field dependence of the rate of emission of particles trapped on them in proportion to $\exp(\alpha\mathcal{E}^{\gamma}/kT)$, where $\alpha$ is a proportionality factor, whose form depends on the nature and parameters of the spots,[14] $\mathcal{E}$ is the external electric field, and $1/2<\gamma<2/3$. In the case of charged ''circular'' spots ($\gamma=1/2$) we have $\alpha>\alpha_0=q^{3/2}[(\varkappa_2-\varkappa_1)/\varkappa_1(\varkappa_1+\varkappa_2)]^{1/2}$ ($\varkappa_1$ and $\varkappa_2$ are the dielectric constants of the contacting media) when lowering of the barrier height occurs because of the image forces[17,18] (the normal Schottky effect).

[1] A. P. Baraban, V. V. Bulavinov, and P. P. Konorov, *Electronics of $SiO_2$ Layers on Silicon* [in Russian], Izd. LGU, Leningrad (1988).
[2] V. N. Vertoprakhov, B. M. Kuchumov, and E. G. Sal'man, *Structure and Properties of $Si/SiO_2/M$ Structures* [in Russian], Nauka, Sib. Otd., Novosibirsk (1981).
[3] Yu. A. Gorokhovatskiĭ and G. A. Bordovskiĭ, *Thermally Stimulated Current Spectroscopy of High-Resistivity Semiconductors and Insulators* [in Russian], Nauka, Moscow (1991).
[4] B. R. Singh and K. Singh, Microelectron. Reliab. **15**, 385 (1976).
[5] T. Ando, A. B. Fowler, and F. Stern, ''Electronic properties of two-dimensional systems,'' Rev. Mod. Phys. **54**, 437–672 (1982) [Mir, Moscow (1985)].
[6] E. Rosencher and R. Coppard, J. Appl. Phys. **55**, 971 (1984).
[7] M. W. Hillen and D. G. Hemmes, Solid-State Electron. **24**, 773 (1981).
[8] J. G. Hwu, J. Z. Hwang, and Y. L. Chiou, Thin Solid Films **125**, 17 (1985).
[9] V. V. Batavin, Yu. A. Kontsevoĭ, and Yu. V. Fedorovich, *Measurement of the Parameters of Semiconductor Materials and Structures* [in Russian], Radio i Svyaz', Moscow (1985).
[10] T. Hino and K. Yamashita, J. Appl. Phys. **50**, 4879 (1979).
[11] T. W. Hickmott, J. Appl. Phys. **46**, 2583 (1975).
[12] P. K. Nauta and M. W. Hillen, J. Appl. Phys. **49**, 2862 (1978).
[13] M. R. Boudry and J. P. Stagg, J. Appl. Phys. **50**, 942 (1979).
[14] S. G. Dmitriev and Yu. V. Markin, Fiz. Tekh. Poluprovodn. **30**, 1231 (1996) [Semiconductors **30**, 649 (1996)].
[15] A. G. Zhdan and Yu. V. Markin, Fiz. Tekh. Poluprovodn. **28**, 756 (1994) [Semiconductors **28**, 444 (1994)].
[16] V. A. Gergel' and R. A. Suris, Zh. Éksp. Teor. Fiz. **84**, 719 (1983) [Sov. Phys. JETP **57**, 415 (1983)].
[17] J. P. Stagg and M. R. Boudry, J. Appl. Phys. **52**, 885 (1981).
[18] G. Greeuw and J. F. Verwey, Solid-State Electron. **28**, 509 (1985).

Translated by P. Shelnitz

## LOW-DIMENSIONAL SYSTEMS

# Transformation of nonradiative recombination centers in GaAs/AlGaAs quantum well structures upon treatment in a $CF_4$ plasma followed by low-temperature annealing

K. S. Zhuravlev, A. L. Sokolov, and K. P. Mogil'nikov

*Institute of Semiconductor Physics, Russian Academy of Sciences, Siberian Branch, 630090 Novosibirsk, Russia*

(Submitted April 7, 1998; accepted for publication April 23, 1998)
Fiz. Tekh. Poluprovodn. **32**, 1450–1455 (December 1998)

The influence of low-temperature annealing on the photoluminescence of GaAs/AlGaAs single-quantum-well structures treated in a low-energy $CF_4$ plasma is investigated. It is established that annealing at 160–300 °C causes a decrease of the photoluminescence intensity of the quantum wells located in the near-surface region, while annealing at 350–450 °C leads to partial restoration of their photoluminescence. The activation energy for the diffusion of plasma-produced point defects and the activation energy for the annealing of these defects are determined. These energies are equal to 150 and 540 meV, respectively. It is discovered that the photoluminescence of the quantum wells near the substrate, which had a low intensity in the as-grown sample, increases after treatment in the plasma and decreases after subsequent annealing monotonically with increasing annealing temperature. Repeated treatment in a $CF_4$ plasma leads to a repeated increase in the photoluminescence intensity of these quantum wells. It is theorized that the defects induced by the $CF_4$ plasma form complexes with defects introduced during growth and that these complexes are not recombination centers. After low-temperature annealing, the complexes dissociate, and the nonradiative recombination centers are recreated.  [S1063-7826(98)00812-6]

### 1. INTRODUCTION

Treatment in a low-energy fluorine-containing plasma is widely used to selectively remove $SiO_2$ and $Si_3N_4$ masks from the surfaces of III–V structures during the fabrication of various microelectronic devices and low-dimensional structures. To completely remove the mask material, the structures are subjected to etching, during which the lower-lying layers are bombarded by plasma ions and damaged. The defects introduced as a result significantly alter the luminescence and electrical properties of the near-surface layers of the structures.[1–14]

Wong *et al.*[1] suggested that the defects produced in the near-surface region of structures could be studied by investigating the photoluminescence (PL) spectra of GaAs/AlGaAs single-quantum-well structures. The exposure of such structures to a low-energy plasma leads to a decrease in the PL intensity of the quantum wells (QW's) located in the near-surface region due to the production of point defects which act as nonradiative recombination centers. We discovered that the exposure of GaAs/AlGaAs QW structures to a low-energy plasma ($CF_4$, Ar, or Kr) can cause not only a decrease, but also an increase in the PL of QW's that are deeper than the damaged region.[4] In the present work, to ascertain the reasons for the plasma-induced increase in the PL of QW's, we investigated the influence of the annealing temperature on the PL intensity of QW's in structures exposed to a low-energy $CF_4$ plasma.

### 2. EXPERIMENTAL CONDITIONS

A GaAs/$Al_{0.3}Ga_{0.7}As$ structure grown on a substrate of semi-insulating GaAs(100) was used in the experiment. It consisted of a GaAs buffer layer with a thickness of 1 $\mu$m, an $Al_{0.3}Ga_{0.7}As$ layer with a thickness of 0.5 $\mu$m, and six GaAs QW's with thicknesses of 2.2, 2.8, 3.4, 4.2, 5.6, and 8.5 nm, which were separated by $Al_{0.3}Ga_{0.7}As$ barriers with a thickness of 24 nm. The thickness of the QW's increased with increasing depth within the structure. A short-period GaAs/AlAs superlattice was grown within a 0.5-$\mu$m $Al_{0.3}Ga_{0.7}As$ layer to prevent the diffusion of impurities and point defects into the structure from the substrate. The structure was covered by a GaAs overlayer with a thickness of 10 nm. The treatment was carried out in a $CF_4$ plasma at a pressure of 0.07 Torr, a power density of 1 W/cm$^2$, and a self-bias voltage equal to roughly $-300$ V. Rapid thermal anneals were carried out in an argon atmosphere successively at temperatures from 160 to 450 °C for 30 s at each temperature. The structures were heated by 20 kW incandescent halogen lamps. The vaporization of arsenic from the surface was prevented by covering the sample with a GaAs wafer. The PL was excited by a He–Ne laser operating at a wavelength of 632.8 nm with a power density of 20 W/cm$^2$. The

 

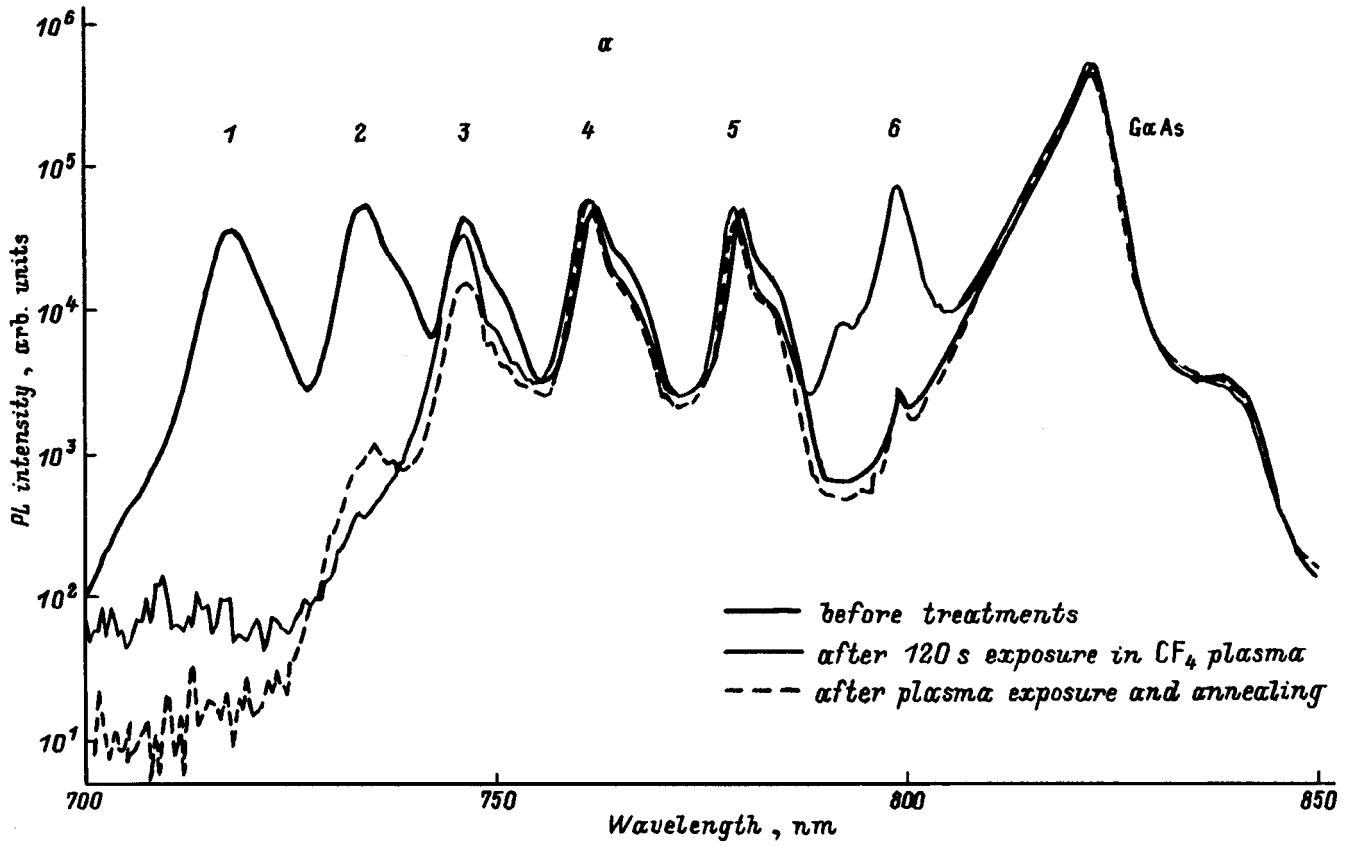


FIG. 1. a) Variation of the PL spectrum of a GaAs/AlGaAs quantum-well structure as a result of treatment of the structure in a low-energy $CF_4$ plasma followed by annealing: thick line — PL spectrum of the as-grown sample; thin line — PL spectrum of the sample after exposure to the plasma; dashed line — PL spectrum after annealing of the sample at 450 °C. The numbers *1–6* correspond to the PL lines from the quantum wells with thicknesses equal to 2.2, 2.8, 3.4, 4.2, 5.6, and 8.5 nm, respectively. b) Variation of the PL spectrum as a result of repeated treatment of the structure in the $CF_4$ plasma and repeated annealing: thick line — PL spectrum of the sample after the first treatment in the plasma and the first anneal; dashed line — PL spectrum of the sample after repeated plasma treatment; thin line — PL spectrum of the sample after repeated annealing. The numbers *1–6* correspond to the PL lines from the quantum wells with thicknesses equal to 2.2, 2.8, 3.4, 4.2, 5.6, and 8.5 nm, respectively.

absorption coefficients of GaAs and $Al_{0.3}Ga_{0.7}As$ for that wavelength at 77 K are equal to $3\times10^4$ and $1\times10^4$ $cm^{-1}$, respectively; therefore, about 3% of the exciting radiation was absorbed near each quantum well in the structure used, ensuring their uniform excitation.

### 3. RESULTS

Figure 1a shows the PL spectra of a GaAs/AlGaAs QW structure before exposure, after 120 s of exposure to the low-energy $CF_4$ plasma, and after low-temperature ($T=450$ °C) annealing of the plasma-treated structure. It is seen from the figure that the spectrum of the as-grown sample contains seven lines. The PL line with a maximum at 822 nm corresponds to a band-to-band transition in the GaAs layer. The other six lines correspond to transitions between size-quantized levels of electrons and heavy holes ($1ehh$) in the six QW's of different thickness. The intensities of the PL lines of the five QW's closest to the surface of the structure are also roughly identical, attesting to the good quality of the QW's. At the same time, the PL intensity of the line of the QW that is farthest from the surface of the structure is significantly smaller, apparently because of the large concentration of defects formed when this QW was grown, which act as nonradiative recombination centers. After exposure of the structure to the $CF_4$ plasma for 120 s, the intensity of the PL lines of the two QW's closest to the surface decreases, and the intensity of the PL lines of the deepest QW increases. After the structure is annealed at $T=450$ °C, the intensity of the PL lines of the QW's closest to the surface is partially restored, while the intensity of the PL line of the deepest QW decreases and essentially returns to the PL intensity level observed in the structure before exposure to the plasma. It should be noted that the energetic position of the PL lines does not vary as a result of exposure of the structure to the plasma and subsequent annealing.

As can be seen from Fig. 1b, repeated exposure of the annealed structures to the $CF_4$ plasma again leads to an increase in the PL intensity of the deepest QW, and subsequent annealing of the structure causes a drop in its PL. Such behavior of the PL is an indication of the reversible character of the processes occurring in the vicinity of the QW closest to the substrate during treatment in the $CF_4$ plasma and low-temperature annealing.

Figure 2 shows the variation of the PL intensities of the QW's normalized to the PL intensity of the QW's in the as-grown structure as a result of treatment in the $CF_4$ plasma at various temperatures. The PL of a GaAs layer, which was placed fairly far from the surface of the structure and was not

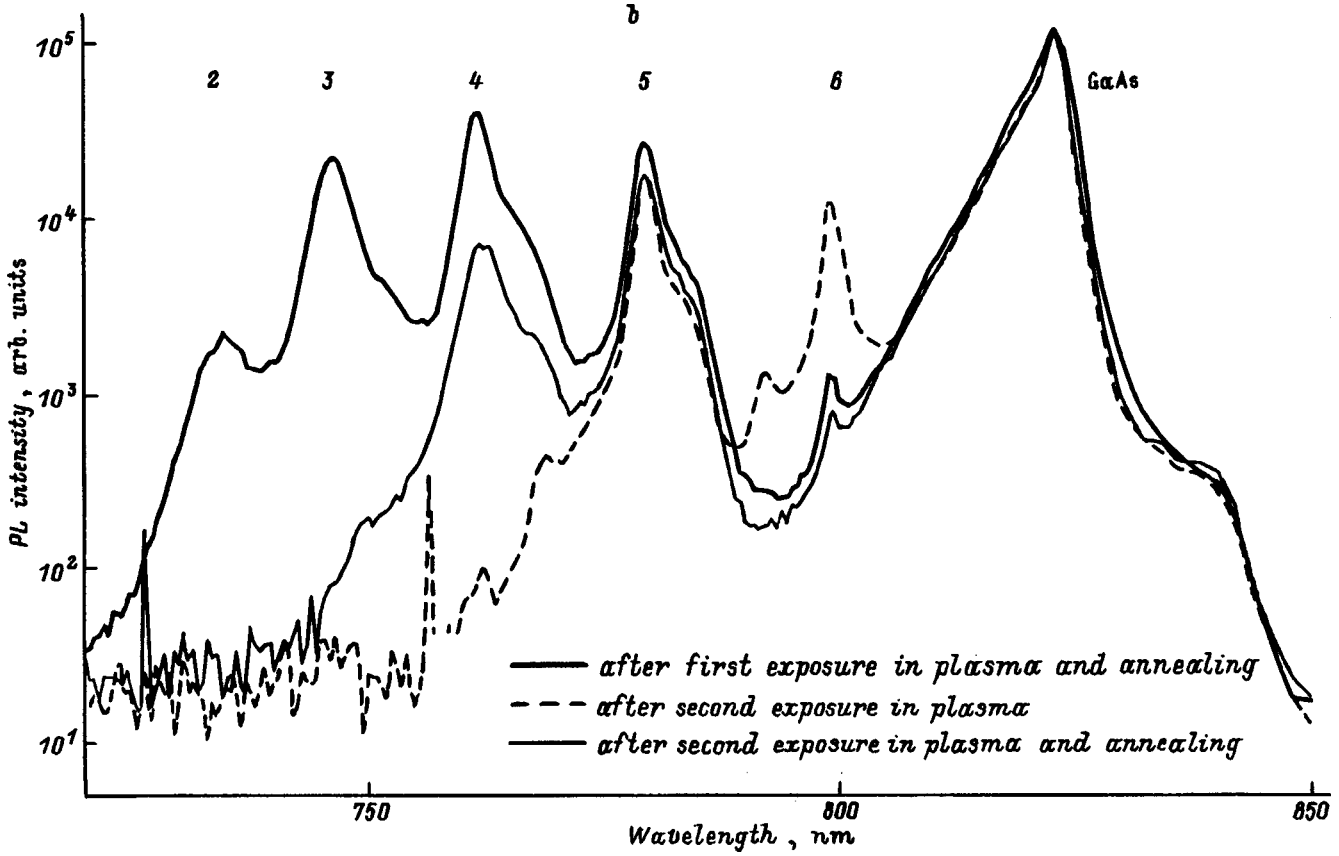


FIG. 1. (continued).

damaged during exposure to the plasma, served as a marker for the normalization. The PL line of the QW closest to the surface was not detected after exposure to the plasma. The PL intensity of the next four QW's decreased after treatment in the plasma and continued to decrease as the annealing temperature was raised from 160 to 300 °C. When the annealing temperature was increased further from 300 to 450 °C, the PL intensity of these QW increased. It can also be seen from the figure that the PL intensity of the deepest QW, unlike the intensity of the PL lines of the other QW's, increased by more than 10 fold after exposure to the plasma and decreased monotonically upon subsequent annealing of the structure.

#### 4. DISCUSSION

The experimental results obtained provide evidence that two competing processes take place during annealing in the portion of the structure damaged by the plasma. At low annealing temperatures (below 300 °C) the process leading to an increase in the rate of nonradiative recombination in the QW's dominates. In the vicinity of each QW there is probably an increase in the concentration of point defects, which diffuse from the near-surface plasma-damaged region in the structure. The data obtained permit determination of the thermal activation energy for the diffusion of these defects. In fact, after exposure to the $CF_4$ plasma, the PL of the second QW from the surface of the structure (2.8 nm) drops by roughly 100 fold, and nonradiative recombination is the dominant process in it. In this case the PL intensity $I_{PL}$ is inversely proportional to the concentration of nonradiative recombination centers ($N_{NR}$), and if it is assumed that one type of nonradiative recombination centers dominates, the following relation holds:

$$I_{PL}/I_0 = 1/(a \cdot N_{NR}). \tag{1}$$

Here $I_0$ is the intensity of the exciting light, and $a$ is a coefficient, which depends on the cross section for the trapping of carriers on the recombination centers, which cannot be determined from the available data.

Figure 3a shows the dependence of the concentration of nonradiative recombination centers for the second QW well from the surface of the structure on annealing temperature, which was constructed using (1), as well as an approximation of this dependence by an expression of the form

$$N_{NR} = N_0 \exp(-x^2/(4 \cdot t \cdot D))/(2\sqrt{\pi \cdot D \cdot t}), \tag{2}$$

which describes the variation of the defect density in the case of diffusion from an infinitely thin source.[15] Here $N_0$ is the initial concentration of nonradiative recombination centers, $x$ is the distance from the surface of the structure to the QW, $t$ is the annealing time, and $D$ is the diffusion coefficient of the defects, whose temperature dependence has the form

$$D = D_0 \exp[-E_a/kT], \tag{3}$$

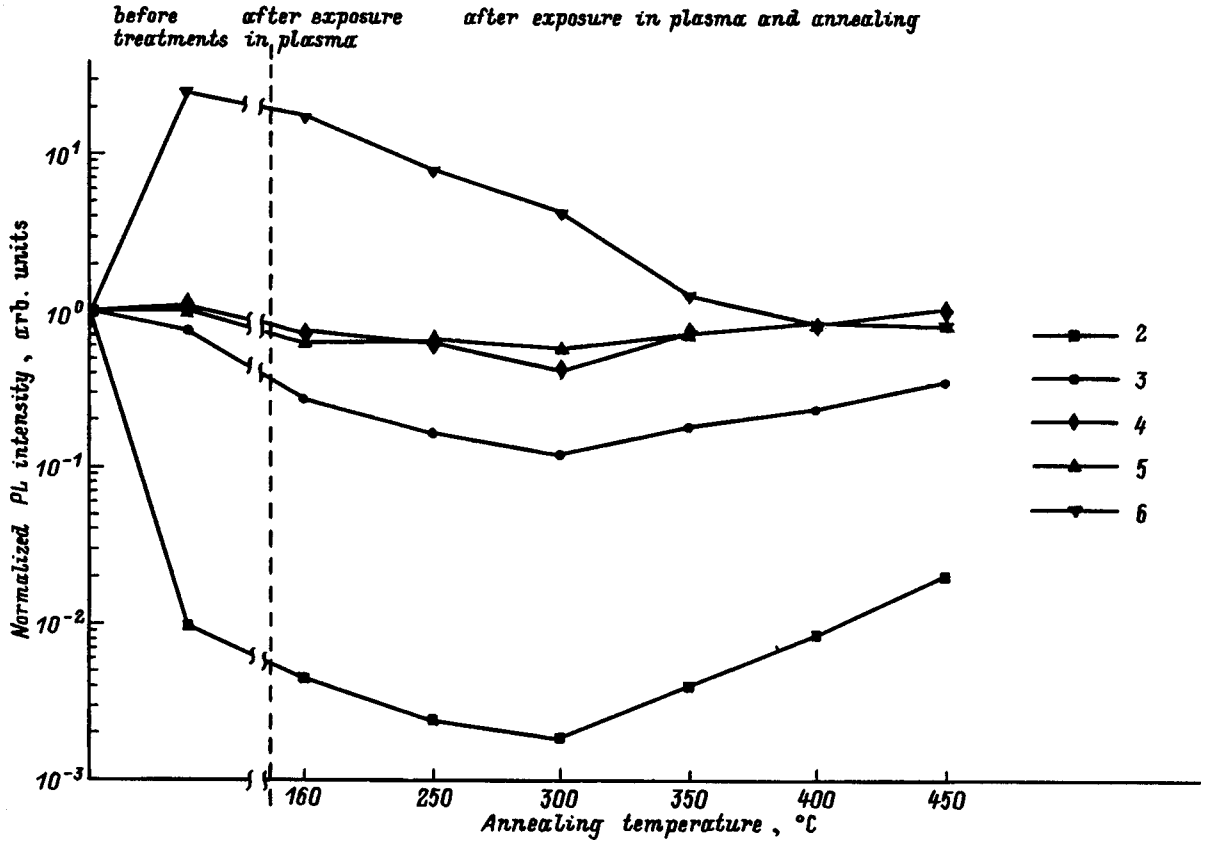


FIG. 2. Variation of the normalized PL intensity of different QW's (from the second to the sixth) as a consequence of plasma treatment followed by annealing at various temperatures.

where $D_0$ is the preexponential factor, $E_a$ is the activation energy for the diffusion of defects, $T$ is the temperature, and $k$ is Boltzmann's constant.

The best fit between the experimental and calculated curves in the temperature range 160–300 °C is achieved for the values $E_a = 0.15 \pm 0.07$ eV and $D_0 = (8.4 \pm 6.6) \times 10^{11}$ cm$^2$/s. It should be noted that the value of $E_a$ obtained is considerably smaller than the values of the activation energies for the diffusion of intrinsic point defects in GaAs, which are equal to 1.5−3 eV.[16] The diffusion of defects is probably facilitated significantly in the plasma-damaged region of the structure.

At annealing temperatures above 300 °C the PL of the QW's is partially restored, probably as a result of the annealing of the plasma-induced defects. Figure 3b presents the experimental dependence of the defect density in the region of the second QW from the surface on reciprocal temperature and its approximation by a curve of the form

$$N_{\mathrm{NR}} = N_0 \exp(-E_A/kT). \tag{4}$$

The thermal activation energy of this process is $E_A = 0.54 \pm 0.04$ eV.

As can be seen from Fig. 2, the PL-quenching defects reach only the fourth QW from the surface (4.2 nm) and do not go deeper. Nevertheless, the PL intensity of the sixth or deepest QW, which increases after exposure to the plasma, decreases when the structure is annealed. The increase in the PL intensity of this QW after exposure of the structures to the plasma can be due to the annihilation or transformation of the defects which act as nonradiative recombination centers and existed in the structure before the treatment as a result of their interaction with point defects formed during exposure of the structures to the plasma. We previously theorized that the increase in PL is a result of the annihilation of vacancies introduced during growth of the QW with interstitial atoms which diffuse with anomalous speed from the damaged region.[4] This hypothesis is not confirmed by the results obtained in this work. In fact, the energy for the formation of vacancies amounts to at least 1 eV (Ref. 16), and the probability of their formation is very small at the annealing temperatures used in this work. The increase in PL is probably due to the formation of complexes consisting of rapidly diffusing plasma-induced defects and defects introduced into the QW's when the structure was grown. These complexes are not recombination centers. When the structures are annealed, the complexes dissociate, and the growth defects, which are nonradiative recombination centers, are released. Evidence that annealing leads to the restoration of defects of this type, rather than to the introduction of new defects, is provided by the possibility of removing the defects introduced during an anneal by repeated treatment in the plasma.

During exposure to the plasma, intrinsic point defects of the semiconductor can form, or chemical impurities present in the chamber of the plasma-treatment system can be im-

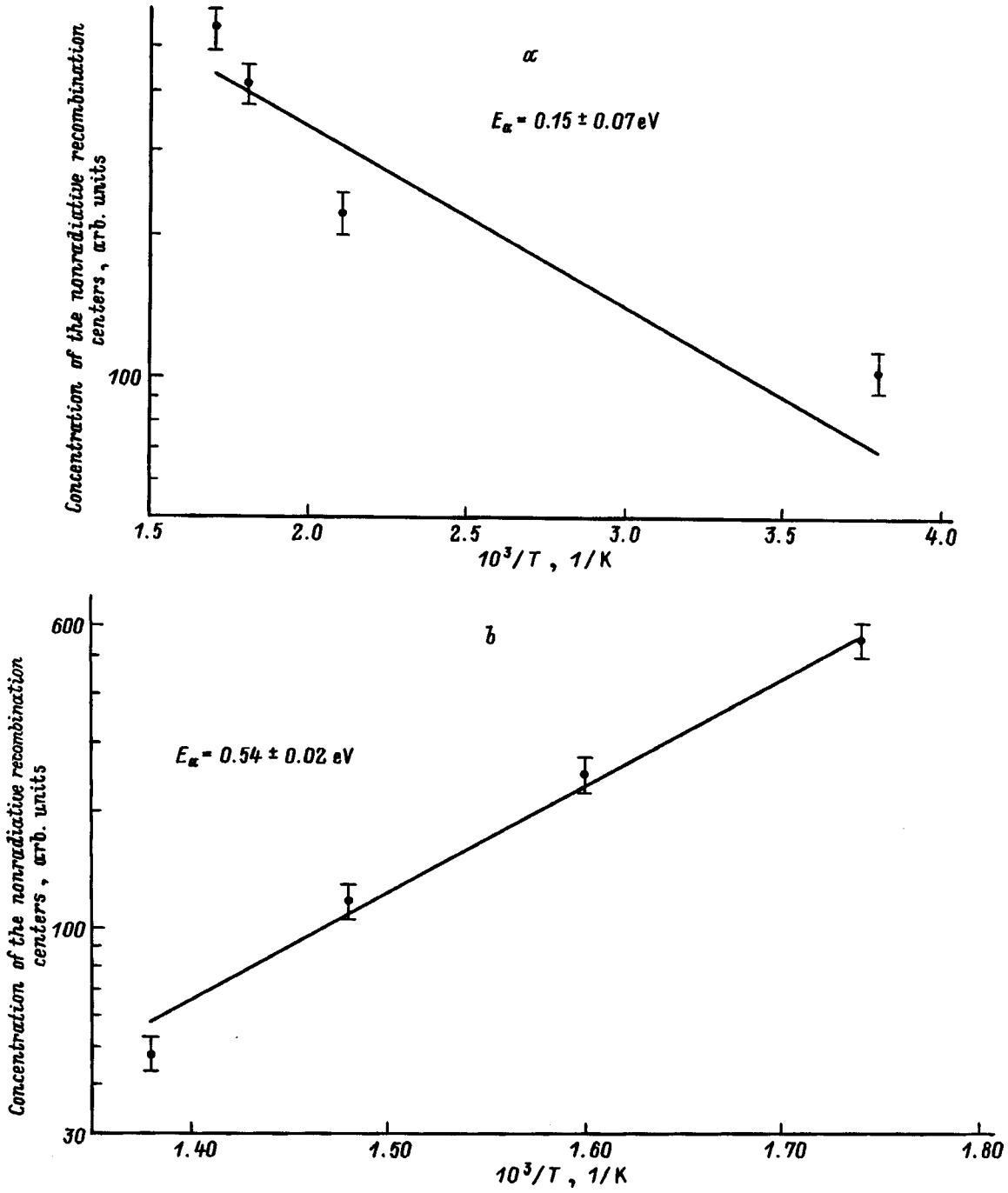


FIG. 3. Dependence of the concentration of nonradiative recombination centers in the vicinity of the second QW from the surface of the structure on reciprocal annealing temperature in the temperature ranges 300–450 °C (a) and 160–300 °C (b). Individual points — experimental data, solid line — calculated curve.

planted. As far as we know, the possibility of passivating nonradiative recombination centers by intrinsic point defects has not been discussed in the literature. On the other hand, it has been established that the defects which act as nonradiative recombination centers in GaAs and GaAs/AlGaAs structures can be passivated by hydrogen, which forms complexes with these defects.[10–12] It is also known that such complexes dissociate when these structures are subjected to low-temperature ($T \leqslant 450$ °C) annealing.[10] Hydrogen might be present in the plasma-treatment system and implanted in the structures; therefore, we have undertaken investigations aimed at elucidating the role of hydrogen in the phenomena described above.

## 5. CONCLUSION

The influence of low-temperature annealing on the PL of GaAs/AlGaAs single-quantum-well structures that were treated in a low-energy $CF_4$ plasma has been studied in this work. It has been discovered that annealing at 160–300 °C leads to a decrease in the PL intensity of QW's located in the plasma-damaged near-surface region and that annealing at

350–450 °C leads to partial restoration of their PL. The decrease in the PL intensity is associated with an increase in the concentration of defects diffusing from the surface into the structure, and the restoration of the PL is associated with annealing of these defects. The activation energy for diffusion of the defects (0.15 eV) and the activation energy for recombination of the defects (0.54 eV) have been determined. It has been established that the PL intensity of the deepest QW, which increases after exposure to the plasma, decreases monotonically with increasing annealing temperature and that repeated exposure of the annealed structure to the plasma restores the PL of that QW. It has been postulated that the increase in the PL intensity of the QW's during exposure to the plasma is caused by the passivation of defects introduced into the structure during growth as a result of the formation of complexes of those defects with plasma-induced defects. These complexes dissociate during low-temperature annealing.

[1] H. F. Wong, D. L. Green, T. Y. Liu, D. G. Lishan, M. Bellis, E. L. Hu, P. M. Petroff, P. O. Holtz, and J. L. Merz, J. Vac. Sci. Technol. B **6**, 1906 (1988).
[2] A. V. Murel', A. P. Kasatkin, and V. M. Kogan, Izv. Ross. Akad. Nauk, Ser. Fiz. **56**, 161 (1992).
[3] B. S. Ooi, A. C. Bryce, C. D. W. Wilkinson, and J. H. Marsh, Appl. Phys. Lett. **64**, 598 (1994).
[4] K. S. Zhuravlev, V. A. Kolosanov, M. Holland, and I. I. Marakhovka, Fiz. Tekh. Poluprovodn. **31**, 1436 (1997) [Semiconductors **31**, 1241 (1997)].
[5] K. S. Zhuravlev, V. A. Kolosanov, V. G. Plyukhin, and T. S. Shamirzaev Zh. Tekh. Fiz. **64**(11), 185 (1994) [Tech. Phys. **39**, 1188 (1994)].
[6] C. Juang, J. K. Hsu, I. S. Yen, and H. S. Shiau, J. Appl. Phys. **72**, 684 (1992).
[7] S. V. Dubonos and S. V. Koveshnikov, Phys. Status Solidi A **77**, 120 (1990).
[8] W. Beinstingl, R. Christanel, J. Smoliner, C. Wirner, E. Gornik, G. Weinmann, and W. Shlapp, Appl. Phys. Lett. **57**, 177 (1990).
[9] F. Ren, J. W. Lee, C. R. Abernathy, C. Constantine, C. Barratt, and R. J. Shul, Appl. Phys. Lett. **70**, 2410 (1997).
[10] J. C. Nabity, Michael Stavola, J. Lopata, W. C. Dautremont–Smith, C. W. Tu, and S. J. Pearton, Appl. Phys. Lett. **50**, 921 (1987).
[11] A. W. Leich, T. Prescha, and J. Weber, Phys. Rev. B **44**, 1375 (1991).
[12] É. M. Omel'yanovskiĭ, A. V. Pakhomov, and A. Ya. Polyakov, Fiz. Tekh. Poluprovodn. **21**, 842 (1987) [Sov. Phys. Semicond. **21**, 514 (1987)].
[13] É. M. Omel'yanovskiĭ, A. V. Pakhomov, A. Ya. Polyakov, and L. V. Kulikova, Fiz. Tekh. Poluprovodn. **21**, 1762 (1987) [Sov. Phys. Semicond. **21**, 1068 (1987)].
[14] J. M. Zavada, H. A. Jenkinson, R. G. Sarkis, and R. G. Wilson, J. Appl. Phys. **58**, 3731 (1985).
[15] B. I. Boltaks, *Diffusion in Semiconductors* (Academic Press, New York 1963; GIFML, Moscow, 1961).
[16] J. F. Wager, J. Appl. Phys. **69**, 3022 (1991).

Translated by P. Shelnitz

# Weak localization and intersubband transitions in $\delta$-doped GaAs

G. M. Min'kov, S. A. Negashev, O. É. Rut, and A. V. Germanenko

*Ural University, 620083, Ekaterinburg, Russia*

V. V. Valyaev and V. L. Gurtovoĭ

*Institute of Semiconductor Technology and Microelectronics, Russian Academy of Sciences, 142432 Chernogolovka, Russia*

(Submitted April 1, 1998; accepted for publication May 13, 1998)
Fiz. Tekh. Poluprovodn. **32**, 1456–1460 (December 1998)

The negative magnetoresistance in $\delta$-doped GaAs is investigated experimentally. It is shown for highly perfect structures that the value of the prefactor in the expression for the negative magnetoresistance significantly exceeds the theoretical value for a two-dimensional film with a single filled size-quantized subband. The role of a large number of filled subbands and intersubband transitions is discussed. It is shown that the symmetry of the wave functions and the scattering potential in $\delta$-doped layers can cause the times of interband transitions between subbands with different parity ($\tau_{i,j}$) to be greater than the phase-relaxation time of the wave function ($\tau_\varphi$). Such a relation between $\tau_{i,j}$ and $\tau_\varphi$ should be manifested as a significant increase in the prefactor. © *1998 American Institute of Physics.* [S1063-7826(98)00912-0]

Since the pioneering work in Refs. 1 and 2, weak localization and the associated phenomenon of negative magnetoresistance have been investigated in detail in various systems: three-dimensional and classical thin films ($1/k_F \ll d \ll D\tau_\varphi$, where $d$ is the film thickness, $D$ is the diffusion coefficient, $\tau_\varphi$ is the phase-relaxation time of the carrier wave function, and $k_F$ is the quasimomentum of an electron at the Fermi level) and structures with size-quantized states ($d \approx 1/k_F$). In the latter case two situations are possible: one or several size-quantized subbands are filled. Weak localization and negative magnetoresistance have been studied most thoroughly in structures with two-dimensional (2D) carriers when only one size-quantized subband is filled. In this case the negative magnetoresistance, which is caused by magnetic-field suppression of the interference correction to the conductivity, is given in the isotropic case with $\mathbf{B} \| \mathbf{n}$ ($\mathbf{n}$ is a normal to the plane of the structure) by the known expression[3]

$$\Delta\sigma(B) = \alpha G_0 \varphi_1 = \alpha G_0 \left[ \Psi\left(0.5 + \frac{l^2}{4D\tau_\varphi}\right) - \Psi\left(0.5 + \frac{l^2}{4D\tau_p}\right) + \ln\left(\frac{\tau_\varphi}{\tau_p}\right) \right], \quad (1)$$

with the prefactor $\alpha = 1$. Here

$$G_0 = \frac{e^2}{2\pi^2\hbar}, \quad l^2 = \frac{c\hbar}{eB}, \quad D = \frac{\sigma}{e^2 N_F}, \quad N_F = \frac{m^*}{\pi\hbar^2},$$

$D$ is the diffusion coefficient, $N_F$ is the density of states at the Fermi level, $m^*$ is the effective mass, $\tau_p$ and $\tau_\varphi$ are the momentum and phase relaxation times of the wave function, respectively, and $\Psi(x)$ is a digamma function. (We shall not discuss the contribution of the electron-electron interaction to the negative magnetoresistance in the structures investigated further.)

In structures with several filled size-quantized subbands the negative magnetoresistance depends significantly on the relation between the intersubband transition times ($\tau_{i,j}$) and $\tau_\varphi$.[4] It is easy to understand the results in two extreme cases: $\tau_{i,j} \gg \tau_\varphi$ and $\tau_{i,j} \ll \tau_\varphi$. In the former case each subband makes an independent contribution to the conductivity, and the expression for $\Delta\sigma(B)$ can be written in the form

$$\Delta\sigma(B) = \sum_i \Delta\sigma_i(B). \quad (2)$$

In the latter case ($\tau_{i,j} \ll \tau_\varphi$) the expression for $\Delta\sigma(B)$ coincides with (1), in which the values of $D$ and $\tau_\varphi$ should be replaced by their effective values:[4,5]

$$D_{\text{eff}} = \sum_i D_i \frac{N_F^i}{N_F}, \quad \frac{1}{\tau_\varphi^{\text{eff}}} = \sum_i \frac{1}{\tau_\varphi} \frac{N_F^i}{N_F},$$

$$N_F = \sum_i N_F^i, \quad (3)$$

where $D_i$ and $N_F^i$ are the diffusion coefficient and the density of states in the $i$th subband.

It has usually been assumed in analyses of negative magnetoresistance in metal-insulator-semiconductor structures and heterostructures[6] that $\tau_{i,j} \ll \tau_\varphi$. This is probably true for such structures, since at the low temperatures used to investigate negative magnetoresistance $\tau_\varphi$ is of the order of $10^{-11}-10^{-12}$ s and is thus $2-3$ orders of magnitude greater than $\tau_p$. Although $\tau_{i,j}$ exceeds $\tau_p$ by several fold,[7] it is still much smaller than $\tau_\varphi$.

 

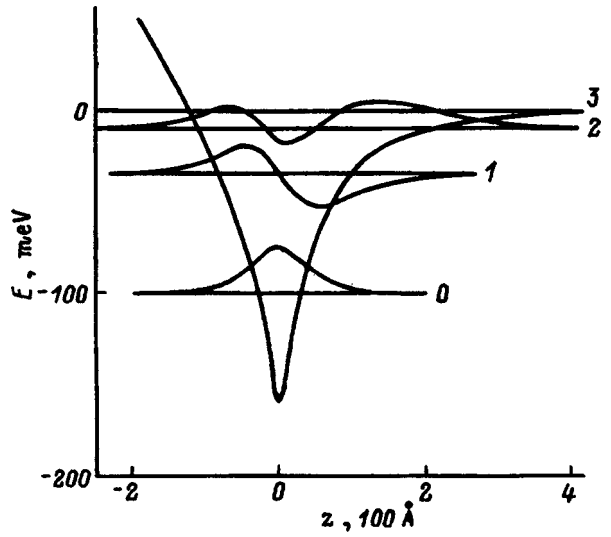


FIG. 1. Energy diagram and wave functions of a structure with a $\delta$ layer. The parameters of sample $1L$ were used in the calculation. The wave function of subband 3 is not shown to avoid cluttering the figure.

From the standpoint of intersubband transitions, $\delta$-doped layers stand out as an entirely separate case. There are several reasons for this.

1. In the case of $\delta$-doped layers at a fairly large distance from the semiconductor surface, where the field created by the Schottky barrier is small, the potential $V(z)$, which forms the size-quantized levels, is essentially symmetric relative to the doping plane near the $\delta$ layer (Fig. 1); therefore, the electronic wave functions $F_n(x,y,z)=f(z)_n f_n(x,y)$ have a definite parity with respect to $z$.

2. Intersubband transitions occur in response to the scattering potential $V_{sc}$, which is equal to the difference between the local potential $[\Sigma e/\kappa(r-r_i)+V_e$, where $e/\kappa(r-r_i)$ is the potential of a single impurity and $V_e$ is the electron potential] and the mean potential, which is equal to the sum of the potential of a uniformly charged plane $(E_0/|z|)$ with the charge density $en_e$ ($n_e$ is the concentration of the charged impurity) and the electron potential. This potential

$$V_{sc}=\sum e/\kappa(r-r_i)-E_0|z|$$

decays rapidly in the $z$ direction with a parameter of the order of 20 Å.

Transitions between subbands with different parity can occur only in response to the odd part of the scattering potential, which appears only when the position of the impurity deviates from the doping plane, and thus in an ideal structure such transitions are forbidden by virtue of the symmetry conditions. In real $\delta$-doped structures the thickness of the layer containing the impurity ($d$) usually equals $10-15$ Å, and the matrix element for transitions between states with different parity is small, being of the order of $d/\langle z\rangle$, where $\langle z\rangle \simeq 100-200$ Å is the characteristic size of the wave function in the $z$ direction.

Thus, in $\delta$ layers the relation $\tau_{i,j}>\tau_\varphi$ can be satisfied for transitions between states with different parity. The time of a transition between states with the same parity is probably not significantly greater than $\tau_p$, and the reverse relation $\tau_{i,j}<\tau_\varphi$ holds for them, i.e., $\delta$ layers can exhibit an unusual (for interference effects) situation, in which the entire electronic system is divided into two subsystems: carriers in even subbands and carriers in odd subbands. The condition $\tau_{i,j}<\tau_\varphi$ holds within each of them, and the condition $\tau_{i,j}>\tau_\varphi$ is satisfied for transitions between them. In this case the negative magnetoresistance is determined by a correction to the conductivity in the form of the sum of the contributions from the even ($\Delta\sigma_{even}$) and odd ($\Delta\sigma_{odd}$) subbands,

$$\Delta\sigma=\Delta\sigma_{even}+\Delta\sigma_{odd}, \tag{4}$$

each of which is given by (1) with the corresponding effective parameters (3). The direct application of this expression to the analysis of experimental results is senseless, since it requires knowledge of a large number of parameters, viz., $D$, $\tau_p$, and $\tau_\varphi$, for each of the systems of subbands. If the expression (1) is used in such an analysis, as we shall do in our analysis of all the experimental results, then the special feature of $\delta$ layers indicated above should be manifested as a need to introduce a prefactor $\alpha>1$. When the values of $D$ and $\tau_\varphi$ in the even and odd subbands are equal, the prefactor should be equal to 2.

TABLE I. Parameters of the samples investigated.

| Sample No. [a] | $n_e, 10^{12}$ cm$^{-2}$ | $\mu$, $10^3$ cm$^2$/(V·s) | $B_{th}$, kOe | $\alpha$ ($T=4.2$ K) | Number of of subbands [b] |
|---|---|---|---|---|---|
| $1L$ | 4.3 | 2.9 | 1.4 | $1.6\pm0.08$ | 4 |
| $2L$ | 3.2 | 2.7 | 1.6 | $1.4\pm0.08$ | 3 |
| $1D$ | 4 | 2.2 | 2.5 | $1.08\pm0.08$ | 4 |
| $2D$ | 3 | 1.3 | 7.2 | $1.17\pm0.08$ | 3 |
| $3D$ | 6 | 1.6 | 3.2 | $0.75\pm0.08$ | 4 |
| $4D$ | 0.8 | 0.44 | 150 | $0.7\pm0.08$ | 2 |

[a]The letters in the sample number have the following meanings: $D$ — measurements in the dark, $L$ — after illumination.
[b]The number of filled subbands was determined from the Fourier spectra for the Shubnikov–de Haas oscillations.

The negative magnetoresistance in $\delta$-doped layers was investigated in fairly great detail in Refs. 8–13, but emphasis was placed in those studies on the determination of the phase-relaxation time and its temperature and concentration dependences. Unfortunately, no conclusion regarding the value of the prefactor and the role of intersubband transitions in the negative magnetoresistance can be drawn from the results presented in those papers.

In this paper we present the results of experimental investigations of negative magnetoresistance in silicon $\delta$-doped GaAs layers grown by MOCVD. The substrate used was compensated GaAs, on which an $n^-$-GaAs buffer layer of thickness 500 nm, a layer $\delta$-doped with silicon, and an $n^-$-GaAs surface layer of thickness 100 nm were grown. The electron concentration determined from Hall measurements in a magnetic field $B=25$ T and the Hall conductivity $\mu=R(25\ \text{T})\sigma(B=0)$ are listed in Table I. Measurements were performed on both samples cooled in the dark and samples subjected to illumination (in a state of frozen photoconductivity). The nature of the frozen photoconductivity in $\delta$-doped GaAs is not entirely known, and we shall con-

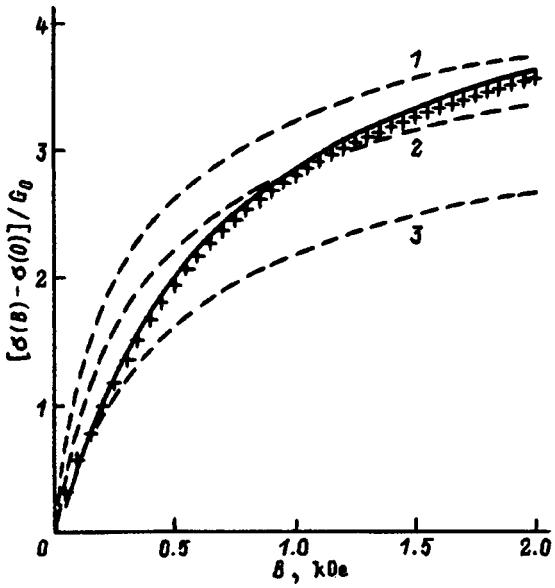


FIG. 2. Magnetic-field dependence of the magnetoconductivity $\delta\sigma(B) \equiv \sigma(B)-\sigma(0)$ for sample $1L$ at $T=4.2$ K (crosses) and the theoretical dependence (1) with the parameters $\alpha=1.6$ and $\tau_\varphi=4.5\times10^{12}$ s (solid line). The dashed lines depict the theoretical dependences for $\alpha=1$ and various values of $\tau_\varphi$, $10^{-11}$ s: *1* — 2.1, *2* — 1.4, *3* — 0.7.

sider the results obtained on a single sample before and after illumination as the results for different samples. The measurements were performed in a magnetic field parallel to a normal to the plane of the structure in the temperature range 1.5−20 K.

Let us first consider the results obtained on samples $1L$ and $2L$. The magnetic-field dependence of the conductivity of sample $1L$ at $T=4.2$ K is shown in Fig. 2. The solid curve in this figure depicts the result of fitting the experimental data to the expression (1) using the expressions $\tau_p=\mu m^*/e$ and $D=\sigma/(e^2N_FN)$ and the fitting parameters $\alpha$ and $\tau_\varphi$ [$N$ is the number of filled subbands (see Table I)]. Equation (1) was derived in the diffusion approximation, and the dependences were therefore treated in magnetic fields $B<B_{\text{th}}=c\hbar/(4eD\tau_p)$ (see Table I). The dashed curves correspond to the expression (1) with $\alpha=1$ and various values of $\tau_\varphi$. It can be seen that agreement with experiment can be obtained only for a value of $\alpha$ significantly greater than unity.

Let us analyze to what extent this conclusion depends on the approximations made in the treatment.

1. The number of filled subbands in the $\delta$-doped layers is known to within 1 (since the electron concentration in the upper subband is small and may not be manifested in the Fourier spectra for the Shubnikov–de-Haas oscillations, which were measured for all the samples investigated), and, as a result, the value of the diffusion coefficient is known to an accuracy of 30−50%. However, when $D$ is varied in this range, the expression (1) still faithfully describes the negative magnetoresistance. In this case the experimentally determined value of $\tau_\varphi$ varies, but the value of the prefactor $\alpha$ remains essentially unchanged.

2. In fitting the magnetoresistance to the expression (1) we used the value of $\tau_p$ determined from the Hall conductivity, which corresponds to an averaged value of $\tau_p$ for all the subbands. However, in this case, too, the variation of $\tau_p$ over a broad range (by several fold) scarcely alters the value of $\alpha$.

3. The use of the expression (1) implies the neglect of spin-orbit coupling, which corresponds to the condition $\tau_s\gg\tau_\varphi$ ($\tau_s$ is the spin relaxation time). When spin-orbit coupling is taken into account, the magnetoresistance depends on both $\tau_\varphi$ and $\tau_s$ and is described by the expression obtained in Ref. 3. (This expression holds when spin relaxation is described by the single time $\tau_s$ and is thus a good approximation for quantum wells in III–V semiconductors at high electron densities[14,15]). In this case the character of the magnetoresistance undergoes a qualitative change when $\tau_s\leqslant\tau_\varphi$: a segment of positive magnetoresistance should appear in weak fields. No such segment was observed for any of the samples investigated. When $\tau_s>\tau_\varphi$, the use of the expression (1) in treating the experimental dependences of $\Delta\sigma(B)$ produces a considerable error in the determination of $\tau_\varphi$ [a value close to $(1/\tau_\varphi+1/\tau_s)^{-1}$ is actually determined], but the value of the prefactor varies only slightly (by less than 10%).

Thus, the results presented show that the value of the prefactor $\alpha$ in (1), which describes the negative magnetoresistance, is significantly greater than unity at least for some $\delta$-doped layers, in agreement with the special feature of intersubband transitions in $\delta$-doped layers described above.

The deviation of the value of the prefactor from 2 might be due to violation of the condition $\tau_{i,j}\gg\tau_\varphi$. A marked temperature dependence of the prefactor should be observed in such a case, since at low temperatures $\tau_{i,j}$ does not depend on $T$, while $\tau_\varphi\sim1/T$ (Fig. 3a), and the relation between $\tau_{i,j}$ and $\tau_\varphi$ varies markedly with temperature in this case. However, as can be seen from Fig. 3b, the prefactor $\alpha$ scarcely depends on $T$ over the entire temperature range $1.5<T<20$ K, in which $\tau_\varphi$ varies from $10^{-11}$ to $10^{-12}$ s. In our opinion, this means that the times of transitions between subbands with different parity are greater than $10^{-11}$ s in the samples with $\alpha>1$.

A value of the prefactor somewhat less than 2 can be associated with the significant difference between the effective diffusion coefficients and $\tau_\varphi$ in the even and odd subbands. As was shown in some studies (see Ref. 16 and the references therein), the conductivities in different subbands of $\delta$ layers and, therefore, the diffusion coefficients differ by no more than a factor of 1.5−2 (the decrease in concentration with increasing subband number is compensated by an increase in mobility). If the expression $1/\tau_\varphi=(\pi G_0kT/\hbar\sigma)\ln(\sigma/2\pi G_0)$ (Ref. 17) is used to estimate $\tau_\varphi$, then in the case of several filled subbands the values of $D\tau_\varphi$ can differ by a factor of 3−4. Assuming that the negative magnetoresistance is described by the expression (4) and correlating $\Delta\sigma(B)$ with the expression (1), as we did in treating the experimental results, we can see that a fourfold difference in $D\tau_\varphi$ leads to a decrease in the value of $\alpha$ from 2 to 1.6.

In many studies[12,18] the decrease in the prefactor was associated with the contribution of the electron-electron ($e$-$e$) interaction to the negative magnetoresistance. In weak

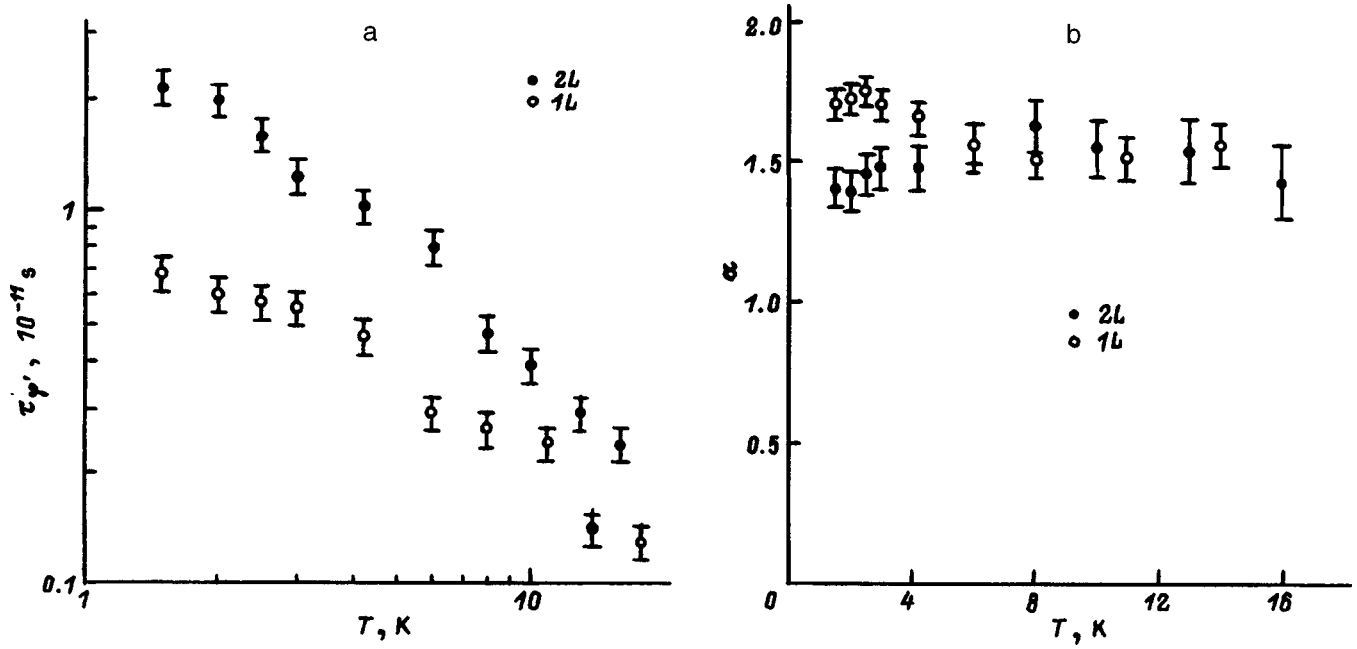


FIG. 3. Temperature dependences of $\tau_\varphi$ (a) and $\alpha$ (b) for samples $1L$ and $2L$.

magnetic fields the following two terms of the interaction in a Cooper channel contribute to the negative magnetoresistance:[17]

$$\Delta\sigma_1^{ee} = -\beta(g)G_0\varphi_1 \quad \Delta\sigma_2^{ee} = -g(T)G_0\varphi_2.$$

The first, which is known as the Maki–Thompson correction, has the same field dependence as the expression (1). In this case the function $\beta(g)$ is always positive and does not depend on the sign of the $e$-$e$ interaction constant $g(T)$, but does depend on its absolute value. The second term has somewhat different field and temperature dependences (the function $\varphi_2$ was presented in Ref. 19). The constant $g(T)$ can be positive or negative in the cases of effective repulsion or attraction between electrons, respectively. In order to estimate the extent to which the $e$-$e$ interaction can alter the prefactor, we calculated the total negative magnetoresistance for various values of $g(1.5\ \mathrm{K})$ with the values of $D$, $\tau_\varphi$, and $\tau_p$ corresponding to the samples investigated. Describing it by the expression (1), precisely as we did with the experimental dependence of $\Delta\sigma(B)$, and using $\alpha$ and $\tau_\varphi$ as fitting parameters, we can see that good agreement is obtained in this case. Moreover, when $g(T)$ is negative, the value of the prefactor is close to unity and scarcely depends on $T$. This is because the two contributions of the $e$-$e$ interaction essentially completely compensate one another in weak magnetic fields. When $g(1.5\ \mathrm{K}) \leqslant 0.3$, the value of the prefactor decreases by $0.2-0.25$, and when $g(1.5\ \mathrm{K}) \geqslant 0.3$, it decreases by a larger amount, but it exhibits a strong temperature dependence. No appreciable temperature dependence of the prefactor was discovered experimentally for any of the samples investigated; therefore, in our opinion, the small value of $\alpha$ in samples $1D-4D$ is not attributable to the $e-e$ interaction.

There is still the question of why the experimentally determined value of the prefactor is close to unity or even less than unity in many samples (see Table I).

One possible cause of the decrease in the prefactor in real samples may be macroscopic conductivity inhomogeneities. The contribution of such inhomogeneities to the negative magnetoresistance can be estimated by utilizing the theory of galvanomagnetic phenomena in two-component media,[20] assigning the dependence of $\sigma_i(B)$ in each of the components of an expression of the type (1), and varying their relative volume and the values of $n^i$, $\mu^i$, and $\tau_\varphi^i$. Treating the negative magnetoresistance of a two-component medium calculated in this manner according to (1) with the fitting parameters $\alpha$ and $\tau_\varphi$, we can easily see that any inhomogeneity only decreases the value of the prefactor $\alpha$.

Evidence of the presence of such inhomogeneities in the samples investigated is provided by the large value of the frozen photoconductivity. It follows from the results of investigations of Shubnikov–de-Haas oscillations that illumination does not lead to appreciable redistribution of electrons between the subbands and that it increases the concentration of carriers only slightly (by $10-15\%$), but increases their mobility significantly (by $1.5-2$ fold). In our opinion, such behavior can be understood only by assuming that the samples contain substantial inhomogeneities, which are shielded by the photocarriers. Indirect evidence that inhomogeneities are responsible for the decrease in the value of the prefactor in the samples investigated is provided by the increase in $\alpha$ following illumination, under whose effect the role of the macroscopic inhomogeneities presumably lessens.

Thus, the results presented show that the times for transitions between size-quantized subbands with different parity in $\delta$-doped layers are greater than $10^{-11}$ s, i.e., greater than the phase-relaxation time of the wave function at low tem-

peratures. (Unfortunately, we were unable to find values of $\tau_{i,j}$ in the literature that were correctly calculated with allowance for fluctuations in the distribution of impurities both in the transverse direction in and the doping plane). This causes the value of the prefactor $\alpha$ in the expression for the negative magnetoresistance to become close to 2 for highly perfect $\delta$-doped layers. The small value of $\alpha$ observed in many of the $\delta$-doped layers can be attributed to macroscopic inhomogeneities, a large thickness of the doped layer, and asymmetry of the potential due to proximity of the Schottky barrier.

This work was supported by grants from the Russian Fund for Fundamental Research (No. 97-02-16168) and the Physics of Solid-State Nanostructures Program.

[1] E. Abrahams, P. W. Anderson, D. C. Licciardello, and T. V. Ramakrishnan, Phys. Rev. Lett. **42**, 673 (1979).
[2] B. L. Altshuler, D. Khmelnitskii, A. I. Larkin, and P. A. Lee, Phys. Rev. B **22**, 5142 (1980).
[3] S. Hikami, A. I. Larkin, and Y. Nagaoka, Prog. Theor. Phys. **63**, 707 (1980).
[4] S. Iwabuchi and Y. Nagaoka, J. Phys. Soc. Jpn. **58**, 1325 (1988).
[5] N. S. Averkiev and G. E. Pikus, Fiz. Tverd. Tela (St. Petersburg) **39**, 1659 (1997) [Phys. Solid State **39**, 1481 (1997)].
[6] A. M. Kreshchuk, S. V. Novikov, T. A. Polyanskaya, and I. G. Savel'ev, Fiz. Tekh. Poluprovodn. **31**, 459 (1997) [Semiconductors **31**, 391 (1997)].
[7] P. T. Coleridge, Semicond. Sci. Technol. **5**, 961 (1990).
[8] G. M. Gusev, Z. D. Kvon, D. I. Lubyshev, V. P. Migal', V. N. Ovsyuk, V. V. Preobrazhenskiĭ, and S. I. Stenin, Fiz. Tverd. Tela (Leningrad) **30**, 3148 (1988) [Sov. Phys. Solid State **30**, 1810 (1988)].
[9] M. Asche, K. J. Fridland, P. Kleinert, H. Kostial, J. Gerzog, and R. Hey, Superlattices Microstruct. **10**, 425 (1990).
[10] G. M. Gusev, Z. D. Kvon, D. I. Lubyshev, V. P. Migal', and A. G. Pogosov, Fiz. Tekh. Poluprovodn. **25**, 601 (1991) [Sov. Phys. Semicond. **25**, 364 (1991)].
[11] M. V. Budantsev, Z. D. Kvon, and A. G. Pogosov, Fiz. Tekh. Poluprovodn. **26**, 1565 (1992) [Sov. Phys. Semicond. **26**, 879 (1992)].
[12] V. A. Kulbachinskii, N. B. Brandt, V. G. Kytin, V. I. Kadushkin, A. P. Senichkin, and E. L. Shangina, Phys. Low-Dimens. Semicond. Struct. **12**, 237 (1995).
[13] W. Poirier, D. Mailly, and M. Sanquer, Cond-mat/9706287.
[14] W. Knap, C. Skierbiszewski, A. Zduniak, E. Litwin-Staszewska, D. Bertho, F. Kobbi, J. L. Robert, G. E. Pikus, F. G. Pikus, S. V. Iordanskii, V. Mosser, K. Zekentes, and Yu. B. Lyanda-Geller, Phys. Rev. B **53**, 3912 (1996).
[15] T. Hassenkam, S. Pedersen, K. Baklanov, A. Kristensen, C. B. Sorensen, P. E. Lindelof, F. G. Pikus, and G. E. Pikus, Phys. Rev. B **55**, 9298 (1997).
[16] A. Ya. Shik, Fiz. Tekh. Poluprovodn. **26**, 1161 (1992) [Sov. Phys. Semicond. **26**, 649 (1992)].
[17] B. L. Altshuler, A. G. Aronov, and D. E. Khmelnitsky, J. Phys. C: Solid State Phys. **15**, 7367 (1982).
[18] A. I. Larkin, Pis'ma Zh. Éksp. Teor. Fiz. **31**, 239 (1980) [JETP Lett. **31**, 219 (1980)].
[19] B. L. Al'tshuler, A. G. Aronov, A. L. Larkin, and D. E. Khmel'nitskiĭ, Zh. Éksp. Teor. Fiz. **81**, 768 (1981) [Sov. Phys. JETP **54**, 411 (1981)].
[20] B. Ya. Balagurov, Zh. Éksp. Teor. Fiz. **82**, 1333 (1982) [Sov. Phys. JETP **55**, 774 (1982)].

Translated by P. Shelnitz

# Quantum corrections to the conductivity of a two-dimensional system with antidots

M. M. Makhmudian and M. V. Éntin

*Institute of Semiconductor Physics, Russian Academy of Sciences, Siberian Branch, 630090 Novosibirsk, Russia*

(Submitted February 13, 1998; accepted for publication April 20, 1998)
Fiz. Tekh. Poluprovodn. **32**, 1461–1466 (December 1998)

The quantum corrections to the conductivity of a two-dimensional electron system with antidots in the limit of a small antidot density are investigated. The corrections to the conductivity and magnetoconductivity due to the presence of antidots in a magnetic field perpendicular to the plane of the system are considered. It is assumed that the mean free path $l$ of electrons on the impurities is far smaller than the antidot radius. © *1998 American Institute of Physics.* [S1063-7826(98)01012-6]

## 1. INTRODUCTION

Recent advances in technology have made it possible to create and investigate artificial media with scales commensurate with both electron momentum relaxation distances and with quantum dimensions (the electron wavelength and the magnetic length). In this context it has been possible to create, for example, two-dimensional (2D) electron systems with a spatially modulated electron concentration. One special case of such systems is characterized by so-called ''quantum dots,'' i.e., regions in which the motion of electrons is confined in three dimensions. Another example is a system of ''antidots,'' i.e., regions within a 2D electron gas where the concentration of 2D electrons vanishes.

The magnetotransport properties of 2D electron systems with a periodic antidot lattice, which are associated with the commensurate values of the cyclotron diameter and the lattice period, are well known.[1,2] These features have a classical nature and are determined by the stochastic character of electron motion in these systems.

However, apart from the classical effects, these systems display some interesting quantum properties associated with the interference of electron waves.[3–6] In particular, the observation of negative magnetoresistance in a disordered antidot lattice was reported in Ref. 5, and the observation of Aharonov–Bohm oscillations in a periodic antidot lattice in weak magnetic fields was described in Ref. 6. Similar periodic oscillations have also been detected in stronger magnetic fields ($2R_c \approx d$).[7,8] Such systems have been studied theoretically as classical objects, i.e., ''electron billiards,'' and from the quantum standpoint in both the ballistic regime and in the quantum limit. The ballistic regime, in which the scattering of electrons by impurities can be neglected, has been studied for the most part.

The present work is a study of the so-called quantum (interference) corrections to the conductivity of 2D systems with antidots in another possible limit, where the electron mean free path before scattering by impurities is small compared with the characteristic dimensions of the system. In this limit the motion of electrons between antidots is described mainly using the kinetic equation. We shall take into account the presence of a magnetic field perpendicular to the plane of the system.

The problem has several parameters: the electron mean free path before scattering by impurities $l$, the electron phase-breaking (relaxation) length $L_\varphi = \sqrt{D\tau_\varphi}$ ($D$ is the diffusion coefficient and $\tau_\varphi$ is the phase-breaking time), the magnetic length $a_H = \sqrt{c\hbar/2eH}$, the electron wavelength $\lambda = \hbar/p$ ($p$ is the electron momentum), the antidot radius $\rho_a$, and the antidot density $n$. In the limit under consideration there are several relations between these parameters. In order that the description of electrons using wave packets would have meaning, the condition $l \gg \lambda$ must hold. On the other hand, in agreement with previous statements, we shall assume that the mean free path is small compared with the antidot radius: $l \ll \rho_a$. Only in this case does the motion of an electron around an antidot have a diffusive character. The phase-breaking length $L_\varphi$ is determined by inelastic scattering. The absence of interference effects for the diffusing electrons requires satisfaction of the condition $l \ll L_\varphi$, which holds at low temperatures (the residual-resistance region). In addition, we shall consider the limit of a small antidot density, which requires that $n_a \rho_a^2$ be small ($n_a \rho_a^2 \ll 1$). This condition also means that the antidot radius must be small compared with the distance between them. The latter condition ensures that $l$ is small in comparison to the mean distance between the antidots $n^{-1/2}$ ($l \ll n_a^{-1/2}$) and thus corresponds to the diffusive character of the motion of electrons between the antidots. In the limit under consideration the contribution of the antidots is a small addition to the quantum corrections to the conductivity of the 2D system.

## 2. CALCULATION OF QUANTUM CORRECTIONS

The conventional theory of transport phenomena is based on the classical kinetic equation for conduction electrons. This means that an electron moves along a classical trajectory during the time between two collisions. This approximation is valid when the interference between two waves scattered by different centers is negligible, i.e., when the mean free path of an electron is much greater than its

 

wavelength ($l \gg \lambda$). Then, the electron can be described quasiclassically between two collisions. Such a description leads to the familiar Drude equation:

$$\sigma = \frac{n_e e^2 \tau}{m_e}, \tag{1}$$

where $n_e$ is the concentration of electrons and $m_e$ is their mass.

As was shown in Ref. 9, allowance for interference leads to the appearance of quantum corrections to the conductivity $\sigma$ (1). The quantum corrections can be calculated quantitatively using a Feynman diagram technique by taking into account the diagrams describing the conductivity of electrons interacting with impurities. We shall briefly describe the method for calculating quantum corrections,[10] which we shall use later on for a 2D system with antidots.

The principal quantum corrections to the conductivity of noninteracting particles stem from consideration of the Cooper diagrams describing the interference occurring upon multiple backscattering. The amplitude of this interference, $C(\mathbf{r},\mathbf{r})$, is determined by the quantum corrections to the conductivity.

The correction to the conductivity at the frequency $\omega$ is related to $C_\omega(\mathbf{r},\mathbf{r})$ by the expression

$$\delta\sigma(\omega) = -\frac{2e^2}{\pi} D\tau C_\omega(\mathbf{r},\mathbf{r}). \tag{2}$$

Here and below we set $\hbar = 1$, and we shall restore its value in the final formulas. In a magnetic field the quantity $C_\omega(\mathbf{r},\mathbf{r})$ satisfies the equation

$$\left\{ -i\omega + D\left( -i\nabla - \frac{2e}{c}\mathbf{A} \right)^2 + \frac{1}{\tau_\varphi} \right\} C_\omega(\mathbf{r}-\mathbf{r}') = \frac{\delta(\mathbf{r}-\mathbf{r}')}{\tau}, \tag{3}$$

where $\mathbf{A}$ is the vector potential of the magnetic field and $\omega$ is the frequency of the external field. Equation (3) formally coincides with the equation for the Green's functions of a cooperon, a particle with a charge $2e$ and a mass $M = (2D)^{-1}$, moving in a magnetic field. The quantity $E = i\omega - \tau_\varphi^{-1}$ corresponds to the cooperon energy.

Let us consider the 2D case. Let $E_n$ be the eigenvalues (''energy levels'' of the cooperon), and let $\psi_n(\mathbf{r})$ be the normalized eigenfunctions of Eq. (3) without the right-hand side, i.e., the Schrödinger equation for a cooperon in a magnetic field:

$$\frac{1}{2M}\left( -i\nabla - \frac{2e}{c}\mathbf{A} \right)^2 \psi_n = E_n \psi_n. \tag{4}$$

Then the expression for $C_\omega(\mathbf{r},\mathbf{r}')$ takes the form

$$C_\omega(\mathbf{r},\mathbf{r}') = \frac{1}{\tau}\sum_n \frac{\psi_n(\mathbf{r})\psi_n^*(\mathbf{r}')}{E_n - E}. \tag{5}$$

In the case of a 2D system with antidots, if we assume that the antidot density is small ($n_a \rho_a^2 \ll 1$), we can neglect the influence of the antidots on one another and calculate the quantum corrections in the case of only a single antidot. The total correction is the sum of the contributions from all the antidots, i.e., it reduces to the product of the contribution in the case of one antidot and the number of antidots. Thus, to calculate the quantum corrections to the conductivity of a 2D system we must solve Eq. (3) for $C_\omega(\mathbf{r},\mathbf{r}')$ in a magnetic field for a round 2D sample of large radius, whose center is occupied by one antidot, with the boundary condition[10]

$$\left\{ \frac{\partial}{\partial \mathbf{n}} + \frac{2ie}{c}(\mathbf{A}\cdot\mathbf{n}) \right\} C_\omega(\mathbf{r},\mathbf{r}')\big|_{r=\rho_a} = 0. \tag{6}$$

The condition (6) means that the flow of particles through the antidot boundary is equal to zero. The relation (2) for the quantum corrections to the conductivity in this case has the form

$$\delta\sigma(\omega) = -\frac{2e^2}{\pi} D\tau \int C_\omega(\mathbf{r},\mathbf{r}) \frac{d\mathbf{r}}{S}. \tag{7}$$

Here $S$ is the area of the sample. The expression for the quantum corrections with consideration of the contributions from all the antidotes is obtained from (7) using (5) by multiplication by the number of antidots $N_a$. Then, bearing in mind that $N_a/S = n_a$, we arrive at the following expression:

$$\delta\sigma(\omega) = -n_a \frac{2e^2 D}{\pi} \sum_n \frac{1}{E_n - E}. \tag{8}$$

We shall henceforth consider the static conductivity. The quantum corrections due to the presence of antidots, which we shall denote by $\delta^2\sigma(H,\rho_a)$, are equal to the difference between the quantum corrections to the conductivity of a 2D system with antidots and the same system without antidots:

$$\delta^2\sigma(H,\rho_a) = \delta\sigma(H,\rho_a) - \delta\sigma(H,0) = -n_a \frac{2e^2 D}{\pi}\left( \sum_n \frac{1}{E_n - E} - \sum_n \frac{1}{E_n^0 - E} \right), \tag{9}$$

where the $E_n^0$ are the cooperon energy levels in the absence of antidots. Thus, to find the quantum corrections, it is sufficient for us to determine the cooperon energy levels in a constant magnetic field for a 2D system with antidots and for the same system without antidots.

In the polar coordinates $\rho, \varphi$ the vector potential of a uniform magnetic field has the components $A_\varphi = H\rho/2$ and $A_\rho = 0$, and the Schrödinger equation (4) takes the form

$$-\frac{1}{2M}\left[ \frac{1}{\rho}\frac{\partial}{\partial\rho}\left( \rho\frac{\partial\psi}{\partial\rho} \right) + \frac{1}{\rho^2}\frac{\partial^2\psi}{\partial\varphi^2} \right] + \frac{i\omega_H}{2}\frac{\partial\psi}{\partial\varphi} + \frac{M\omega_H^2}{8}\rho^2\psi = E\psi, \tag{10}$$

where $\omega_H = 4DeH/c$. The boundary condition (6) in polar coordinates has the form

$$\left.\frac{\partial\psi}{\partial\rho}\right|_{\rho=\rho_a} = 0. \tag{11}$$

We seek a solution in the form

$$\psi = e^{im\varphi} R(\rho), \tag{12}$$

and for the radial part of the wave function we obtain the equation

$$\frac{1}{2M}\left(R''+\frac{1}{\rho}R'-\frac{m^2}{\rho^2}R\right)+\left(E-\frac{M\omega_H^2}{8}\rho^2+\frac{m\omega_H}{2}\right)R=0. \tag{13}$$

Introducing the new independent variable $\xi=(M\omega_H/2)\rho^2$, we rewrite the equation in the form

$$\xi R''+R'+\left(-\frac{\xi}{4}+\beta-\frac{m^2}{4\xi}\right)R=0, \tag{14}$$

where we have introduced the notation $\beta=E/\omega_H+m/2$. When $\xi\to\infty$, the function sought behaves as $e^{-\xi/2}$, and when $\xi\to 0$, it behaves as $\xi^{|m|/2}$. Accordingly, we seek a solution in the form

$$R(\xi)=e^{-\xi/2}\xi^{|m|/2}w(\xi), \tag{15}$$

and for $w(\xi)$ we obtain equations for the degenerate hypergeometric function

$$\xi w''+(1+|m|-\xi)w'-\left(\frac{1+|m|}{2}-\beta\right)w=0. \tag{16}$$

The general solution of Eq. (16) can be written in the form[11,12]

$$w=AM(a,b;\xi)+BU(a,b;\xi).$$

Here $M(a,b;\xi)$ and $U(a,b;\xi)$ are Kummer and Tricomi functions, respectively, where $a=(1+|m|)/2-\beta=(|m|-m)/2+1/2-\varepsilon$, $\varepsilon=E/\omega_H$, and $b=1+|m|$. In these expressions $A$ and $B$ are arbitrary constants.

For $\xi\to\infty$

$$M(a,b;\xi)=\frac{\Gamma(b)}{\Gamma(a)}e^{\xi}\xi^{a-b}\left[1+O\left(\frac{1}{\xi}\right)\right],$$

$$U(a,b;\xi)=\xi^{-a}\left[1+O\left(\frac{1}{\xi}\right)\right].$$

It follows from the boundary condition at infinity $R(\xi)|_{\xi\to\infty}=0$ that $A=0$. Then the solution (15) of Eq. (14) takes the form

$$R(\xi)=Be^{-\xi/2}\xi^{|m|/2}U(a,b;\xi). \tag{17}$$

The boundary condition (11) gives

$$\left.\frac{\partial R(\xi)}{\partial\xi}\right|_{\xi=\xi_a}=0. \tag{18}$$

Substituting (17) into (18), we obtain the equation for $a$

$$\frac{1}{2}\left(1+\frac{|m|}{\xi_a}\right)U(a,1+|m|;\xi_a)-U(a,2+|m|;\xi_a)=0. \tag{19}$$

The solution of Eq. (19) for $a$ specifies the cooperon energy levels $\varepsilon$ and, through (9), the quantum corrections to the conductivity.

### 3. 2D SYSTEM WITH ANTIDOTS OF SMALL RADIUS

Let us consider the limit where the antidot radius is small compared with the characteristic dimensions of the problem: $\rho_a\ll\min(a_H,L_\varphi)$. This corresponds to $\xi_a\ll 1$. The condition $\xi_a\ll 1$ permits the expansion of (19) in the small parameter $\xi_a$. Isolating the principal terms in the expansion, we find

$$\left(\frac{1}{2}-a\right)\psi(a)=\frac{1}{\xi_a}\quad\text{for}\quad m=0,$$

$$|m|(a-1)\ldots(a-|m|)(-1)^{|m|-1}\psi(a)=\frac{(|m|!)^2}{\xi_a^{|m|}}\quad\text{for}\quad m\neq 0, \tag{20}$$

where $\psi(a)=\Gamma'(a)/\Gamma(a)$. Substituting the asymptote[11] into (20), we obtain

$$\psi(a)|_{a\to -n_\rho}\sim -\left.\frac{1}{a+n_\rho}\right|_{a\to -n_\rho},$$

where $n_\rho$ is a nonnegative integer. Using the relation $\varepsilon=1/2+(|m|-m)/2-a$, we find the energy levels (in units of $\omega_H$)

$$\varepsilon_{n,m}=\left(n+\frac{1}{2}\right)(1-a_{n,m}), \tag{21}$$

where $n=n_\rho+(|m|-m)/2$ is the principal quantum number,

$$a_{n,0}=-\xi_a,$$

$$a_{n,m\neq 0}=\frac{|m|}{n+\frac{1}{2}}\left(n-\frac{|m|-m}{2}+1\right)\ldots\left(n-\frac{|m|-m}{2}+|m|\right)\frac{\xi_a^{|m|}}{(|m|!)^2}.$$

It follows from the inequality $\xi_a\ll 1$ that $a_{n,m}\ll 1$.

The cooperon energy levels in the absence of antidots are obtained by setting the antidot radius equal to zero:

$$E^0_{n,m}=E_{n,m}|_{\rho_a=0}.$$

Substituting (21) into (9) and taking into account that $\alpha_{n,m}\ll 1$, we obtain

$$\delta^2\sigma(H,\rho_a)=-n_a\frac{2e^2D}{\pi\omega_H}\sum_{n,m}\frac{\alpha_{n,m}\left(n+\frac{1}{2}\right)}{\left(n+\frac{1}{2}-\varepsilon\right)^2}. \tag{22}$$

Hence it can be seen that the main contribution to the sum is made by $m=-1,0,1$. Then (22) reduces to

$$\delta^2\sigma(H,\rho_a)=-n_a\rho_a^2\frac{e^2}{2\pi}\times\sum_{n_\rho=0}^{\infty}\left[\frac{\xi}{\left(n_\rho+\frac{1}{2}-\varepsilon\right)^2}+\frac{1}{n_\rho+\frac{1}{2}-\varepsilon}\right]. \tag{23}$$

The sum (23) can be rewritten using the generalized zeta function $\xi(s,\nu)=\Sigma_{n=0}^{\infty}(n+\nu)^{-s}$ with $s=1$ and $s=2$. The

zeta function with $s=1$ diverges, but this divergence is eliminated by taking into account the limiting value of the cooperon energy, which determines the upper level of the sum: $(n_\rho)_{\max}=D/\omega_H l^2$. As a result, to logarithmic accuracy we obtain

$$\delta^2\sigma(H,\rho_a)=-n_a\rho_a^2\frac{e^2}{2\pi}\left[\varepsilon\zeta\left(2,\frac{1}{2}-\varepsilon\right)-\psi\left(\frac{1}{2}-\varepsilon\right)+\ln\frac{D}{\omega_H l^2}\right]. \quad (24)$$

Here $\psi(y)$ is the logarithmic derivative of the gamma function. Going over to the variable $x=\omega_H\tau_\varphi=4DeH\tau_\varphi/c=-1/\varepsilon$, we have

$$\delta^2\sigma(H,\rho_a)=n_a\rho_a^2\frac{e^2}{2\pi}\left[f_1\left(\frac{4DeH\tau_\varphi}{c}\right)-\ln\frac{D\tau_\varphi}{l^2}\right], \quad (25)$$

where

$$f_1(x)=\frac{1}{x}\zeta\left(2,\frac{1}{2}+\frac{1}{x}\right)+\psi\left(\frac{1}{2}+\frac{1}{x}\right)+\ln x=\begin{cases}1-5x^2/24 & \text{for } x\ll 1,\\ \ln x & \text{for } x\gg 1.\end{cases}$$

The second term in (25) is independent of magnetic field and specifies the magnitude of the quantum corrections due to the presence of antidots in a zero magnetic field:

$$\delta^2\sigma(\rho_a)=-n_a\rho_a^2\frac{e^2}{2\pi\hbar}\ln\frac{D\tau_\varphi}{l^2}. \quad (26)$$

Equations (24)–(26) contain the electron mean free path $l$. The mean free path is determined by both impurity scattering and the antidots. Strictly speaking, Eqs. (24)–(26) are valid for isotropic impurity scattering. In the case of scattering anisotropy, for these equations to be valid, the characteristic electron momentum transfers upon scattering must be greater than the characteristic cooperon momentum $q\sim(D\tau_\varphi)^{-1/2}$.

The presence of antidots leads to a change in $l$. However, in the limit $l\ll\rho_a$ the corrections to the mean free path are small with respect to the parameter $n_a\rho_a l$, and the changes in the final formulas associated with them contain the small parameter $l/\rho_a$. In fact, only electrons found in a layer of thickness $l$ near an antidot boundary experience the influence of the antidot on their relaxation. As a result, the relative increase in the collision frequency in a two-dimensional medium containing antidots is determined by the fraction of electrons undergoing collisions with an antidot boundary, which is of the order of the total perimeter of the antidots per unit area of the sample $2\pi n_a\rho_a$ multiplied by the impurity mean free path $l$.

The expression (26) should be compared with the quantum corrections appearing in a microscopic medium containing cavities. Such a medium can be characterized by an averaged diffusion coefficient $\overline{D}$. The value of $\overline{D}$ can be calculated using the corrections to the averaged conductivity

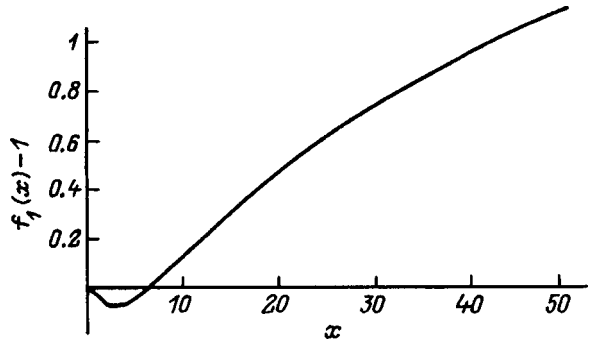


FIG. 1.

of a two-dimensional medium containing round cavities $\overline{\sigma}=\sigma(1-2n_a\pi\rho_a^2)$ and the corrections to the mean concentration $\overline{n_e}=n_e(1-n_a\pi\rho_a^2)$:

$$\overline{D}=D\frac{\overline{\sigma n_e}}{\overline{\sigma}\,\overline{n_e}}\approx D(1-n_a\pi\rho_a^2). \quad (27)$$

The quantum corrections $\delta\sigma$ to the macroscopic conductivity of a 2D system in the absence of a magnetic field have the form[10]

$$\delta\sigma=-\frac{e^2}{2\pi^2\hbar}\ln\frac{D\tau_\varphi}{l^2}. \quad (28)$$

The diffusion coefficient in (28) should apparently be replaced by the effective diffusion coefficient (27). With consideration of the smallness of the parameter $n_a\rho_a^2$, we obtain

$$\delta^2\sigma(\rho_a)=\frac{e^2}{2\pi\hbar}n_a\rho_a^2. \quad (29)$$

The formula (29) is distinguished from (26) both by the absence of the large logarithm and by its sign. These differences are due to the interference effects associated with the diffusive trajectories bending around the antidots, which were not taken into account in (29).

The magnetoconductivity is given by the first term in (25), which specifies the magnetic-field dependence of the quantum corrections:

$$\delta^3\sigma(H,\rho_a)=\delta^2\sigma(H,\rho_a)-\delta^2\sigma(0,\rho_a)=n_a\rho_a^2\frac{e^2}{2\pi\hbar}\left[f_1\left(\frac{4DeH\tau_\varphi}{c\hbar}\right)-1\right]. \quad (30)$$

The characteristic multiplier accompanying the quantum corrections $n_a\pi\rho_a^2$ is equal to the ratio of the area occupied by the antidots to the total area of the sample. The behavior of the quantum corrections in a magnetic field is assigned by the function $f_1(x)-1$, which is shown in Fig. 1. At strong fields the corrections exhibit the same logarithmic behavior as in the case of a 2D system without antidots,[10] and at weak fields the behavior of the corrections is also quadratic with respect to the field, but with a negative sign.

## 4. 2D SYSTEM WITH ANTIDOTS OF LARGE RADIUS

When the antidot radius is large, i.e., when $\rho_a \gg \max(a_H, L_\varphi)$, we can proceed in the following manner. Since the quantum corrections occur over distances of the order of $\min(a_H, L_\varphi)$, when $\rho_a \gg \max(a_H, L_\varphi)$, we can refer to the averaged corrections to the conductivity of a 2D system with antidots. In this case a 2D system with antidots can be regarded as a macroscopic medium with a certain conductivity $\sigma$, including the quantum corrections, in which holes of radius $\rho_a$ have been cut out, and it can be characterized by a certain effective conductivity $\overline{\sigma}$, where $\overline{\sigma}/\sigma = \overline{D}/D$. Then, finding the quantum corrections to the conductivity of the 2D system with antidots reduces to finding the corrections for a medium with the conductivity $\overline{\sigma}$:

$$\delta^2\sigma(\rho_a) = -2n_a\pi\rho_a^2\delta\sigma, \tag{31}$$

where $\delta\sigma$ is given by (28).

Let us consider the corrections to the magnetoconductivity due to the presence of antidots of large radius. In a weak magnetic field the quantum corrections to the magnetoconductivity exceed both the Hall conductivity and the classical magnetoconductivity; therefore, we shall neglect the classical corrections. In analogy to the preceding case, we find

$$\delta^2\sigma(H,\rho_a) = -n_a\rho_a^2\frac{e^2}{\pi\hbar}f_2\left(\frac{4DeH\tau_\varphi}{c\hbar}\right), \tag{32}$$

$$f_2(x) = \psi\left(\frac{1}{2}+\frac{1}{x}\right)+\ln x = \begin{cases} x^2/24 & \text{for} \quad x \ll 1, \\ \ln x & \text{for} \quad x \gg 1. \end{cases}$$

This result can be explained qualitatively in the following manner. The quantum corrections occur over distances of the order of $\min(a_H, L_\varphi)$, and since $\rho \gg \max(a_H, L_\varphi)$, trajectories with interference cannot bend around the antidots. This means that the introduction of antidots into a 2D system in this case is equivalent to the removal of the area occupied by the antidots (the excluded area) from the 2D system. Then the relative variation of the quantum corrections is determined by the fraction of all possible trajectories that are inaccessible to electrons, which is equal to the ratio of the excluded area to the total area of the 2D system: $N_a\pi\rho_a^2/S = n_a\pi\rho_a^2$. Then, taking into account that the quantum corrections decrease and that each self-intersecting trajectory corresponds to two alternate routes, we arrive at (32).

## 5. CONCLUSION

The quantum corrections to the conductivity of a 2D system due to the presence of antidots have been obtained as a function of the magnetic field perpendicular to the plane of the system in this work. The limits of the problem for antidots of small and large radius have been investigated in the approximation of a small antidot density. In the case of antidots of small radius the quantum corrections change sign as a function of magnetic field. The corrections in the case of antidots of large radius, as expected, are negative and are associated with a decrease in the fraction of self-intersecting trajectories, from which quantum corrections arise. In the limit considered the contribution of the antidots is a small addition to the quantum corrections to the conductivity of the 2D system.

However, this contribution is perfectly measurable. As we know, the antidot radius can easily be modulated using a field electrode or illumination. The variation of the quantum corrections in this case is due to both variation of the surface electron density and variation of the size of the depleted regions around the antidots. The first effect is parasitic in our problem. Its concentration dependence arises through the concentration dependence of the phase-breaking time and the momentum relaxation time. We suggest that it can be eliminated experimentally by comparison with a homogeneous sample.

The limiting cases investigated do not exhaust all the limits of the problem studied, and further treatment is required. For example, we can expect to obtain periodic oscillations of the magnetoconductivity associated with the Aharonov–Bohm effect when electron waves traveling around antidots interfere. For the Aharonov–Bohm effect to be manifested, $L_\varphi$ must be greater than the antidot perimeter, and the number of magnetic flux quanta passing through the area of an antidot must be greater than or of the order of unity. However, consideration of this effect requires a computer calculation based on Eqs. (19) and (9).

This work was partially supported by the Russian Fund for Fundamental Research (Grants 95-02-04432 and 97-02-18397) and by a grant from Volkswagen Stiftung.

[1] G. M. Gusev, V. T. Dolgopolov, Z. D. Kvon *et al.*, Pis'ma Zh. Éksp. Teor. Fiz. **54**, 369 (1991) [ JETP Lett. **54**, 364 (1991)].
[2] É. M. Baskin, A. G. Pogosov, and M. V. Entin, Zh. Eksp. Teor. Fiz. **110**, 2061 (1996) [ JETP **83**, 1135 (1996)].
[3] K. Ensslin and P. Petroff, Phys. Rev. B **41**, 12 307 (1990).
[4] D. Wiess, M. L. Roukes, A. Menschig, P. Grambow, K. von Klitzing, and D. Weimann, Phys. Rev. Lett. **66**, 2790 (1991).
[5] G. M. Gusev, P. Basmaji, Z. D. Kvon, L. V. Litvin *et al.*, Surf. Sci. **305**, 443 (1994).
[6] G. M. Gusev, Z. D. Kvon, L. V. Litvin *et al.*, Pis'ma Zh. Éksp. Teor. Fiz. **55**, 129 (1992) [ JETP Lett. **55**, 123 (1992)].
[7] F. Nihey and K. Nakamura, Physica B **184**, 398 (1993).
[8] D. Wiess, K. Richter, A. Menschig *et al.*, Phys. Rev. Lett. **70**, 4118 (1993).
[9] L. P. Gor'kov, A. I. Larin, and D. E. Khmel'nitskiĭ, Pis'ma Zh. Éksp. Teor. Fiz. **30**, 248 (1979) [ JETP Lett. **30**, 228 (1979)].
[10] B. L. Altshuler, A. G. Aronov, D. E. Khmelnitskii, and A. I. Larkin, *Quantum Theory of Solids*, I. M. Lifshitz [Ed.], Mir, Moscow (1982).
[11] *Bateman Manuscript Project. Higher Transcendental Functions, Vol. 1*, edited by A. Erdélyi (McGraw-Hill, New York, 1953; Vol. 1, Nauka, Moscow, 1965).
[12] *The Handbook of Mathematical Functions*, edited by M. Abramowitz and I. A. Stegun (Dover, New York, 1976; Nauka, Moscow, 1969).

Translated by P. Shelnitz

## PHYSICS OF SEMICONDUCTOR DEVICES

# Transient processes in photocathodes at high laser intensities

B. I. Reznikov

*A. F. Ioffe Physicotechnical Institute, Russian Academy of Sciences, 194021 St. Petersburg, Russia*

A. V. Subashiev

*State Technical University, 195251 St. Petersburg, Russia*

(Submitted July 2, 1998; accepted for publication July 6, 1998)
Fiz. Tekh. Poluprovodn. **32**, 1467–1475 (December 1998)

The transient characteristics of a photocathode observed following the instantaneous onset and termination of optical excitation in one- and two-pulse excitation regimes are considered within a nonlinear diffusion model. The critical values of the illumination intensity corresponding to the manifestation of charge-confinement effects and to the cessation of photoelectron emission are determined. It is shown that the emission charge in a pulse is a nonmonotonic function of the excitation intensity and depends strongly on the values of the negative electron affinity and the effective transparency of the barrier in the activation layer. In the charge-confinement regime the time for establishing a stationary photovoltage and emission current following the onset of excitation is determined mainly by the establishment of equilibrium between the electron and hole fluxes reaching the surface and is inversely proportional to the illumination intensity. The time for restoration of the photocathode characteristics following the termination of illumination is inversely proportional to the trapping rate of holes on deep neutral centers during their tunneling to the surface through the barrier in the space-charge region and can be as large as several microseconds. © *1998 American Institute of Physics.* [S1063-7826(98)01112-0]

### 1. INTRODUCTION

Semiconductor photocathodes that utilize the emission of optically oriented electrons from the surface of a GaAs epitaxial film activated to a negative electron affinity are used in high-energy physics in linear accelerators[1,2] to obtain beams of polarized electrons. The important parameters of such cathodes include the maximum current (in a continuous regime) and the maximum charge in a pulse (in a pulsed regime) that can be achieved under intense optical excitation. Such excitation is associated with confinement of the current and emission charge as a consequence of the photovoltaic effect, which diminishes the near-surface band bending and increases the work function.[3]

Emission-confinement effects have been investigated experimentally in both a quasistationary regime[4] and with pulsed excitation.[4–6] The relationship between the observed laws and the photovoltaic effect was discussed in Ref. 7. It was shown that consideration of the photovoltaic effect permits a description of the experimental dependences from Ref. 5, but the quantitative results in Ref. 7 were obtained in the form of a model numerical calculation.

We previously[8] investigated the stationary characteristics of a photocathode under intense excitation. It was shown that to obtain a quantitative description of the observed dependences of the quantum efficiency on photovoltage and excitation intensity it must be assumed that the transparency of the effective barrier in the activation layer on the surface decreases significantly with increasing photovoltage, attesting to a dependence of the barrier transmission probability on energy. The transient characteristics of a photocathode would also be of considerable interest, especially in connection with the use of photocathodes in multiple-pulse regimes.[9]

In the present work the mechanisms determining the establishment of a stationary emission current following the onset of excitation and the relaxation of the photocathode following its termination are investigated, and the possibilities of characterizing photocathode structures on the basis of experimental data obtained during nonstationary excitation are ascertained.

### 2. STATEMENT OF THE PROBLEM

2.1. The activation of an atomically clean surface of a *p*-GaAs epitaxial film by applying a monolayer Cs–O coating leads to pinning of the Fermi level on donorlike localized surface states in the band gap, band bending at the surface, and the formation of a space-charge region, whose thickness $w$ is determined by the position of the Fermi level and the acceptor concentration $N_a$.

In addition, a layer (the activation layer), which creates a negative electron affinity and acts as an energy barrier to photoelectrons, forms on the film surface.

 

The energy diagram of a photocathode structure with a working region of thickness $d$ was presented in, for example, Refs. 7 and 8. We shall described the kinetics of photoelectrons in the quasineutral region $w \leqslant x \leqslant d$ and in the space-charge region $0 \leqslant x \leqslant w$ by the diffusion equation

$$\frac{\partial n}{\partial t} + \frac{\partial q_n}{\partial x} = \alpha I_i e^{-\alpha x} - \frac{n}{\tau}, \quad q_n = -D_n \frac{\partial n}{\partial x} - \mu_n E n, \quad (1)$$

matching the solutions at the boundary $x = w$ (for further details, see Ref. 8). Here $n$ is the electron concentration; $x$ is the coordinate measured to the right of the barrier; $I_i$ is the maximum intensity of the optical radiation entering the semiconductor; $\alpha$ is the absorption coefficient; and $\mu_n, D_n$, and $\tau$ are the electron mobility, diffusion coefficient, and lifetime.

2.2. The boundary conditions for Eq. (1) at $x = w$ correspond to continuity of the electron flux and concentration. The solution of the diffusion equation in the space-charge region for $\alpha w \ll 1$ gives

$$q_n(0) \approx q_n(w) + I_i \alpha w, \quad q_n(w) = -D_n \partial n / \partial x(w). \quad (2)$$

The condition of surface recombination with the rate $s_1$ is assigned on the right-hand boundary of the working region at $x = d$:

$$D_n \partial n / \partial x(d) = -s_1 n(d).$$

Here we have neglected the equilibrium dark electron concentration, which is much smaller than the characteristic concentrations in the working region upon illumination.

The boundary condition on the surface at $x = 0$ describes the recombination of electrons with positively charged centers and their emission into the vacuum.[8] The recombination flux $q_{sn} = \alpha_n n_0 N_s^+ = s_n n_0 (1-f)$ is proportional to the density of electrons and positively charged centers at the surface $N_s^+ = N_s(1-f)$ and the capture coefficient $\alpha_n$ on centers and depends on the filling of the centers with electrons $f$. Here $N_s = N_a w_0$ is the surface density of centers before illumination, and $s_n = \langle \alpha_n N_s \rangle$ is the rate of surface recombination.

A study of the energy distribution of the escaping electrons at a weak excitation intensity[10,11] shows that their energies are distributed in the band of width $\Delta E = E_c - E_{\text{vl}}$ between the conduction band edge and the vacuum level, which is close to the magnitude of the negative electron affinity $\Delta E \approx \chi$. This attests to the rapid trapping of electrons in the well of the space-charge region, slow energy relaxation in the well, and a small transparency of the near-surface effective potential barrier. The mean depth of the well in the space-charge region $V_{bi}$ significantly exceeds $\Delta E$; therefore, a decrease in the depth of the well in the space-charge region diminishes the emission current. Accordingly, the effective rate of electron emission from the space-charge region can be written in the form $v_{\text{emi}} = v_n T_n T_w$, where $v_n$ is the mean electron velocity and $T_n$ is the transparency of the effective barrier in the activation layer. The multiplier $T_w$ takes into account the decrease in the width $\Delta E$ of the energy band available for electron emission and the depth of the well in the space-charge region at a high excitation intensity as a consequence of the photovoltaic effect.

The final form of the boundary condition at $x = 0$ is

$$q_n(0) = -q_{sn} - q_{\text{emi}} = -[s_n(1-f) + v_{\text{emi}}] n_0. \quad (3)$$

2.3. The variation of the filling of the surface states is regulated by the difference between the fluxes of electrons and holes trapped by centers:

$$N_s \frac{df}{dt} = q_{sn} - q_{sp}, \quad q_{sp} = s_p p_0 f. \quad (4)$$

The initial value $f_0 = 0$ is assigned by the condition $q_{sn} = q_{sp} = 0$. The value of $q_{sp}$, like $q_{sn}$, is proportional to the density of the holes overcoming the energy barrier $p_0$, the density of neutral centers $N = N_s f$, and the rate of trapping on neutral centers $s_p = \alpha_p N_s$ ($\alpha_p$ is the hole capture coefficient). The hole density $p_0$ is determined by the total hole flux reaching the surface from the working region

$$p_0 = q_{p0}/V_p, \quad q_{p0} = q_{pth} + q_{pt}, \quad (5)$$

which contains two components, the thermionic emission current $q_{pth}$ and the tunneling current $q_{pt}$ through the barrier into the space-charge layer. The fluxes $q_{pth}$ and $q_{pt}$ are written in the standard manner (see Ref. 12). The expressions for them were presented in Ref. 8.

2.4. The flux of holes toward the surface restores the number of positively charged surface states and the surface charge. The variation of the filling of the centers alters the surface charge density $eN_s^+ = eN_s(1-f)$, the height $V_{bi}$, and the width $w$ of the energy barrier to holes

$$V_{bi} = 2\pi \frac{e^2 N_s^{+2}}{\varepsilon_s N_a} = V_{bi}^0 (1-f)^2,$$

$$w = \sqrt{\frac{2V_{bi}}{kT}} L_d = w_0 (1-f) \quad (6)$$

($L_d$ is the Debye radius) and leads to a photovoltaic effect consisting of the appearance of a photovoltage $\delta V$, which alters the position of the conduction band edge relative to the vacuum level:

$$\delta V = V_{bi}^0 - V_{bi} = V_{bi}^0 f(2-f), \quad E_{\text{vl}} = E_{\text{vl}}^0 + \delta V. \quad (7)$$

This decreases the fraction of electrons overcoming the barrier. The total charge of the electrons emitted by the photocathode from a unit area (in units of $e$) equals

$$Q = v_n \int_0^\infty T_n T_w n_0 \, dt. \quad (8)$$

The dependence of the transparency $T_w$ on the degree of band bending is associated with the energy distribution of the electrons in the well of the space-charge region. In the approximation of a uniform distribution

$$T_w = \frac{E_c - E_{\text{vl}}}{V_{bi}} = \frac{r-y}{1-y}, \quad y = \delta V / V_{bi}^0,$$

$$r = \frac{E_c - E_{\text{vl}}^0}{V_{bi}^0} = T_{w0}. \quad (9)$$

It can be seen from (9) that the ''well transparency'' decreases as the photovoltage (the filling of the centers) in-

creases. The equation describing the kinetics of the filling of surface centers (4) with consideration of (7) and (9) is conveniently written relative to $y$ in the form

$$\frac{N_s}{2\sqrt{1-y}}\frac{dy}{dt}=q_{sn}-[q^0_{sth}(e^{U_0y}-1)+q^0_{st}(e^{\lambda_0 y}-1]f, \tag{10}$$

where

$$f=1-\sqrt{1-y}, \quad U_0=V^0_{bi}/kT,$$

$$\lambda_0=\lambda U_0, \quad \lambda=2\sqrt{m^*_p kTL_d}/\hbar.$$

It follows from (10) that the hole restoring current depends on the filling $f$ of the centers, which determines the photovoltage $y$. The explicit expressions for the preexponential factors $q^0_{sth}$ and $q^0_{st}$ in the hole current were presented in Ref. 8.

### 3. QUASISTATIONARY APPROXIMATION

3.1. The complexity of the combined solution of the diffusion equation (1) and the center filling kinetic equation (10) is due to the nonlinearity of the problem; however, several specific models are amenable to analytic solution. Let us consider the case where the diffusion processes in the working region are considerably faster than the establishment of equilibrium between the electron and hole fluxes reaching the barrier. With the exception of the initial stage with a duration less than $t_*=d^2/D_n$, the distribution of the electron concentration and the fluxes correspond to the stationary solutions of the boundary-value problem (1). To analyze the solution of the kinetic equation (10) we replace the electron flux $q_{sn}$ by an approximate expression, which is equal to the stationary value of $q_{sn}$ for $f\to 0$,[8]

$$q_{sn}=I_i\frac{\alpha L_{\rm dif}}{1+\alpha L_{\rm dif}}\frac{\gamma\theta_0}{1+\upsilon_n T_n r/s_n}. \tag{11}$$

Here $L_{\rm dif}=\sqrt{D_n\tau}$, and $\gamma$ and $\theta_0$ are constants, which depend on the parameters characterizing the bulk generation and recombination in the working region and the rate of surface recombination at $x=d$.[8]

Under the assumption that $q_{sn}$ does not depend on time, Eq. (10) can be integrated in quadratures:

$$\int_0^y \frac{dy}{2\sqrt{1-y}\left\{1-\left[\frac{q^0_{sth}}{q_{sn}}(e^{U_0y}-1)+\frac{q^0_{st}}{q_{sn}}(e^{\lambda_0 y}-1)\right](1-\sqrt{1-y})\right\}}=\frac{t}{N_s/q_{sn}}. \tag{12}$$

At low intensities, at which $\lambda_0 y\ll 1$ and $U_0 y\ll 1$, the integral in (12) can be calculated, and the solution has the form

$$y=y_s\tanh(t/\tau_s), \tag{13}$$

$$y_s=\sqrt{\frac{2q_{sn}}{q^0_{sth}U_0+q^0_{st}\lambda_0}},$$

$$\tau_s=\frac{N_s}{\sqrt{2q_{sn}(q^0_{sth}U_0+q^0_{st}\lambda_0)}}. \tag{14}$$

It follows from (14) that $\tau_s$ decreases with increasing intensity as $\tau_s\propto I_i^{-1/2}$ and that $y_s$ increases as $y_s\propto I_i^{1/2}$. We note that at low intensities, at which the charge-confinement effects are weak, the slow relaxation of the photovoltage with the time $\tau_s$ weakly influences the time dependence of the quantum efficiency, which is established simultaneously with the distribution of the electron concentration, i.e., during a time of the order of the diffusion time.

At high excitation intensities an approximate analytic solution can be obtained for the case where one of the components of the hole restoring current (say, the tunneling current) dominates ($q^0_{st}\gg q^0_{sth}$)

$$y=\frac{1}{\lambda_0}\ln\frac{q'}{1+(q'e^{-\lambda_0 y_1}-1)\exp[-\lambda_0 q'\overline{f(1-f)}(\tilde{t}-\tilde{t}_1)]}. \tag{15}$$

Here $\tilde{t}=2tq^0_{st}/N_s$, $q'\approx 1+(q_{sn}/q^0_{st})/\overline{f}$ (a line over a symbol denotes averaging in the interval $[y_1,y]$, where $y_1(t_1)\ll y$ corresponds to the upper boundary of the linear region).

The solution (15) contains the characteristic time scale

$$\tau_s=\frac{N_s}{2\lambda_0 q'\overline{f(1-f)}q^0_{st}}\approx\frac{N_s/q_{sn}}{2\lambda_0\overline{f(1-f)/f}}. \tag{16}$$

It follows from (15) that the time for the establishment of stationary values of the photovoltage and the quantum efficiency is equal to $\tau_{\rm ad}=(3-4)\tau_s\approx N_s/I_i$. It can vary over a broad range, decreasing at large values of the excitation intensity [to the extent that the ratio $\overline{f(1-f)/f}$ is independent of intensity] in inverse proportion to the illumination intensity $I_i$.

3.2. The range of intensities corresponding to significant charge-confinement effects corresponds to a large photovoltage on the barrier and a low transparency $T_w$. The maximum value of the photovoltage $y$, at which the surface barrier is transparent to electrons depends on the initial values of $E_c-E^0_{\rm vl}$ and $V^0_{bi}$ and equals $y_{\max}=r$. In this case $f_{\max}=1-\sqrt{1-r}$, If $\delta V\geqslant E_c-E^0_{\rm vl}$ (i.e., $y\geqslant r$), the barrier becomes nontransparent. The expression for the radiation intensity corresponding to the condition $y=r$ follows from the equality $q_{sn}=q_{sp}$:

$$I^{\rm cr}\approx\frac{[1+(\alpha L_{\rm dif})^{-1}]}{\gamma\theta(r)}[q^0_{st}(e^{\lambda_0 r}-1)+q^0_{sth}(e^{U_0 r}-1)](1-\sqrt{1-r}). \quad (17)$$

We note that the expression (17) is valid for an arbitrary form of the function $T_w(y)$, but it should be assumed that $T_w(r)=0$. It is significant that $I^{\rm cr}$ decreases exponentially with increasing $E^0_{\rm vl}$ (decreasing $r$). Conversely, decreases in $s_n$ and increases in $s_p$ shift the barrier nontransparency boundary to higher intensities.

## 4. TRANSIENT PROCESSES FOLLOWING THE ONSET OF ILLUMINATION

4.1. The electron diffusion equation (1) with the boundary conditions (2) and (3) was solved together with Eq. (10), which describes the kinetics of the filling of positively charged centers by electrons. Difference approximations of second-order accuracy with respect to the coordinate and first-order accuracy with respect to time were used. In solving the system of difference equations, the time step included internal iterations for calculating $f$ for an assigned flux $q_w$ on the boundary of the working region and external iterations for calculating the distribution $n(x)$ in the next time layer.

The results of the calculations for a photocathode with the parameters $d=1\,\mu$m, $D_n=40$ cm$^2$/s (the diffusion time $t_*=d^2/D_n=0.25$ ns), $\alpha=10^4$ cm$^{-1}$, $\tau=10^{-9}$ s, $s_1=10^5$ cm/s, $N_a=5\times10^{18}$ cm$^{-3}$, $V^0_{bi}=0.3$ eV, $E^0_{\rm vl}=1.2$ eV, and $T_n=0.04$ are presented below. The capture coefficients of electrons and holes on surface centers were $\alpha_n=10^{-7}$ cm$^3$/s and $\alpha_p=3\times10^{-8}$ cm$^3$/s. The calculations allowed for the field dependence of the rate of surface recombination of electrons and the decrease in barrier transparency with increasing photovoltage.[8] For the numerical values of the parameters taken $I^{\rm cr}\approx4\times10^{22}$ cm$^{-2}$s$^{-1}$.

4.2. Let us examine the dynamics of the transient processes for a photocathode following the instantaneous onset of illumination. The range of illumination intensities includes values of $I_i$ which are much smaller than the critical value $I^{\rm cr}$ (low intensities) or close to it (high intensities). The numerical values of $I^{\rm cr}$ and, therefore, the values of the ''low'' and ''high'' intensities are determined by the photocathode parameters selected, primarily by $E^0_{\rm vl}$ and $\alpha_p$.

The characteristic time of the transient process following the instantaneous onset of illumination is determined by the time for the diffusion of nonequilibrium electrons to the barrier $t_*$ and the time for equalization of the fluxes of photogenerated electrons and holes $\tau_s$. When the intensity creates an electron density at the barrier much smaller than $N_a$, equilibrium between $q_{sn}$ and $q_{sp}$ is established over a space-charge layer of a considerable width, which is close to the dark value. Therefore, equilibrium between the fluxes is achieved after a time much greater than $t_*$. If the intensity is such that the electron concentration at the barrier becomes comparable to the density of the charged centers, then (in the case of instantaneous recombination) the photovoltage lowers the energy barrier to holes during the diffusion time, and equilibrium between the electron and hole fluxes is achieved during the same time. Equalization of the two characteristic times gives an estimate of the intensity $I_*=N_sD_n/d^2$, at which the time for the establishment of equilibrium equals $t_*$. The value for the parameters taken is $I_*=2\times10^{22}$ cm$^{-2}$s$^{-1}$ and is thus approximately two times smaller than $I^{\rm cr}$, which corresponds to closing of the barrier.

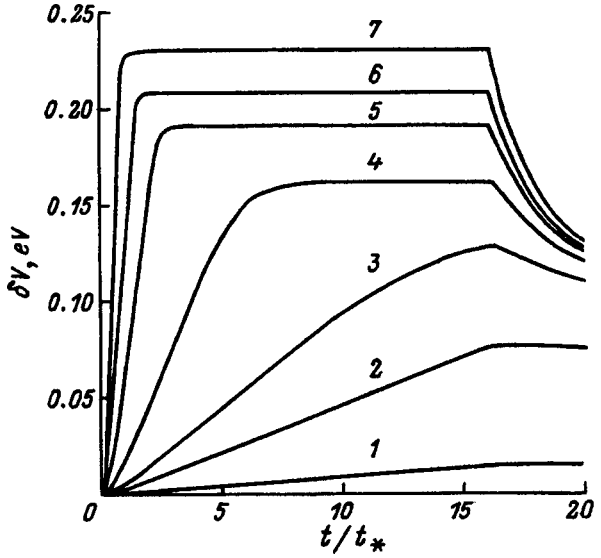


FIG. 1. Dependence of the photovoltage on time (in units of $t_*$) for various values of the illumination intensity $I_i$, $10^{20}$ cm$^{-2}$s$^{-1}$: *1* — 1, *2* — 5, *3* — 10, *4* — 30, *5* — 100, *6* — 200, *7* — 500.

After the onset of illumination the electron concentration $n(x)$ at first increases monotonically with time in the entire working region, and then (at $t\gtrsim2t_*$) bulk and ''surface'' recombination diminish it somewhat, and the distribution of $n(x)$ relaxes downward to the stationary profile. The time for the establishment of a stationary distribution of electrons is of the order of the diffusion time, i.e., $(2-5)t_*$. Numerical calculations show that the flux $q_{sn}$ reaches a stationary value during a time close to $t_*$, regardless of the illumination intensity. The hole flux $q_{sp}\ll q_{sn}$ at $t\simeq t_*$, and the time for the establishment of equilibrium between $q_{sn}$ and $q_{sp}$ depends fairly strongly on the intensity, decreasing according to a $\tau_{\rm ad}\propto N_s/I_i$ law.

The results of the calculation of the dependence of the photovoltage on the barrier $\delta V(t)$ and the quantum efficiency $Y(t)$ for a light pulse of duration $t_{\rm pul}=16t_*$ are shown in Figs. 1 and 2. For the values of the capture coefficients taken in the calculation and intensities corresponding to the manifestation of charge-confinement effects, $\delta V(t)$ and $Y(t)$ reach stationary values at times considerably smaller than $t_{\rm pul}$. We note that, as follows from (7), the time dependences of the photovoltage on the barrier $\delta V(t)$ are determined by the filling $f(t)$ of the centers by electrons. It can be seen from Fig. 1 that the photovoltage on the barrier $\delta V(t)$ increases monotonically with time and that the stationary value of $\delta V$ and the derivative $d\,\delta V/dt$ increase with increasing $I_i$, while the time for the achievement of a stationary state $\tau_{\rm ad}$ decreases. In the range of fairly large intensities $I_i\simeq0.1I_*$ ($I_i\gtrsim10^{21}$ cm$^{-2}$s$^{-1}$) the photovoltage on the barrier is comparable to $E_c-E^0_{\rm vl}$, the stationary value of $f$ approaches 0.5, and $\tau_{\rm ad}$ approaches the diffusion time $t_*$ and

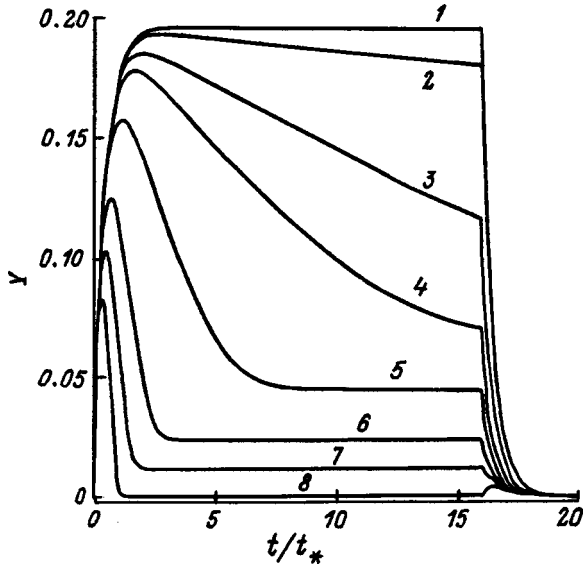


FIG. 2. Quantum efficiency $Y$ of a photocathode as a function of time (in units of $t_*$) for various values of the illumination intensity $I_i$, $10^{20}$ cm$^{-2}$s$^{-1}$: *1* — 0.1, *2* — 1, *3* — 5, *4* — 10, *5* — 30, *6* — 100, *7* — 200, *8* — 400.

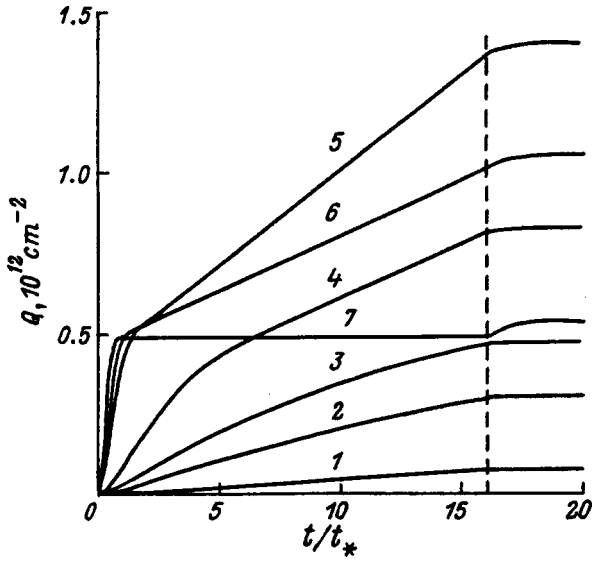


FIG. 3. Photoelectron charge $Q$ (in units of $e$) as a function of time (in units of $t_*$) for various values of the illumination intensity $I_i$, $10^{20}$ cm$^{-2}$s$^{-1}$: *1* — 1, *2* — 5, *3* — 10, *4* — 30, *5* — 200, *6* — 300, *7* — 500.

then drops below it. In this case the filling $f(t)$ of the centers and the photovoltage $\delta V$ at first increase sharply and then rise slowly in the quasistationary regime. In this case the rise in $f(t)$ continues even after achievement of the filling $f_{\max}$, which corresponds to a completely nontransparent barrier ($T_w=0$). Conversely, at low intensities ($I_i \lesssim 0.1 I_*$) the values of $f$ and $y$ are much less than unity, a stationary state is not achieved during a time equal to $16t_*$ (Fig. 1), and when the intensity is lowered to $\lesssim 0.01 I_*$, the time for the achievement of a stationary regime increases to values of the order of fractions of a microsecond. Decreasing the electron capture coefficient $\alpha_n$ leads to a similar effect.

Figure 2 shows plots of the time dependence of the quantum efficiency (the emission current normalized to the light intensity in the pulse) for various illumination intensities. It can be seen from the figure that there are four ranges of intensities that determine the character of the behavior of $Y(t)$. In the range of very low intensities $I_i \lesssim 0.01 I_*$ ($I_i \approx 10^{19}$ cm$^{-2}$s$^{-1}$) the quantum efficiency $Y(t)$ increases monotonically with time and reaches a stationary value, which does not depend on intensity, after a time of the order of $t_*$. In the range of low intensities $I_i \gtrsim 0.1 I_*$ ($I_i \approx 10^{21}$ cm$^{-2}$s$^{-1}$) the quantum efficiency passes through a gently sloping maximum and then decreases to a stationary value. In this intensity range the maximum and stationary values of $Y$ are very close, and the time for achieving the maximum decreases with increasing $I_i$. In the range of moderate intensities $I_i \simeq I_*$ ($I_i \simeq 10^{22}$ cm$^{-2}$s$^{-1}$) the maximum of $Y$ shifts appreciably to the left and becomes sharper, and the difference between the maximum and stationary values becomes quite considerable as the intensity is increased. The stationary value of $Y$ decreases and becomes significantly smaller than the value of $Y_0$ at low intensities. The $Y(t)$ curve acquires a characteristic spike-shaped form. Finally, in the range of high intensities $I_i \gtrsim I^{\rm cr} \approx 4 \times 10^{22}$ cm$^{-2}$s$^{-1}$, after a time less than $t_*$, the increase in the photovoltage to values comparable to $E_c - E_{\rm vl}^0$ leads to fulfillment of the condition $E_{\rm vl} > E_c$, the barrier becomes nontransparent before the photocathode achieves a stationary regime, and the quantum efficiency $Y$ vanishes. When the intensity is increased further, the time for achieving the maximum of $Y$ and the time for achieving complete barrier nontransparency, as well as the value of $Y$, decrease, and the accumulation of charge ends at times appreciably shorter than the diffusion time. The nonmonotonic character of $Y(t)$ is attributed to the decrease in the barrier transparency and the increase in the recombination of photoelectrons near the barrier after a quasistationary state is achieved in the working region. The duration of the descending portion of the $Y(t)$ curve is determined by the time for the establishment of equilibrium between the electron and hole fluxes at the barrier.

These features of the behavior of $Y(t)$ are manifested in the time dependence of the total number of electrons emitted by the photocathode. Figure 3 reveals the intensity dependence of $dQ/dt$, its variation with time, and the cessation of charge accumulation at times smaller than the diffusion time $t_*$ at intensities exceeding the critical value. It can also be seen from Fig. 3 that the increase in the stationary values of $Q(t)$ with increasing illumination intensity gives way to a decrease at small and moderate intensities ($I_i \lesssim 10^{22}$ cm$^{-2}$s$^{-1}$). This is because the charge-confinement effects lead to an appreciable decrease in the amount of charge emitted, i.e., to a nonmonotonic dependence of the accumulated charge on the illumination intensity, at high intensities due to the decreases in the charge accumulation time and the quantum efficiency (see also Sec. 5.1). Thus, for a photocathode with assigned characteristics there is an upper limit on the number of electrons emitted from 1 cm$^2$ of the working region during a light pulse under intense excitation. As follows from Ref. 8, this limit is of the order of $N_s$. For the values of the parameters taken it is equal to roughly

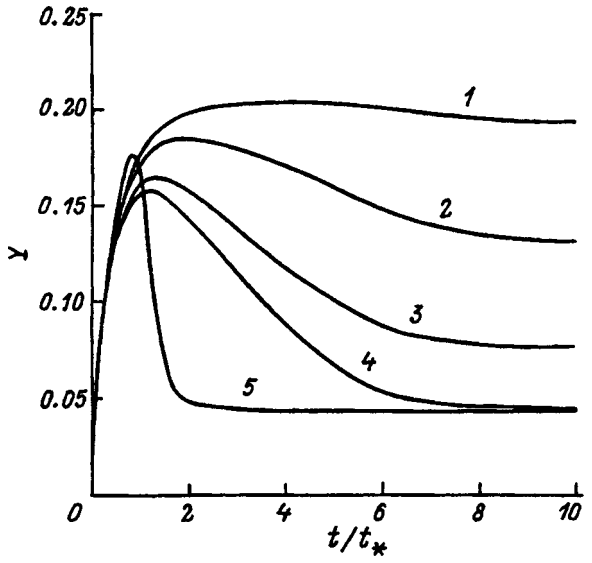


FIG. 4. Calculation of the time dependence of the quantum efficiency $Y(t)$ for various models of the trapping of electrons and the barrier transparency in the activation layer. Illumination intensity $I_i$, $10^{21}$ cm$^{-2}$s$^{-1}$: *1–4* — 3, *5* — 35. Model parameters: *1* — $\alpha_n=\alpha_{n0}$, $T_n=T_{n0}$; *2* — $\alpha_n(E)$, $T_n=T_{n0}$; *3* — $\alpha_n=\alpha_{n0}$, $T_n=T_n(\delta V)$; *4* — $\alpha_n(E)$, $T_n=T_n(\delta V)$; *5* — $\alpha_n=\alpha_{n0}$, $T_n=T_{n0}$.

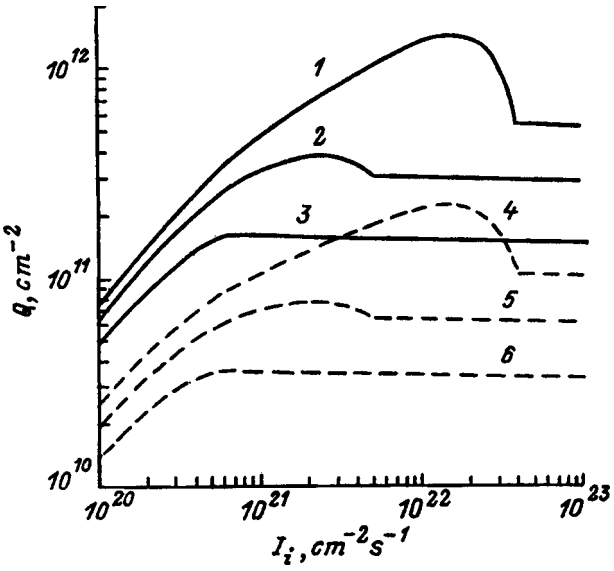


FIG. 5. Dependence of the photoelectron emission charge $Q$ (in units of $e$) on illumination intensity for various values of $E_{nl}^0$ and $T_n$: *1–3* — $T_n=0.04$; *4–6* — $T_n=0.01$; $E_{\rm vl}^0$, eV: *1, 4* — 1.2; *2, 5* — 1.25; *3, 6* — 1.3.

$10^{12}$ electrons and corresponds to an intensity $I_i=10^{22}$ cm$^{-2}$s$^{-1}$, which is roughly four times smaller than the critical value, at which the barrier becomes nontransparent.

Let us now discuss the question of how the features of the model of the photoemission process influence $Y(t)$. The significance of such factors as the field dependence of the rate of surface electron recombination [$\alpha_n(E)\propto E^{-\nu}$] and the dependence of the tunneling transparency of the surface barrier on photovoltage [$T_n(\delta V)$], can be determined by direct simulation. The influence of these factors on the stationary characteristics of a photocathode was investigated in Ref. 8. Figure 4 presents the results of calculations with and without consideration of the field dependence of the surface recombination rate and the dependence of the tunneling transparency of the surface barrier on photovoltage [see Eq. (36) in Ref. 8]. The effect of both factors is like an additional increase in intensity. Both factors diminish the numerical value of the quantum efficiency and shorten the time for achieving the maximum of $Y(t)$ and the time for achieving a stationary state. It is significant that the choice of the model determines the quantitative features of $Y(t)$. Consideration of the dependence of $T_n$ on $\delta V$ is more important in the quantitative respect, since a decrease in the tunneling barrier transparency at high intensities dramatically reduces the fraction of electrons capable of overcoming the barrier. The parameters of $\alpha_n(E)$ and $T_n(\delta V)$ can be determined from the experimental data if $Y(t)$ and $\delta V(t)$ are measured simultaneously (see Ref. 8).

## 5. TRANSIENT PROCESSES FOLLOWING THE TERMINATION OF ILLUMINATION

5.1. A study of the processes occurring in a photocathode following the termination of illumination provides information on the hole current restoring its original state. Below we shall discuss the results of calculations for the case of rapid termination, in which it was assumed that at the time $t=t_0=16t_*$ the intensity begins to decrease according to a Gaussian law with a time constant $10^{-12}$ s.

The calculations show that there are two stages in the restoration of the characteristics of a photocathode following the termination of illumination, of which one takes place in the diffusion time scale $t_*$, while the other is determined by the time of the decrease in the photovoltage to small values near $\delta V\sim kT$ (this time is denoted by $t_r$). The first stage is associated with the escape of electrons from the working region in the absence of photogeneration and with decreases in both the photovoltage on the barrier and the electron flux $q_{sn}$ during a time of the order of $2t_*$. These decreases are clearly displayed in Fig. 1 (curves *4–7*) and Fig. 2 (curves *1–7*). Thereafter the filling of the surface centers varies only under the effect of the hole restoring flux.

At high light intensities near $I^{\rm cr}$, where the barrier transparency decreases dramatically ($I_i\simeq 10^{23}$ cm$^{-2}$s$^{-1}$), a repeated increase in current is possible, despite the decrease in the electron concentration near the barrier, due to the improvement in the effective transparency $T_w$ as a result of the decrease in the photovoltage (curve *8*, Fig. 2). For this reason, charge accumulation not only continues after termination of the excitation for a time roughly equal to $2t_*$, but can also produce an addition to the emission charge (at intensities of the order of $I^{\rm cr}$; see Fig. 3, curves *6* and *7*). As the intensity approaches $I^{\rm cr}$, the total amount of charge emitted in a pulse is a nonmonotonic function of intensity due to the decrease in the barrier transparency and the increase in the recombination rate (Fig. 5). The position and numerical value of the maximum and the details of the behavior of $Q(I_i)$ in the vicinity of the maximum depend on the difference $E_c-E_{\rm vl}^0$ and $T_n$. A clearly expressed maximum appears on the $Q(I_i)$ curve for photocathodes with high values of the

''well transparency'' ($T_{w0}=r$) at low intensities. For photocathodes with small values of $T_{w0}$ the growth of the charge slows sharply as the vicinity of $I^{cr}$ is approached, and after passing through a diffuse maximum the function $Q(I_i)$ approaches a limiting value from above (curves *3* and *6*).

It should be noted that the dependence of the accumulated charge $Q$ on the tunneling barrier transparency $T_n$ is nonlinear and its character depends on the excitation intensity. As can be seen from Fig. 5, in the vicinity of $I^{cr}$ a decrease in $T_n$ leads to a decrease in $Q_{max}$ according to a law that is stronger than a linear relation.

5.2. Let us now consider the stage of restoration of the photocathode characteristics. Figure 1 shows the significant asymmetry of the plots of $\delta V(t,I_i)$ and the difference between the time scales for the onset and termination of illumination, which depends on the excitation intensity. Following the termination of illumination, the photovoltage decreases due to cessation of the supply of electrons from the working region to the space-charge region, and (at high and moderate illumination intensities) it drops to values of about 0.1 V during a time equal to $(1-3)t_*$, regardless of the initial value of the intensity (Fig. 1). The decrease in the photovoltage leads to an increase in the width of the space-charge layer and the height of the barrier to holes, decreasing the hole flux and slowing the decline of the photovoltage on the barrier. The derivative $|d\delta V/dt|_{t_{pul}}$ depends weakly on intensity in the strongly nonlinear case [$\delta V(t_0)\simeq V_{bi}^0$], but when $\delta V(t_0)\ll V_{bi}^0$ or $y_0\ll 1$, it decreases markedly with decreasing intensity. Thus, regardless of the illumination intensity, relaxation in a linear regime takes up a large part of the restoration period, during which the photovoltage decreases from $\delta V_0\lesssim 0.1$ to a value smaller than $kT$.

The restoration time greatly exceeds the time for the achievement of the stationary state and increases with decreasing values of the hole capture coefficient $\alpha_p$. Let us estimate this time using Eq. (10). Assuming that $q_{sn}\ll q_{sp}$ during virtually the entire restoration time, instead of (12) we obtain

$$\int_y^{y_0}\frac{dy}{2\sqrt{1-y}(1-\sqrt{1-y})[\tau_t^{-1}(e^{\lambda_0 y}-1)+\tau_{th}^{-1}(e^{U_0 y}-1)]}=t(y)-t_0. \tag{18}$$

Equation (18) contains two quantities having the dimensions of time, viz., $\tau_t=N_s/q_{st}^0$ and $\tau_{th}=N_s/q_{sth}^0$, and the smaller of them is the characteristic time scale for restoration of the quantum efficiency. An approximate solution of the problem under the condition of dominance of the hole tunneling current ($\tau_t\ll\tau_{th}$) has the form

$$t_r-t_0=\tau_t F(y_r,y_0,\lambda_0),$$

$$F(y_r,y_0,\lambda_0)=\int_{y_r}^{y_0}\frac{dy}{2\sqrt{1-y}(1-\sqrt{1-y})(e^{\lambda_0 y}-1)}. \tag{19}$$

The integral $F(y_r,y_0,\lambda_0)$ can be evaluated to sufficient accuracy if the integrand is replaced by an approximate expression which holds in the region making the largest contribution to the integral. Then

$$F(y)=\frac{1}{\sqrt{1-y_0}}\int_{\lambda_0 y}^{\lambda_0 y_0}\frac{dz}{z(e^z-1)}\approx\frac{1}{\sqrt{1-y_0}\lambda_0 y}\left(1-\frac{y}{y_0}\right). \tag{20}$$

When $y/y_0\ll 1$, $F$ increases proportionally to $1/y$. Let us make some numerical estimates. We assume that the restoration process is completed when the effective transparency $T_w$ of the quantum well increases to the $0.99r$ level. If $E_c-E_{vl}^0=0.224$ eV and $V_{bi}^0=0.3$ eV, this corresponds to a photovoltage $\delta V_r$ roughly equal to 0.01 eV. For $y_0=1/3$ (see Fig. 1) and $\lambda_0\approx 7.5$ we obtain $F\approx 4.4$. A similar estimate for $\delta V_r=kT$, which corresponds to the restoration of $T_w$ to the $0.97r$ level, gives $F\approx 1.4$. Thus, it can be assumed for moderate and high intensities that $F$ depends weakly on $y_0$ and that the restoration time $t_r-t_0\approx(2-3)\tau_t$.

It follows from the definition of $\tau_t$ and $q_{st}^0=s_p N_* e^{-\lambda_0}$, where the effective density of tunneling holes for the parameters chosen $N_*\approx 3\times 10^{17}$ cm$^{-3}$ (see Refs. 8 and 12), that

$$\tau_t=(\alpha_p N_*)^{-1}e^{\lambda_0}. \tag{21}$$

This time decreases with increasing $\alpha_p$ and increases with $\lambda_0$ [see (10)]. Since $\lambda_0\propto(m_p^*/N_a)^{1/2}$, $\tau_t$ decreases exponentially with increasing $N_a$ and increases with the effective mass of the tunneling holes. It is very significant that $\lambda_0$ does not depend on temperature, and thus the temperature dependence of $\tau_t$ is determined only by the preexponential factor and the hole restoring current.[12] If $\alpha_p=3\times 10^{-8}$ cm$^3$/s and $\lambda_0=7.5$, for the parameters used in the calculation the restoration time $t_r=2\tau_t=0.4\mu$s.

In the linear case $U_0 y,\lambda_0 y\ll 1$, and formula (18) is applicable over the entire range of variation of $y$, so that $y_0$ is the stationary value of the photovoltage during illumination. The law governing the variation of $y$ has the form

$$y=\frac{y_0}{1+(t-t_0)/\tau_l},\quad \tau_l=\frac{N_s}{(q_{st}^0\lambda_0+q_{sth}^0U_0)y_0}. \tag{22}$$

Plugging in $y_0$ from (14), we obtain

$$\tau_l=\frac{N_s}{\sqrt{2q_{sn}(q_{st}^0\lambda_0+q_{sth}^0U_0)}}\equiv\tau_s, \tag{23}$$

where $\tau_s\propto I_i^{-1/2}$ is the time for the achievement of a stationary state. Thus, in the case of low intensities, in which the photocathode parameters vary only slightly under the effect of illumination, the processes leading to the establishment of equilibrium following the onset and termination of illumination take place with similar time scales.

5.3. There should be special interest in the simulation of excitation by two pulses of equal duration and intensity ($t_{pul}=4t_*=1$ ns, $I_i=10^{23}$ cm$^{-2}$s$^{-1}$) with a variable interval $\Delta$ between them. Such a regime has been used both for experimental studies of nonlinear effects[4,5] and in accelerators.[9] The excitation intensity chosen is such that the time for achieving the stationary state is several times smaller than the illumination time $t_{pul}$. The emission charge in the second pulse is determined both by the changes in the barrier parameters in response to the first pulse (which depend on the relationship between $I_i$ and $I^{cr}$) and by the relationship between $\Delta$ and the restoration time $t_r$ of the barrier character-

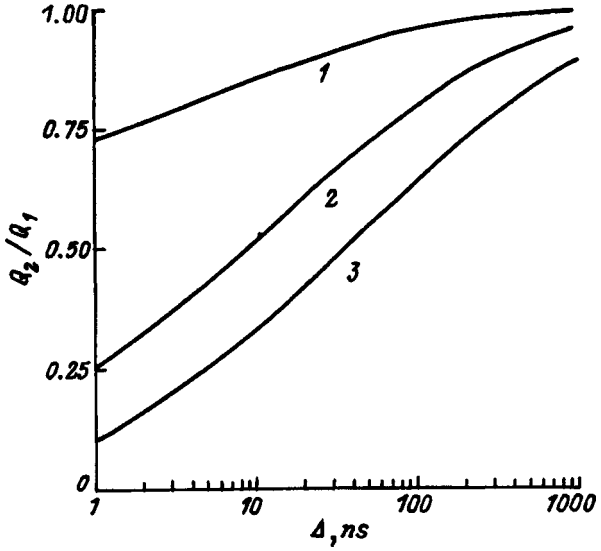


FIG. 6. Ratio of the photoelectron emission charge in the second pulse $Q_2$ to the emission charge in the first pulse $Q_1$ for two-pulse excitation as a function of the delay between the pulses $\Delta$ for various values of $\alpha_p$ $\mathrm{cm^3 s^{-1}}$: *1* — $10^{-7}$, *2* — $3\times10^{-8}$, *3* — $10^{-8}$.

istics. Both $I^{\mathrm{cr}}$ and $t_r$ depend on the capture coefficient of holes on neutral centers. In particular, the value of $I^{\mathrm{cr}}$ decreases with decreasing $\alpha_p$ [see (17)], while the time $\tau_t \propto 1/\alpha_p$ increases. Figure 6 shows plots of the charge ratio $Q_2/Q_1$ as a function of $\Delta$, which were calculated for various values of the capture coefficient of holes on neutral centers $\alpha_p$. It is seen that at $\Delta \ll \tau_t$ the ratio $Q_2/Q_1$ is markedly less than unity and depends strongly on $\Delta$ and $\alpha_p$.

Apart from the dependence of $Q_2/Q_1$ on $\Delta$, it would be interesting to determine the smallest interval between pulses which ensures that $(Q_1-Q_2)/Q_1 \leqslant q$ for an assigned value of $q$. The calculations show that the ratio $Q_2/Q_1$ differs from unity by no more than 5% when $\Delta \simeq (2-3)\tau_t$. In the range $\alpha_p = 10^{-7}-10^{-8}$ $\mathrm{cm^3/s}$ the time $\tau_t$ varies in the range $0.05-0.5\mu$s. For $\alpha_p \leqslant 3\times10^{-8}$ $\mathrm{cm^3/s}$ and the intensity $I_i = 10^{23}$ $\mathrm{cm^{-2}s^{-1}} > I^{\mathrm{cr}}$ we note that the barrier is blocked long before the establishment of equilibrium and that restoration of the position of the vacuum level relative to the conduction band requires considerable time. For this reason the emission charge in the second pulse for $I_i \geqslant I^{\mathrm{cr}}$ is strongly reduced when $\Delta \ll \tau_t$ (see Fig. 6).

## 6. DISCUSSION OF THE EXPERIMENT

A comparison of the results of the theoretical calculations with experimental data[5] on the dependence of the emission charge $Q$ on the laser pulse energy shows that adjustment of the values of $E_c - E_{\mathrm{vl}}^0$ and $T_n$ makes it possible to obtain the range of values of $Q$ which reproduce the experimental data. An inversely proportional intensity dependence of the time for the establishment of a stationary regime following the onset of illumination [formula (16)] was observed in Ref. 6. Calculations of the restoration of the photocathode characteristics following the termination of illumination and simulation of the two-pulse regime reveal the processes which determine the main qualitative effects:[4,5,7] the decreases in the amplitude of the current and charge during the repeated pulse and their increase with the delay between pulses (a memory effect).

The restoration time of the photocathode characteristics depends weakly on temperature [see (21)], providing evidence (together with the experimental results in Ref. 4) supporting the assertion that the light-hole tunneling current is the restoring current. The restoration time is determined by the capture coefficient of holes on neutral centers, and when $\alpha_p \approx 3\times10^{-8}$ $\mathrm{cm^3/s}$, it amounts to 0.1 $\mu$s, which is consistent with the experimental data in Refs. 5 and 7. The exponential dependence of the restoration time on the parameters of the emitter space-charge region leads to strong variability of the observed (for example, in Refs. 4 and 5) restoration times and the dependences of the photocurrent on the delay in the case of two successive excitation pulses, providing evidence of the significantly different parameters of the photoemitters investigated.

According to experiment, the maximum values of the quantum efficiency and the free charge are achieved for large values of the negative electron affinity ($E_c - E_{\mathrm{vl}}^0 \simeq 0.2$ eV), and a small restoration time is attained for a high concentration of acceptors in the space-charge region.

## 7. CONCLUSION

The transient characteristics of photocathodes observed at high excitation intensities (the kinetics of the establishment of a stationary regime and the dependence of the emission charge on illumination intensity and restoration time) are described by a nonlinear diffusion-drift model of a photocathode. The results obtained permit reconstruction of the of the parameters of photoemitters from experimental transient characteristics and can be used to optimize photocathode structures for use in excitation regimes.

This work was supported by a grant from the U.S. Civilian Research and Development Foundation (CRDF, Award No. RPI-351) and by Grant 95-1.23 from the ''Surface and Atomic Structures'' Russian State Program, as well as by Grant 96-02-19187*a* from the Russian Fund for Fundamental Research.

[1] D. T. Pierce, in *Experimental Methods in Atomic, Molecular and Optical Physics: Charged Particles* (*Experimental Methods in the Physical Sciences, Vol. 29A)*, F. B. Dunning and R. G. Hulet [Eds.], Academic Press (1995), p. 1.
[2] K. Abe, *et al.*, (SLAC E143 Collaboration), Phys. Rev. Lett. **75**, 4173 (1995).
[3] M. Hecht, Phys. Rev. B **41**, 7918 (1990).
[4] A. S. Jaroshevich, M. A. Kirillov, D. A. Orlow, A. G. Paulish, H. E. Sheibler, and A. S. Terechov, in *Proceedings of the 7th International Workshop on Polarized Gas Targets and Polarized Beams*, Urbana (1997), p. 485.
[5] H. Tang, R. K. Alley, H. Aoyagy, J. E. Clendenin *et al.*, in *Proceedings of the Workshop on Photocathodes for Polarized Electron Sources for Accelerators (SLAC-432)* (1994), p. 344.
[6] Y. B. Bolkovityaninov, A. M. Gilinsky, C. W. de Jager *et al.*, in *Proceedings of the 12th International Symposium on High-Energy Spin Physics*, C. D. W. de Jager *et al.*, [Eds.], Word Scientific, Singapore (1997), p. 700.
[7] A. Herrera-Gómez, G. Vergara, and W. E. Spicer, J. Appl. Phys. **79**, 7318 (1996).
[8] B. I. Reznikov and A. V. Subashiev, Fiz. Tekh. Poluprovodn. **32**, 1125 (1998) [Semiconductors **32**, 1006 (1998)].

[9] R. Alley, H. Aoyagi, J. Clendenin *et al.*, Nucl. Instrum. Methods Phys. Res. A **365**, 1 (1995).
[10] C. Herman, H.-J. Drouhin, G. Lampel, Y. Lassailly, D. Paget, J. Peretti, R. Houdré, F. Ciccacci, and H. Riehert, in *Spectroscopy of Nonequilibrium Electrons and Phonons*, C. V. Shank and B. P. Zakharchenya [Eds.], Elsevier (1992), p. 135.
[11] A. S. Terekhov, D. A. Orlov, A. S. Yaroshevich, G. M. Soldatenkov, I. V. Savchenko, and L. S. Ronzhin, Fiz. Tverd. Tela (St. Petersburg) **38**, 306 (1996) [Phys. Solid State **38**, 171 (1996)].
[12] S. M. Sze, *Physics of Semiconductor Devices*, 2nd ed. (Wiley-Interscience, New York, 1969; Mir, Moscow, 1984).

Translated by P. Shelnitz

# Features of the current-voltage characteristics of long semiconductor structures under ultrahigh-level double-injection conditions

N. M. Volodin and A. V. Khanova

*S. A. Lavochkin Scientific-Industrial Association, 141400 Khimki, Russia*

P. S. Smertenko and L. L. Fedorenko

*Institute of Semiconductor Physics, Ukrainian National Academy of Sciences, 252028 Kiev, Ukraine*
(Submitted June 20, 1997; accepted for publication April 29, 1998)
Fiz. Tekh. Poluprovodn. **32**, 1476–1481 (December 1998)

The widespread use of low-resistivity materials in modern solid-state electronics calls for an analysis of the current-voltage characteristics of long semiconductor structures under ultrahigh-level double-injection conditions. It is shown that the pure plasma model of semiconductors is not applicable in such an analysis, since the concentration dependence of the carrier mobility $\mu(n)$ must be taken into account. The conditions for the appearance of highly superlinear current-voltage characteristics in the region of the initial variation of $\mu(n)$ due only to the rate of variation of the mobility of the majority carriers (the $\lambda$ effect) are analyzed. The $\lambda$ effect is manifested on the experimental current-voltage characteristics in the form of sharp current jumps and corresponding high values of the differential order of the current-voltage ($J-V$) characteristic ($\alpha = d\log J/d\log V$), which are determined by the variation of the differential order of the concentration dependence of the carrier mobility $\lambda(n) = d\log\mu/d\log n$. A calculation shows that the mechanism for the appearance of the $\lambda$ effect can be determined at injection levels as high as $\sim 10^{17}$ cm$^{-3}$. © *1998 American Institute of Physics.* [S1063-7826(98)01212-5]

## INTRODUCTION

The conditions for the appearance of sharply superlinear current-voltage characteristics of semiconductor structures are analyzed in this paper on the basis of the theory of injection-contact phenomena with consideration of the character of the dependence of the mobility of the charge carriers on their concentration.

The features of the current-voltage characteristics (IVC's) of long semiconductor structures under ultrahigh-level double-injection conditions are considered. Although this question has not been analyzed hitherto, the widespread use of low-resistivity materials in modern solid-state electronics calls for such an analysis.

It should be noted that the statement of the problem is not confined to an examination of low-resistivity materials alone. The condition of low resistivity is equivalent to the condition of high current densities. However, the Joule heating of high-resistivity structures at such high current densities may preclude observation of the features of the ultrahigh-level double-injection regime.

The geometry of the structure investigated is shown in Fig. 1. In the present treatment $L > l_a + l_k$, where $l_a$ and $l_k$ are the ambipolar diffusion lengths at the anode and cathode, respectively. The cathode and anode materials must be good electron and hole injectors.

We shall utilize the theory of injection-contact phenomena developed in Ref. 1 to solve the problem posed.

## 1. INITIAL EQUATIONS AND APPROXIMATIONS

The calculation of IVC's at ultrahigh injection levels requires consideration of the dependence of the electron and hole mobilities ($\mu_n$ and $\mu_p$), the diffusion coefficients ($D_n$ and $D_p$), and, in the general case, the dielectric constant $\varepsilon$ on the electron and hole concentrations ($n$ and $p$).[2–5] In addition, the form of the dependence of the recombination intensity on the carrier concentrations $R(n,p)$ can also differ significantly from that in the Shockley–Read model because of both the occurrence of Auger processes and the complex dependence on $n$ and $p$ under the conditions of semiconductor degeneracy.[3–6]

When the diffusion-free approximation holds, the following system of equations can be obtained, according to Ref. 1, from the current equation, the Poisson equation, and the continuity equation:

$$E(n,j) = \frac{j}{e[\mu_n(n)n + \mu_p(n)p]},$$

$$j_n = j\frac{\mu_n(n)n}{\mu_n(n)n + \mu_p(n)p}, \tag{1}$$

$$dx = \frac{dj_n}{eR(n)} = \frac{j}{eR(n)}d\left[\frac{\mu_n(n)n}{\mu_n(n)n + \mu_p(n)p}\right],$$

where $e$ is the charge of an electron, $n$ and $p$ are the electron and hole concentrations at an arbitrary point $x$ in the semiconductor structure, $j$ is the direct current density, and $E$ is the electric field intensity. The space-charge density is de-

 

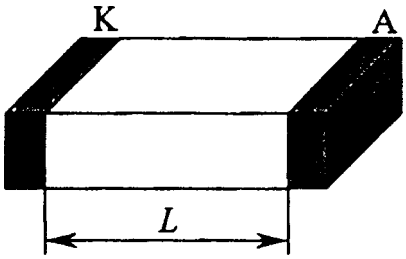


FIG. 1. Geometry of the structure: $L$ — intercontact distance; K — cathode; A — anode. Cathode and anode materials: metal or heavily doped $n^+$- and/or $p^+$-type semiconductor layers.

noted by $\rho(n,p)$, and the form of the functions $R(n,p)$ and $\rho(n,p)$ is specified by the semiconductor model.

The quasineutrality condition $\rho \equiv |\rho_+| - |\rho_-| \approx 0$ signifies fulfillment of the conditions

$$\left|\frac{dE}{dx}\right| \ll \frac{4\pi}{\varepsilon}|\rho_+| \approx \frac{4\pi}{\varepsilon}|\rho_-|,$$

$$\frac{\varepsilon(n)}{4\pi}|r(n)| \ll |\rho_+| \approx |\rho_-|, \tag{2}$$

where $|\rho_+|$ and $|\rho_-|$ denote the positive and negative components of the space charge $\rho(p,n)$, respectively,

$$r(n) = -\frac{\mu_n[1-\lambda_n(n)] + \mu_p(n)\{[dp/dn] - \lambda_p(n)[p(n)/n]\}}{\mu_n(n)\mu_p(n)\{p(n)[1+\lambda_p(n)-\lambda_n(n)] - n[dp/dn]\}} \times R(n) \tag{3}$$

is the ambipolar recombination function, and

$$\lambda(n) = -\frac{n}{\mu}\frac{d\mu}{dn}$$

is the differential order of $\mu(n)$.

If we also introduce the conductivity

$$\sigma(n) = e[\mu_n(n)n + \mu_p(n)p(n)], \tag{4}$$

the IVC from (1) can be determined using the following system of equations:[1]

$$L = \int_0^L dx = -j\int_{\sigma_S(j)}^{\sigma_k(j)} \frac{d\sigma}{\sigma^2 r(\sigma)},$$

$$V = \int_0^E E(x)\,dx = -j^2\int_{\sigma_S(j)}^{\sigma_k(j)} \frac{d\sigma}{\sigma^3 r(\sigma)}, \tag{5}$$

where $\sigma_k(j)$ is the near-cathode conductivity and $\sigma_S(j) = \sigma_{n=n_S(j)}$ is the value of $\sigma(x)$ at the minimum near the anode (it is assumed that $r<0$). The accuracy of the first integral in (5) is determined by fulfillment of the condition $L > l_a + l_k$, and the accuracy of the second integral is determined by the criterion for diffusion-free conditions[1]

$$V(j) \gg \frac{kT}{e}\ln\left|\frac{r_k(j)\sigma_k(j)}{r_a(j)\sigma_a(j)}\right|,$$

where $kT/e$ is the thermodynamic potential.

The system (5) will be solved below in the ''virtual-cathode'' approximation ($\sigma_k \to \infty$), which, on the basis of Ref. 1, means that $V(j) \ll |r_k(j)|L^2/2$, where $r_k(j) = r_{n=n_k(j)}$.

## 2. SPACE-CHARGE MODEL

At high injection levels the quasineutrality condition $\rho(n,p) \approx 0$ can be written in the form

$$p(n) \approx n + \Delta N, \tag{6}$$

where

$$\Delta N = \sum_A \frac{C_{nA}}{C_{nA}+C_{pA}}N_A - \sum_D \frac{C_{pD}}{C_{nD}+C_{pD}}N_D > 0$$

is the absolute value of the difference between the charges in all the acceptor ($A$) and donor ($D$) states, and $C_n$ and $C_p$ are the coefficients for the recombination of electrons and holes on them, respectively.[1,7]

Then, the quasineutrality criterion from (2) and (3) takes on the form [with consideration of the equality $|\rho_+| = ep(n)$]:

$$\frac{\varepsilon(n)|r(n)|}{4\pi e p(n)} = \frac{\varepsilon(n)}{4\pi e}\frac{\mu_n(n)[1-\lambda_n(n)] + \mu_p(n)\{1-\lambda_p(n)-\lambda_p(n)[\Delta N/n]\}}{\mu_n(n)\mu_p(n)\{[\lambda_p(n)-\lambda_n(n)]n + [1+\lambda_p(n)-\lambda_n(n)]\Delta N\}}\frac{R(n)}{p(n)} \ll 1, \tag{7}$$

and it follows from (4) that

$$\sigma(n) = e[\mu_n(n) + \mu_p(n)]n + e\mu_p(n)\Delta N. \tag{8}$$

It can be shown that under conditions for realization of the plasma model of semiconductors, where

$$p \approx n \gg \Delta N,$$

$$\sigma(n) \approx e[\mu_n(n) + \mu_p(n)]n, \tag{9}$$

the quantity $\Delta N$ in $r(n)$ from (3) and (7) can be neglected only under the conditions

$$n \gg \begin{cases} \dfrac{\mu_p(n)\lambda_p(n)}{\mu_n(n)[1-\lambda_n(n)] + \mu_p(n)[1-\lambda_p(n)]}\Delta N, \\ \dfrac{1+\lambda_p(n)-\lambda_n(n)}{\lambda_p(n)-\lambda_n(n)}\Delta N \end{cases} \tag{10}$$

which are more severe than (9), when $\lambda(n) \to 0$ or $\lambda(n) \to 1$.

This situation raises some doubt regarding the use of the pure plasma model in injection problems,[8] since $\lambda(n) \to 0$ and it becomes difficult to satisfy the second condition in (10) when $\mu(n) = \mu = \text{const}$. Therefore, the validity of the

pure plasma model of semiconductors in problems of the type under consideration can be determined only if the character of the dependence of the mobility of the carriers on their concentration, i.e., $\mu(n)$, is determined.

### 3. SCATTERING MODEL

When the electron-hole scattering of carriers in a nondegenerate structure is taken into account, in accordance with the data in Ref. 5 the mobility $\mu^*_{n,p}$ can be written in the form

$$\mu^*_{n,p}(n)=\mu_{n,p}\Bigg/\left\{1+\frac{n}{Q(n)}\ln\left[1+\left(\frac{M(n)}{n}\right)^{2/3}\right]\right\}, \tag{11}$$

where $\mu_{n,p}$ is the carrier mobility for $n\approx p\to 0$,

$$Q(n)=\frac{3\varepsilon^2(n)(kT)^{3/2}}{\sqrt{8\pi}e^3}\sqrt{\frac{m_n+m_p}{m_nm_p}}\,\frac{1}{\mu_{n,p}},$$

$$M(n)=64\,\frac{[\varepsilon(n)kT]^3}{e^6}, \tag{12}$$

and $m_n$ and $m_p$ are the electron and hole effective masses.

In the case of electron-hole scattering, when the quantum effects are taken into account, according to Ref. 7, the result (11) for the region $n\ll M$ remains valid if $Q(n)$ and $M(n)$ are replaced by the quantities

$$Q^*(n)=\frac{2^{9/2}\varepsilon^2(n)(kT)^{3/2}}{3\pi^{3/2}e^3}\sqrt{\frac{m_n+m_p}{m_nm_p}}\,\frac{1}{\mu_{n,p}},$$

$$M^*(n)=\frac{24\pi}{\exp(1)}\,\frac{m_nm_p}{m_n+m_p}\,\varepsilon(n)\left(\frac{kT}{eh}\right)^2. \tag{13}$$

In the case of a narrow-gap semiconductor with strong degeneracy, the Kane effect[4] should be taken into account. According to this effect, as $n$ increases, the effective mass of the carriers in the plasma ($p\approx n$) rises according to the expression

$$m^*_{n,p}(n)=m^*\sqrt{1+\left(\frac{n}{N}\right)^{2/3}},$$

$$N=\frac{\sqrt{8}\pi}{3}\,\frac{(m^*E_g)^{3/2}}{h^3}, \tag{14}$$

where $m^*$ is the effective mass of the carriers when $n\to 0$ ($m^*=m_n,m_p$) and $E_g$ is the gap width of the semiconductor for a given doping level. At room temperature (300 K) for $\varepsilon\approx 10$ we have $M(n)\approx 3.7\times 10^{20}$ cm$^{-3}$. If $Q(n)\ll M(n)$ and $n\ll M(n)$, a significant change (a twofold decrease) in $\mu(n)$ in Eq. (11) is achieved for

$$n\equiv n_m\cong\frac{3}{2}\left\{Q(n)/\ln\left[\frac{2}{3}\,\frac{M(n)}{Q(n)}\ln\frac{2}{3}\,\frac{M(n)}{Q(n)}\right]\right\}. \tag{15}$$

The value of $n_m$ from (15) is of the order of $10^{17}$ cm$^{-3}$ if $\mu\approx 10^3$ cm$^2$/V·s, while the value of $N$ in (14) is of the same order of magnitude only for narrow-gap materials with anomalously low values of $E_g$ and the effective masses of the carriers (InSb etc.). In general, we can single out the class of materials for which $n_m\ll N$ and which, in accordance with (12), (14), and (15), obey the relation

$$\mu\gg\frac{9\varepsilon^2(n)h^3}{8\pi^{3/2}e^3}\left(\frac{kT}{E_g}\right)^{3/2}\sqrt{\frac{m_n+m_p}{m_nm_p}\,\frac{1}{(m^*)^3}}, \tag{16}$$

which places a lower bound on the initial (at small values of $n$) carrier mobilities at a level of a few cm$^2$/V·s, if $\varepsilon\approx 10$, $T\approx 300$ K, $E_g\approx 1$ eV, and $m_n\approx m_p\approx m$. This means that the Kane effect can be disregarded under the conditions

$$n\ll n_m(n)\ll N\ll M(n) \tag{17}$$

when (16) is satisfied. In this case from (11) we can easily obtain

$$\mu(n)\approx\mu,\quad \lambda(n)\approx\frac{2}{3}\,\frac{n}{Q(n)}\left[\ln\frac{M(n)}{n}-1\right]\ll 1. \tag{18}$$

However, when the strong inequality (16) is reversed, under the conditions

$$n\ll N\ll n_m(n)\ll M(n) \tag{19}$$

only the Kane effect need be taken into account at relatively small values of $n$, so that

$$\mu(n)\approx\mu,\quad \lambda(n)\approx\frac{1}{3}\left(\frac{n}{N}\right)^{2/3}\ll 1. \tag{20}$$

### 4. RECOMBINATION MODEL

The conditions (16), (18), and (20) can be satisfied (or violated) for both types of carriers. However, we shall consider (for the sake of fixing ideas and simplicity) the situation where the majority carriers are holes under the condition $r<0$ in (3) and (5), so that the conditions $n\gg\Delta N>0$, $\mu_p(n)\approx\mu_p\gg\mu_n(n)\approx\mu_n$, and $m_p(n)\approx m_p\ll m_n(n)\approx m_n$ will hold at not excessively high values of $n$. In accordance with (3), (4), and (6), we then have

$$r(n)=-\frac{R(n)}{\mu_n[\lambda_p(n)n+\Delta N]},$$

$$n(\sigma)=\frac{\sigma}{e\mu_p}, \tag{21}$$

and from (7) the quasineutrality condition can be written in the form

$$\frac{\varepsilon}{4\pi e}\,\frac{R(n)}{\mu_n n[\lambda_p(n)n+\Delta N]}\ll 1, \tag{22}$$

where it is henceforth assumed that

$$\varepsilon=\text{const}\left|(n/\varepsilon)(d\varepsilon/dn)\right|\ll 1.$$

### 5. CALCULATION OF THE CURRENT-VOLTAGE CHARACTERISTIC

Let $R(n)=\gamma n^2$, which is true both for band or level recombination in shallow traps in the absence of degeneracy[1,8] and for normal Auger recombination in the presence of degeneracy.[7] In this case from (16), (18), and (21) we can obtain

$$r(\sigma)=-\frac{3}{2}\frac{Q_p\gamma}{\mu_n}\frac{\sigma^2}{\sigma^2[\ln(\sigma_M/\sigma)-1]+\sigma_\Delta^2}, \tag{23}$$

where

$$\sigma_M\equiv e\mu_p M, \quad \sigma_\Delta\equiv e\mu_p\sqrt{\frac{3}{2}Q_p\Delta N},$$

$$Q_p\equiv Q_{\mu=\mu_p}=\frac{3\varepsilon^2(kT)^{3/2}}{\sqrt{8\pi}e^3\sqrt{m_p}}\frac{1}{\mu_p}. \tag{24}$$

Using (23) and the methodology in Ref. 1 to determine the order of the function $r(\sigma)$

$$\delta(\sigma)=\frac{\sigma}{r}\frac{dr}{d\sigma}=\frac{\sigma^2+2\sigma_\Delta^2}{\sigma^2[\ln(\sigma_M/\sigma)-1]+\sigma_\Delta^2}, \tag{25}$$

we can predict the existence of a minimum $\delta_{\min}(\sigma_{\min})$ for $\delta(\sigma)$ and a corresponding maximum $\alpha_{\max}$ for the order of the IVC $\alpha=d(\log J)/d(\log V)$. The minimum of $\delta(\sigma)$ from (25) is specified by the equations

$$\frac{2}{\delta_{\min}}+\ln\left(\frac{2}{\delta_{\min}}-1\right)=2\ln\frac{\sigma_M}{\sqrt{2}\sigma_\Delta}-3,$$

$$\sigma_{\min}=\sigma_M\exp\left[-\left(\frac{1}{\delta_{\min}}+\frac{3}{2}\right)\right], \tag{26}$$

which yields a value of the maximum order of the IVC at the level

$$\alpha_{\max}\equiv\alpha_e\approx 1+\frac{1}{\delta_{\min}}\approx\ln\frac{\sigma_M}{2\sqrt{\exp(1)}\sigma_\Delta}, \tag{27}$$

since $\alpha_e\gg 1/2|\ln(\alpha_e-3/2)|$ and from (17) and (24) $\sigma_M\gg\sigma_\Delta$.

After the region of the extremum of the order of the IVC, where $\sigma_S^2(j)\gg\sigma_\Delta^2$, from (5) and (23) we can obtain the expressions

$$\sigma_S(V)\approx\sigma_M\exp\left[-\left(1+\frac{3\gamma Q_pL^2}{4\mu_nV}\right)\right],$$

$$j(V)\approx\frac{2\sigma_MV}{L}\exp\left[-\left(1+\frac{3\gamma Q_pL^2}{4\mu_nV}\right)\right], \tag{28}$$

and from (15) and (17) we have

$$V\ll V_M=\frac{3\gamma Q_pL^2}{4\mu_n}\left\{\ln\left[\frac{2M}{3Q_p}\ln\left(\frac{2M}{3Q_p}\right)\right]\right\}^{-1},$$

$$\sigma_S(V)\ll\frac{3}{2}e\mu_pQ_p\left\{\ln\left[\frac{2M}{3Q_p}\ln\left(\frac{2M}{3Q_p}\right)\right]\right\}^{-1}\ll\sigma_M. \tag{29}$$

Thus, fairly high orders of the IVC (sharp current jumps) should be observed in the injection regime under consideration due to the existence of a dependence of $\lambda_p$ on $n$ long before any appreciable variation of $\mu_p(n)$ is observed. Figure 2 presents qualitative plots of the IVC and $\alpha$ vs $V$ for the cases considered.

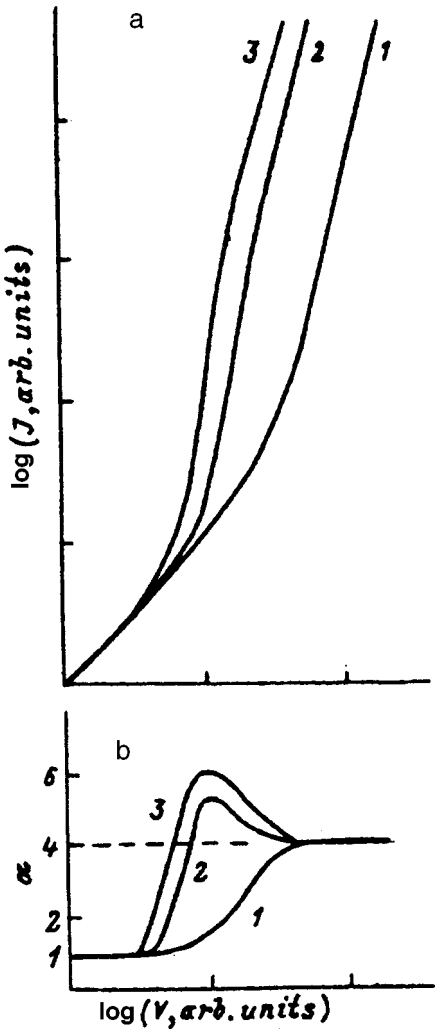


FIG. 2. Qualitative plots of the IVC (a) and $\alpha$ vs $V$ (b) for the ultrahigh-level double-injection regime. Curves *1–3* correspond to different values of $\Delta N$: $\Delta N_3<\Delta N_2<\Delta N_1$.

## 6. MEASUREMENT POSSIBILITIES OF THE ULTRAHIGH-LEVEL DOUBLE-INJECTION REGIME

An exact calculation of the parameters of the order extrema ($J_e, V_e$, and $\alpha_e$) from (23) and (25) using the methods in Ref. 1 makes it possible to determine the values of $\Delta N$ and $\gamma$ from experimentally observed IVC's in the region of their order extrema and the formulas

$$\Delta N=\frac{2}{3}\left(\frac{LJ_e}{e\mu_pSV_e}\right)^2\frac{1}{Q_p}\frac{\alpha_e^2}{(2\alpha_e-1)^2}\times\frac{\delta_{se}\ln(\sigma_M/\sigma_{se})-(1+\delta_{se})}{2-\delta_{se}},$$

$$\gamma=\frac{2}{3}\frac{\mu_nV_e}{Q_pL^2}\frac{(2\alpha_e-1)(\alpha_e-1)}{\alpha_e^2}\frac{2\ln(\sigma_M/\sigma_{se})-3}{2-\delta_{se}}, \tag{30}$$

where $J_e=Sj_e$, $S$ is the area of the sample normal to the current,

$$\frac{\sigma_M}{\sigma_{se}}=\frac{e\mu_pMSV_e}{LJ_e}\left(2-\frac{1}{\alpha_e}\right),$$

$$\delta_{se}=\frac{1}{\alpha_e-1}\left[1-\frac{\alpha_e''V_e^2}{\alpha_e(2\alpha_e-1)(\alpha_e-1)}\right],$$

$$\alpha_e''=\left(\frac{d^2\alpha}{dV^2}\right)_{V=V_e}, \quad \alpha_e=\frac{V_e}{J_e}\left(\frac{dJ}{dV}\right)_{V=V_e}.$$

When the strong inequality (16) is reversed, under conditions for the realization of (19), (20), and (22) from (21) we obtain

$$r(\sigma)=-\frac{3N_p^{2/3}\gamma}{\mu_n(e\mu_p)^{1/3}}\frac{\sigma^2}{\sigma^{5/3}+\sigma_p^{5/3}}, \tag{31}$$

where

$$N_p=N_{(m^*=m_p)}=\frac{\sqrt{8}\pi}{3}\frac{(m_pE_g)^{3/2}}{h^3},$$

$$\sigma_p\equiv e\mu_p(3\Delta N N_p^{2/3})^{3/5}.$$

For $\sigma_s(j)\gg\sigma_p$ it follows from (31), (26), and (27) that we can use approximations of the form

$$\sigma_s(j)=\left(\frac{e\mu_p}{N_p^2}\right)^{1/4}\left(\frac{\mu_n j}{4\gamma L}\right)^{3/4},$$

$$j(V)=\frac{9\cdot 7^4}{8\pi^2\cdot 4^7}\frac{eh^6\mu_p\mu_n^3}{(\gamma m_pE_g)^3}\frac{V^4}{L^7}, \tag{32}$$

whence follows the formula for analyzing measurement results

$$\gamma\approx 0.256\left(\frac{e\mu_pS}{J_e}\right)^{1/3}\frac{h^2\mu_nV_e^{4/3}}{m_pE_gL^{7/3}}, \tag{33}$$

where $V_e$ and $J_e$ are determined at the point of the order maximum $\alpha\approx\alpha_e=4$.

In the case of weak asymmetry of the carrier mobilities and effective masses, the IVC from (32) can be written in the form

$$j(V)=\frac{9\cdot 7^4}{8\pi^2\cdot 4^7}\frac{eh^6}{(\gamma E_g)^3}\left[\frac{\mu_n\mu_p(m_n-m_p)}{m_nm_p}\right]^3 \times\frac{1}{(\mu_n+\mu_p)^2}\frac{V^4}{L^7}. \tag{34}$$

It can be shown on the basis of (22), (18), and (20) for fairly small values of $\Delta N$ $[\Delta N\ll\lambda_p(n)n]$ that the conditions for carrier drag (quasineutrality) under the conditions considered can be written in the form

$$\sigma_s(j)\gg\frac{3\varepsilon\gamma}{8\pi}Q_n[\ln(a\ln a)-1],$$

$$\sigma_s(j)\gg e\mu_pN_p\left[\frac{3\varepsilon\gamma}{4\pi e\mu_n}\right]^{3/2}, \tag{35}$$

respectively, for the cases of electron-hole scattering and the Kane effect. Here $a\equiv\varepsilon\gamma M/(8\pi e\mu_nQ_p)$.

## 7. CONCLUSION

The appearance of highly superlinear IVC's in the region of the initial variation of $\mu(n)$ due only to the rate of variation of the mobility of the majority carriers (the λ effect) is very interesting. According to the data presented above, it requires fulfillment of the following conditions (for a *p*-type semiconductor):

$$\mu_p\gg\mu_n\gg\frac{\varepsilon\gamma}{4\pi e},$$

$$N_p\gg\frac{3}{2}Q_p\left\{\ln\left[\frac{2M}{3Q_p}\ln\frac{2M}{3Q_p}\right]\right\}^{-1}\gg\Delta N,$$

$$\frac{3}{2}Q_p\left\{\ln\left[\frac{2M}{3Q_p}\ln\frac{2M}{3Q_p}\right]\right\}^{-1}\gg N_p\gg\Delta N,$$

of which the first ensures satisfaction of the quasineutrality criterion, the second refers to the case of electron-hole scattering ($\alpha_e>4$), and the third applies to the Kane effect ($\alpha_e=4$). In the case of electron-hole scattering in comparatively wide-gap semiconductors ($E_g\approx 1$ eV), these conditions impose a lower bound on the value of $\mu_p(m_p/m_n)^2$ at a level of several $\mathrm{cm^2/V\cdot s}$ (when $\mu_p\gg\mu_n$) and an upper bound on the value of $\mu_p\Delta N$ at the $10^{21}$ $\mathrm{cm^{-1}V^{-1}s^{-1}}$ level when $\mu_p/\gamma\gg 6\times 10^6$ $\mathrm{cm^{-1}V^{-1}}$. In the latter case (the Kane effect) for narrow-gap materials with small values of $m_p$ (like InSb) violation of the condition (16) places an additional upper bound on $\mu_p$ at the $10^4$ $\mathrm{cm^2/V\cdot s}$ level. All these conditions are attained comparatively easily, so that the achievement of injection levels as high as $n_s(j)\approx 10^{17}$ $\mathrm{cm^{-3}}\gg\Delta N$ in a semiconductor can permit verification of the existence of a given λ mechanism.

[1] A. Ya. Zyuganov and S. V. Svechnikov, *Injection-Contact Phenomena in Semiconductors* [in Russian], Nauka Dumka, Kiev (1981).
[2] H. Brooks, Phys. Rev. A **83**, 879 (1951).
[3] N. H. Fletcher, Proc. IRE **45**, 862 (1967).
[4] E. O. Kane, J. Phys. Chem. Solids **1**, 249 (1957).
[5] A. Anselm, *Introduction to Semiconductor Theory* (Prenctice-Hall, Englewood Cliffs, N.J., 1981; Mir, Moscow, 1978).
[6] A. Haug, Solid-State Electron. **21**, 1281 (1978).
[7] G. N. Galkin, Tr. FIAN **128**, 3 (1981).
[8] M. A. Lampert and P. Mark, *Current Injection in Solids* (Academic Press, New York, 1970; Mir, Moscow, 1973).

Translated by P. Shelnitz

# Continuous stimulated emission at $T=293$ K from separate-confinement heterostructure diode lasers with one layer of InAs quantum dots grown on vicinal GaAs(001) surfaces misoriented in the [010] direction in the active region

V. P. Evtikhiev, I. V. Kudryashov, E. Yu. Kotel'nikov, V. E. Tokranov, A. N. Titkov, I. S. Tarasov, and Zh. I. Alferov

*A. F. Ioffe Physicotechnical Institute, Russian Academy of Sciences, 194021 St. Petersburg, Russia*
(Submitted June 29, 1998; accepted for publication July 1, 1998)
Fiz. Tekh. Poluprovodn. **32**, 1482–1486 (December 1998)

The electroluminescence and stimulated emission of lasers with one layer of InAs quantum dots (QD's) grown in a single molecular-beam epitaxial process on vicinal GaAs(001) surfaces misoriented in the direction [010] by 2, 4 and 6° are investigated. It is discovered that an increase in the misorientation angle leads to a blue shift and a decrease in the full width at half maximum (FWHM) of the electroluminescence spectrum. This effect is attributed to a decrease in the size of the quantum dots and improvement in their size uniformity. A strong dependence of the threshold current density on the width of the spontaneous luminescence spectrum is discovered. The room-temperature threshold current density of the lasers with one layer of quantum dots and the spontaneous luminescence spectrum having the smallest FWHM (54 meV) equals 210 A/cm$^2$. © *1998 American Institute of Physics.* [S1063-7826(98)01312-X]

Quantum-dot (QD) arrays are very interesting objects for use as active media in the next generation of injection heterostructure lasers. The calculations in Ref. 1 showed that because of the delta-shaped character of the energy dependence of the QD density of states, QD lasers can have extremely low threshold current densities ($>10$ A/cm$^2$), which depend weakly on temperature. The threshold current densities that have been achieved in quantum-dot lasers are still far from the predicted values. Significant progress in improving the characteristics of QD lasers has been achieved as a result of the use of several layers of vertically coupled QD's[2] and tunnel-coupled QD arrays and quantum wells.[3] However, since these solutions unavoidably lead to broadening of the density-of-states function, the interest in the possibility of creating a ''classical'' quantum-dot laser has not waned.

The main obstacle to obtaining low-threshold lasing at room temperature is the complexity of growing uniform high-density arrays of isolated QD's by molecular-beam epitaxy (MBE) according to the Stranski–Krastanov method. The use of GaAs(001) substrates misoriented in the [010] direction in ordinary MBE according to the Stranski–Krastanov method to improve the size uniformity of QD's was first proposed in Ref. 4. Growth steps oriented in two directions, viz., [110] and $[\bar{1}10]$, should appear on such a vicinal surface. The intersection of these steps forms a network of bounded terraces, whose size depends on misorientation angle, on the vicinal surface. The energy barriers in the surface potential located on the terrace boundaries prevent the movement of atoms diffusing over the surface from terrace to terrace. In fact, detailed atomic force microscopic (AFM) investigations of InAs QD arrays grown by the Stranski–Krastanov method on GaAs(001) substrates misoriented in the [010] direction[5] showed that a quantum dot grows on each terrace predominantly from the material deposited on that terrace. An increase in the misorientation angle leads to an increase in the density of QD's, a decrease in their size, a decrease in the number of coalescing ''large'' islands, and improvement in the uniformity of the QD size.

Our work is devoted to studying the electroluminescence (EL) of separate-confinement laser heterostructures with one layer of InAs QD's in the active region, which are grown by ordinary MBE according to the Stranski–Krastanov method on GaAs(001) substrates misoriented in the [010] direction. The laser heterostructures were grown in a TsNA-4 system in one MBE process on a set of substrates misoriented in the [010] direction by 0, 2, 4, and 6°. The growth rates, substrate temperature, and V/III flux ratio were chosen and monitored using reflection high-energy electron diffraction (RHEED). As in Ref. 5, the growth temperature of the InAs QD's was 470 °C, and the V/VIII flux ratio was equal to 2. After 2.9 monolayers of InAs were deposited, growth was interrupted for 15 sec for the final stage of formation of the QD's. The QD layer was enclosed on both sides in waveguide superlattice layers with effective variation of the composition from $Al_{0.1}Ga_{0.9}As$ near the QD layer to $Al_{0.6}Ga_{0.4}As$ near the emitters. The heterostructure was an ordinary separate-confinement laser structure with $Al_{0.6}Ga_{0.4}As$ emitters, each having a thickness of 0.8 $\mu$m, a waveguide layer of variable composition and thickness 0.6 $\mu$m, and a *p*-type GaAs(Be) contact layer of thickness 0.4 $\mu$m. Lasers having a very simple stripe design with $SiO_2$ insulation and a stripe width of 100 $\mu$m were fabricated from the structures. Highly reflective dielectric coatings with 80–90% reflectivity were deposited on the mirrors of some of the lasers. The EL spectra were investigated under a continuous pump current.

Figure 1 shows the AFM images of QD arrays grown in

 

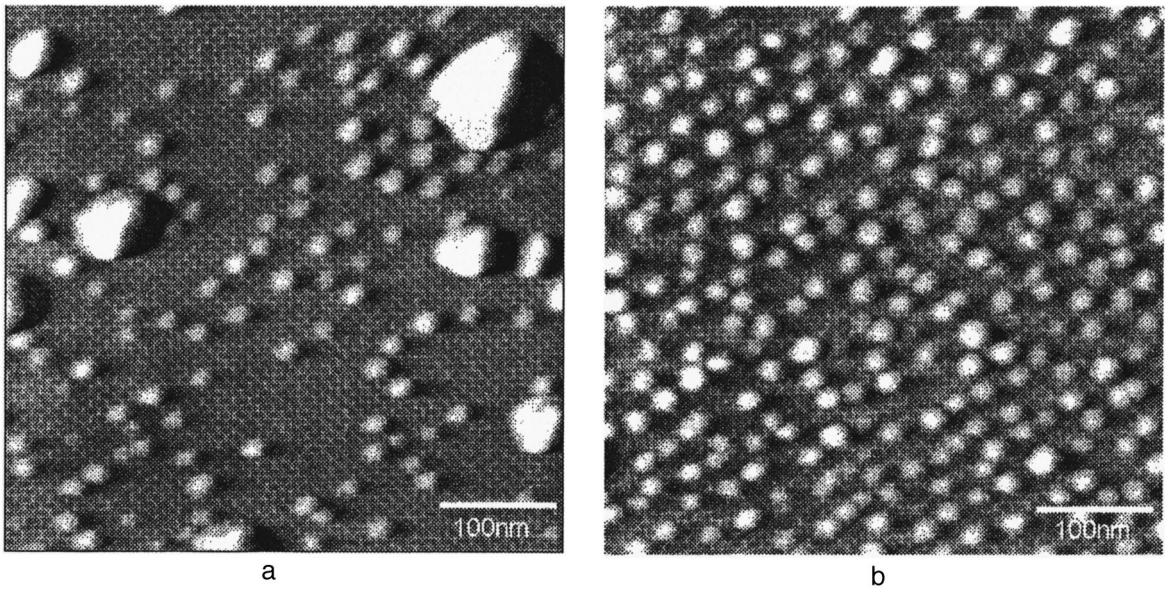


FIG. 1. AFM images of GaAs(001) surfaces coated by a 2.9 monolayer thick InAs layer with different misorientation angles in the [010] direction: 0 (a) and 6° (b).

a single MBE process on an exactly oriented GaAs(001) substrate (a) and a substrate misoriented by 6° (b) under conditions corresponding completely to the growth of the laser heterostructures. The surfaces of the samples were investigated by atomic force microscopy on an SPM-4 (NT-MDT) microscope. The surface images were obtained with scanning of the tip over the sample surface at a constant pressure (in the contact mode). The spatial resolution achieved using a $Si_3N_4$ tip with a radius $R<300$ Å mounted on a $V$-shaped cantilever was far better than the diameter of most of the features observed on the surface. A comparison of the AFM images in Fig. 1 shows that substrate misorientation leads to the formation of a more uniform array of InAs QD's without ''large'' InAs islands. An estimate of the QD density from the AFM images gives $4\times10^{10}$ cm$^{-2}$ and $\approx10^{11}$ cm$^{-2}$ for an exactly oriented surface and a surface misoriented by 6°. An analysis of the height distribution of the QD's revealed a decrease of the mean QD height from 35 to 20 Å with increasing misorientation and a decrease in the height dispersion from 15 to 10%.

Laser diodes with a cavity length of 1700 $\mu$m not having dielectric coatings on the mirrors were used to investigate the electroluminescence. The transition to a lasing regime could be observed with such a cavity length. A comparison of the photo- and electroluminescence spectra presented in the inset in Fig. 2 for a sample with 4° misorientation showed that self-absorption effects[6] do not alter the qualitative picture of the spectrum and do not interfere with the comparative study of the spectra of the laser structures. Figure 2 presents the EL spectra of four laser diodes without coatings on the mirrors, which were fabricated from heterostructures with various misorientation angles. The spectra were recorded at 20 °C with a pump current density equal to 300 A/cm$^2$.

The spectrum of the exactly oriented sample has the complex form previously observed in Ref. 7. Apart from the long-wavelength maximum, which is associated with recombination from the ground state of the quantum dots, it contains a short-wavelength shoulder, which separates into two peaks of Gaussian shape upon curve fitting. An increase in the misorientation angle leads to a blue shift of the luminescence spectra, reduction of the short-wavelength shoulder, and a decrease in the full width at half-maximum (FWHM) of the ground-state peak. Due to the large height of the barrier ($Al_{0.1}Ga_{0.9}As$) bounding the dots, none of the samples displayed luminescence from the wetting layer (the calculated position of the peak is indicated by an arrow). The observed blue shift and the decrease in the FWHM (Fig. 2) agree well with the data from the AFM investigations and can be attributed to variation of the size distribution of the dots with the misorientation angle. Variation of the temperature in the range $20-50\,^{\circ}$C and the pump current up to a subthreshold value did not lead to changes in the shape and FWHM of the long-wavelength maximum and only slightly altered the contribution of the short-wavelength shoulder to the luminescence. The decrease in the contribution of the short-wavelength shoulder to the spectrum with increasing misorientation angle is evidence that the complex form of the spectra is clearly due to recombination not only through excited states of the QD's, but also through states created by the presence of tunnel-coupled dots with a different mean radius (Refs. 8 and 9).[1)]

A further increase in the pump current ($T=20\,^{\circ}$C) in the samples without dielectric mirrors led to the appearance of lasing. Figure 3 presents the electroluminescence spectra of a sample with 4° misorientation for various pump currents. When the current equals 690 mA, a series of individual narrow (1–2 meV) peaks appears along with general narrowing of the luminescence maximum. Luminescence with such a pattern is clearly caused by the stimulated emission of a few groups of QD's of very similar size. Increasing the pump current to 715 mA causes the appearance of lasing lines in the spectrum, which coincide in position with the peaks of

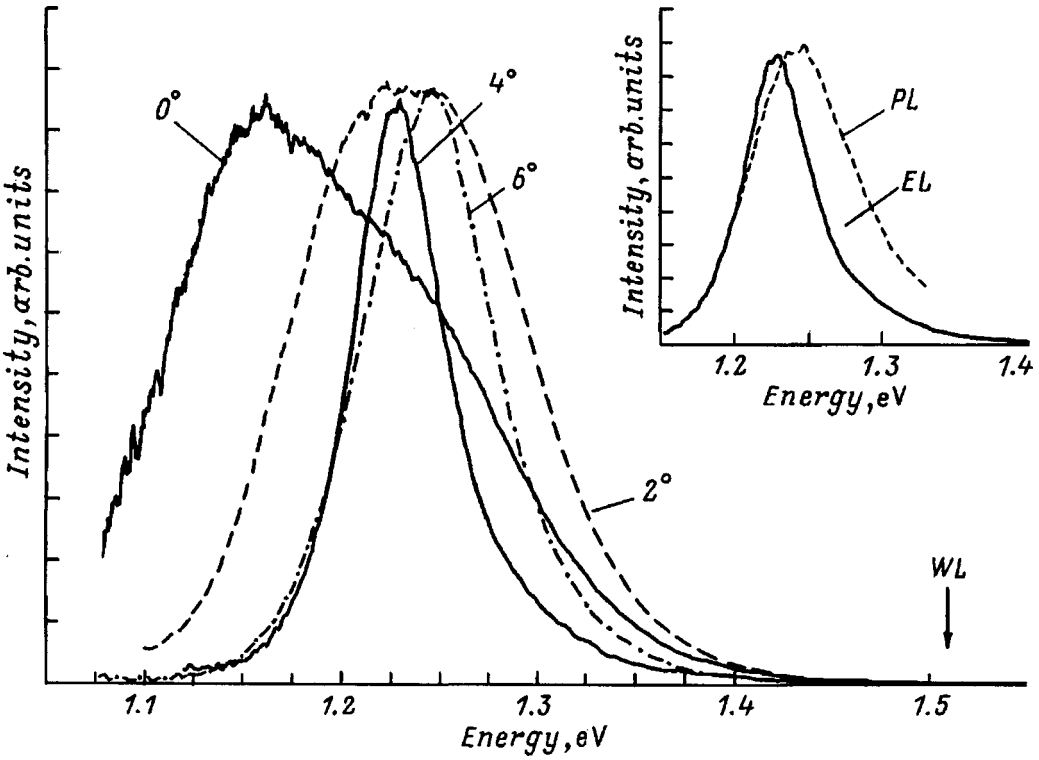


FIG. 2. Electroluminescence spectra ($T=293$ K; $I=300$ mA) of four laser diodes fabricated from heterostructures with various substrate misorientation angles. The inset shows the photo- and electroluminescence spectra for a sample with 4° substrate misorientation.

stimulated EL. Variation of the pump current up to twice the threshold value did not lead to variation of the positions of the initial lasing peaks. Only new peaks caused by stimulated emission from other groups of QD's were added to the spectrum.

Highly reflective dielectric coatings were deposited to diminish the losses due to the escape of radiation in the mirrors of the stripe lasers. The values of the threshold current density measured for the best structures ranged from 210 A/cm$^2$ for a sample with 4° misorientation to 5000 A/cm$^2$ for an exactly oriented sample. In our opinion, such strong variation of the threshold current density cannot be explained by the value of the quantum efficiency in the heterostructures. We measured the quantum efficiency ($\eta$) in samples with a short cavity ($L=100\mu$m) according to the method described in Ref. 10 (inset in Fig. 4). The relative increase in $\eta$ with increasing misorientation angle does not exceed a factor of 2. This finding can be attributed to a decrease in the contribution of radiationless recombination through ''large islands.'' The threshold current density turned out to be lower in the sample with 6° misorientation than in the sample with 2° misorientation, despite the smaller value of $\eta$. In Fig. 4 the values of the threshold current density $J_{th}$ are plotted as a function of the FWHM of the spontaneous EL spectra. The rapid increase in $J_{th}$ with the FWHM corresponds to the predictions of the theory of QD lasers developed in Ref. 11. According to this theory, the maximum gain in such a laser is proportional to the surface density of QD's and also depends on the size dispersion $\varepsilon$ of the dots as $1/\varepsilon$. Since the FWHM of the luminescence spectra is directly related to the size uniformity of the QD's, the low values of the threshold current density for the samples with 2, 4, and 6° misorientation are due to the fact that quantum dots could be obtained in them with a large surface density and a low size dispersion.

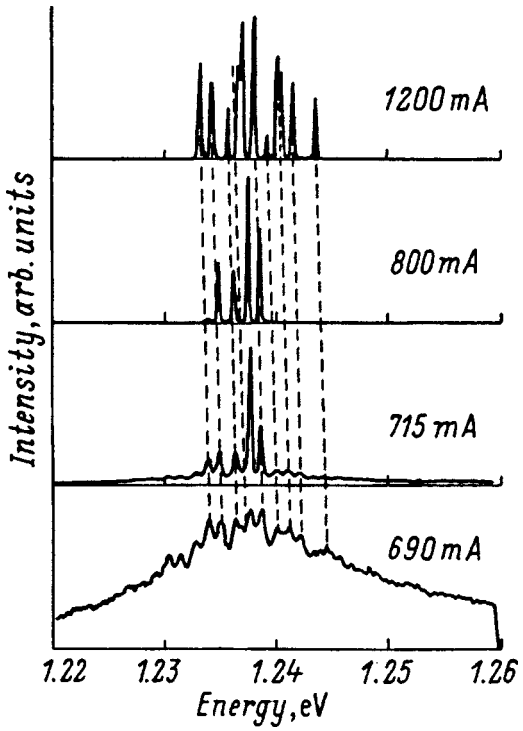


FIG. 3. Electroluminescence spectra of a sample with 4° substrate misorientation for various pump currents at $T=293$ K.

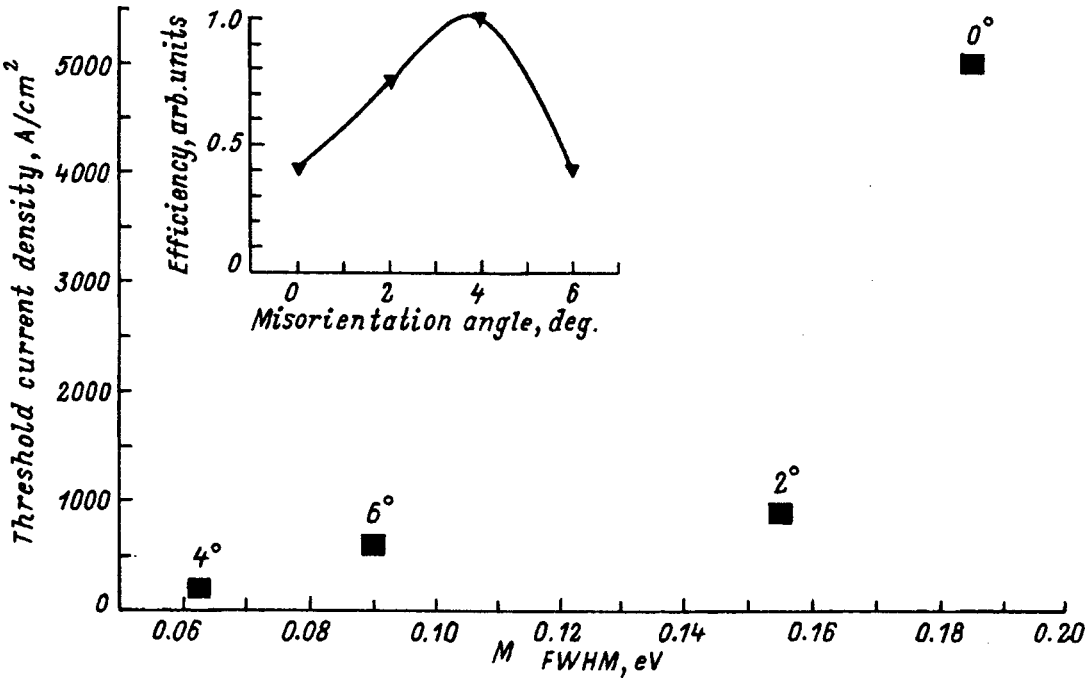


FIG. 4. Dependence of the threshold current density $J_{th}$ on the FWHM of the spontaneous EL spectra for samples with various substrate misorientation angles: 0, 2, 4, and 6°. The inset shows the relative variation of the quantum efficiency in samples with a short cavity ($L=100\mu$m) on substrate misorientation angle.

The lowest threshold current density (210 A/cm$^2$) was exhibited by the lasers displaying spontaneous EL with the smallest FWHM (4° substrate misorientation). The EL and lasing spectra of this laser are shown in Fig. 5. This value is a record for injection lasers with one layer of InAs QD's in the active region.

In conclusion, we note that the employment of GaAs(001) substrates misoriented in the [010] direction in a conventional MBE process has allowed us to grow laser heterostructures with a single uniform QD array having a high surface density ($\approx 10^{11}$ cm$^{-2}$) in the active region, on which it was possible to obtain continuous lasing at 293 K through the ground state of the carriers in the QD's. The value of 210 A/cm$^2$ obtained for the threshold current density at 293 K in the lasers with 4° misorientation is the best value known to us for separate-confinement heterostructure lasers with one layer of quantum dots in the active region.

We thank L. V. Asryan for some fruitful discussions and N. F. Kadoshchuk for depositing the mirrors.

This work was supported by the Russian Fund for Fundamental Research (Grants 97-02-18153, 97-02-18151, and 97-02-18291).

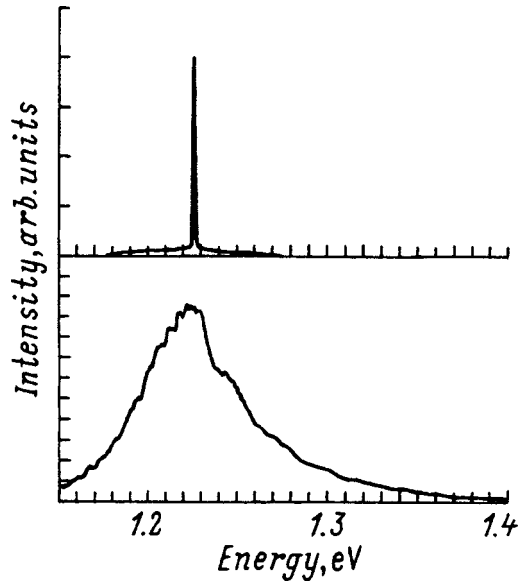


FIG. 5. Spontaneous EL ($J=170$ A/cm$^2$) and lasing ($J=210$ A/cm$^2$) spectra of a laser with 4° substrate misorientation at $T=293$ K.

[1)] We intend to publish the results of an investigation of the form of the photoluminescence spectra of QD arrays on misoriented wafers in the near future.

[1] Y. Arakawa and H. Sakaki, Appl. Phys. Lett. **40**, 939 (1982).
[2] N. N. Ledentsov, V. M. Ustinov, V. A. Shchukin, P. S. Kop'ev, and Zh. I. Alferov, Fiz. Tekh. Poluprovodn. **32**, 385 (1998) [Semiconductors **32**, 343 (1998)].
[3] F. Heinrishsdorff, M.-H. Mao, N. Kirstaedter, A. Krost, and D. Bimberg, Appl. Phys. Lett. **71**, 22 (1997).
[4] V. P. Evtikhiev, A. K. Kryganovskii, A. B. Komissarov, A. N. Titkov, M. Ichida, and A. Nakamura, Inst. Phys. Conf. Ser. **155**, 351 (1996).
[5] V. P. Evtikhiev, V. E. Tokranov, A. K. Kryzhanovskiĭ, A. M. Boĭko, R. A. Suris, A. N. Titkov, A. Nakamura, and M. Ichida, Fiz. Tekh. Poluprovodn. **32**, 860 (1998) [Semiconductors **32**, 765 (1998)].
[6] D. Z. Garbuzov, V. P. Evtikhiev, V. V. Agaev, V. B. Khalfin, and V. P. Chalyĭ, Fiz. Tekh. Poluprovodn. **17**, 1653 (1983) [Sov. Phys. Semicond. **17**, 1052 (1983)].
[7] H. Shoji, Y. Nakata, K. Mukai, Y. Sugiyama, M. Sugawara, N. Yoloyama, and H. Ishikawa, IEEE J. Sel. Top. Quantum Electron. **3**, 188 (1997).

[8] D. G. Vasil'ev, V. P. Evtikhiev, V. E. Tokranov, I. V. Kudryashov, and V. P. Kochereshko, Fiz. Tverd. Tela (St. Petersburg) **40**, 855 (1998) [Phys. Solid State **40**, 787 (1998)].
[9] N. P. Kobayashi, T. R. Ramachandran, P. Chen, and A. Madhukar, Appl. Phys. Lett. **68**, 3299 (1996).
[10] D. Z. Garbuzov, A. T. Gorelenok, M. K. Trukan, A. S. Usikov, and V. P. Chalyĭ, Fiz. Tekh. Poluprovodn. **15**, 505 (1981) [Sov. Phys. Semicond. **15**, 286 (1981)].
[11] L. V. Asryan and R. A. Suris, Semicond. Sci. Technol. **11**, 554 (1996).

Translated by P. Shelnitz

## PERSONALIA

# Solomon Meerovich Ryvkin (On his 80th Birthday)

Fiz. Tekh. Poluprovodn. **32**, 1533–1534 (December 1998)

[S1063-7826(98)01412-4]

November 23 marks the 80th birthday of the renown Russian scientist, Prof. Solomon Meerovich Ryvkin, who was the first editor-in-chief of Fizika i Tekhnika Poluprovodnikov [Semiconductors].

He was born in Belorussia in 1918. In 1936 he enrolled in the faculty of physics and mechanics of the Leningrad Polytechnic Institute, from which he graduated a few days before the beginning of World War II. In 1941–1945 he defended his homeland, travelled as a member of the signal corps from Voronezh to Vienna, and finished the war as the commander of the telephone-telegraph section of the Third Ukrainian Front.

In 1945 S. M. Ryvkin started working in the Physicotechnical Institute, where, thanks to his remarkable talent, tremendous industriousness, and unreserved devotion to science, advanced in a short time from a junior research worker to a doctor of physical and mathematical sciences, a professor, and a great scientist, who enjoyed well-deserved worldwide fame. In 1957 he set up the Laboratory for Nonequilibrium Processes in Semiconductors, which he headed until his premature retirement in 1981.

Already in his early papers S. M. Ryvkin was the first to use the concept of the exciton to explain the anomalous dependences of the photoconductivity of cuprous oxide that he observed. The optical spectrum of this quasiparticle was subsequently discovered in a crystal of cuprous oxide. Ryvkin's scientific studies of the mechanisms and kinetics of the photoconductivity of solids are regarded as classical and, to a large extent, fundamental. Ryvkin's monograph *Photoelectric Effects in Semiconductors*, which summarized those studies, was republished in the United States and Germany and became a reference book for a whole generation of researchers.

S. M. Ryvkin's name is associated with the discovery of many fundamental effects in physics. They include the current-convective instability in a semiconductor plasma, the phenomenon of light scattering in crystals with variation of the frequency due to the nonlinear polarizability of the medium, and electron drag by photons. The phenomena associated with the charge exchange of local centers that he discovered, as well as the discovery of the magnetoconcentration effect and some new nonlinear phenomena in hot electron-hole plasmas (Gunn oscillations in strained germanium, intervalley current instability, and the shock avalanche breakdown of excitons in germanium) also aroused great interest in the scientific community. His pioneering work on the observation of induced emission in III-V semiconductors

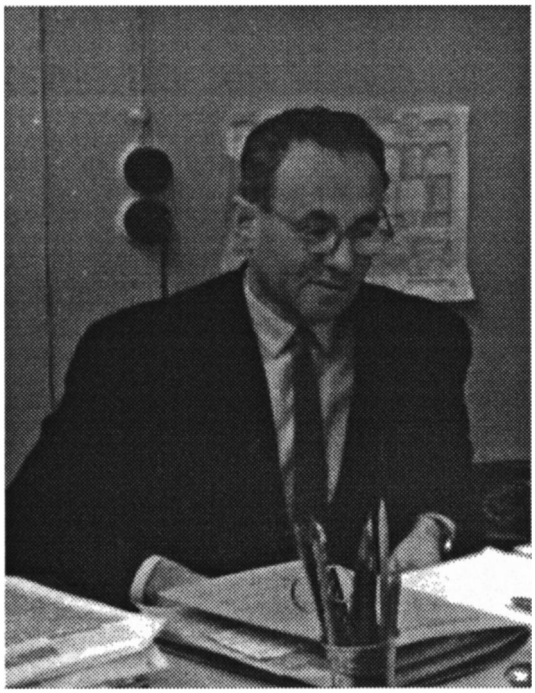

subsequently led to the creation of semiconductor lasers and was acknowledged by a Lenin Prize in 1964 (which he shared with D. N. Nasledov, A. A. Rogachev, and B. V. Tsarenkov). In the nineteen-seventies S. M. Ryvkin was one of the first to recognize the importance and prospects of studying manifestations of disorder in semiconductors and initiated appropriate research projects in his laboratory.

S. M. Ryvkin was typified by a combination of interest in basic science and the practical application of its results. For example, the work of Ryvkin and his coworkers on the effect of nuclear radiations on semiconductors led to the extensive development of research on radiation effects in Russia and, at the same time, to the development of a new branch of semiconductor instrument building, viz., the production of nuclear radiation detectors. Fundamentally new, uncooled detectors of infrared laser radiation were created on the basis of the phenomenon of carrier drag by photons. On the basis of the principle of controlled sensitivity that they formulated, S. M. Ryvkin and his coworkers created a new class of image detectors, i.e., semiconductor photographic systems and ionization-type converters, which have found application in the high-speed photographic diagnostics of infrared laser radiation.

 

Together with his students, S. M. Ryvkin boldly created new areas of research, achieving outstanding results. This trend was undoubtedly promoted by the inquisitive atmosphere that prevailed in his laboratory. One object of his constant concern was the laboratory seminar, which earned a favorable reputation among specialists in semiconductor physics. The spirit of the seminar, which was known for its relaxed and friendly atmosphere, was always Ryvkin himself. More than 50 doctors and candidates of science, many of whom presently head scientific teams, were trained under his guidance.

S. M. Ryvkin performed a great deal of scientific administrative work. He initiated the publication of Fizika i Tekhnika Poluprovodnikov [Semiconductors], which has earned a reputation among specialists from all over the world, and until 1981 he headed its editorial board. Reviewing everything done by S. M. Ryvkin, we can single out the establishment of a scientific school for investigating nonequilibrium processes in semiconductors, which is being continued by his students, as his primary accomplishment.

*Students and Friends*
*Editorial Board*
*Board of Directors*
*A. F. Ioffe Physicotechnical Institute*
*Russian Academy of Sciences*

Translated by P. Shelnitz

## ERRATA

# Erratum: Autosolitons in InSb in a magnetic field [Semiconductors 32, 625–628 (June 1988)]

I. K. Kamilov, A. A. Stepurenko, and A. S. Kovalev

*Kh. I. Amirkhanov Physics Institute, 367003 Makhachkala, Russia*
Fiz. Tekh. Poluprovodn. **32**, 1535 (December 1998)

[S1063-7826(98)01512-9]

The sentence beginning on the 14th line from the top of the right-hand column on p. 627 reads: It turned out that the velocity of the autosoliton decreases as it moves into the hotter region of the EHP. It should read: It turned out that the velocity of the autosoliton increases as it moves into the hotter region of the EHP and that the velocity of the autosoliton decreases as it moves into the colder region of the EHP.

 